VOLUME 11 NUMBER 1 2020 ISSN 2218-7987
eISSN 2409-5508

International Journal of Mathematics and Physics

Al-Farabi Kazakh National University

The International Journal of Mathematics and Physics is a peer-reviewed international journal covering all branches of mathematics and physics. The Journal welcomes papers on modern problems of mathematics and physics, in particular, Applied Mathematics, Algebra, Mathematical Analysis, Differential Equations, Mechanics, Informatics, Mathematical Modeling, Applied Physics, Radio Physics, Thermophysics, Nuclear Physics, Nanotechnology, and etc.

International Journal of Mathematics and Physics is published twice a year by al-Farabi Kazakh National University, 71 al-Farabi ave., 050040, Almaty, Kazakhstan
website: http://ijmph.kaznu.kz/

Any inquiry for subscriptions should be send to:
Prof. Tlekkabul Ramazanov, al-Farabi Kazakh National University
71 al-Farabi ave., 050040, Almaty, Kazakhstan
e-mail: Tlekkabul.Ramazanov@kaznu.kz

EDITORIAL

The most significant scientific achievements are attained through joint efforts of different sciences, mathematics and physics are among them. Therefore publication of the Journal, which shows results of current investigations in the field of mathematics and physics, will allow wider exhibition of scientific problems, tasks and discoveries.

One of the basic goals of the Journal is to promote extensive exchange of information between scientists from all over the world. We propose publishing service for original papers and materials of Mathematical and Physical Conferences (by selection) held in different countries and in the Republic of Kazakhstan.

Creation of the special International Journal of Mathematics and Physics is of great importance because a vast amount of scientists are willing to publish their articles and it will help to widen the geography of future dissemination. We will also be glad to publish papers of scientists from all the continents.

The Journal will publish experimental and theoretical investigations on Mathematics, Physical Technology and Physics. Among the subject emphasized are modern problems of Applied Mathematics, Algebra, Mathematical Analysis, Differential Equations, Mechanics, Informatics, Mathematical Modeling, Astronomy, Space Research, Theoretical Physics, Plasma Physics, Chemical Physics, Radio Physics, Thermophysics, Nuclear Physics, Nanotechnology, and etc.

The Journal is issued on the base of al-Farabi Kazakh National University. Leading scientists from different countries of the world agreed to join the Editorial Board of the Journal.

The Journal is published twice a year by al-Farabi Kazakh National University. We hope to receive papers from many laboratories which are interested in applications of the scientific principles of mathematics and physics and are carrying out researches on such subjects as production of new materials or technological problems.

IRSTI 27.35.63 https://doi.org/10.26577/ijmph.2020.v11.i1.01

[1]B.G. Mukanova, [1]D.S. Rakisheva

[1]L.N. Gumilyov Eurasian National University, Nur-Sultan, Kazakhstan,
e-mail: mbsha01@gmail.com, dilya784@mail.ru

THE METHOD OF INTEGRAL EQUATIONS AND FOURIER TRANSFORMS FOR THE PROBLEMS OF MODELING THE ELECTRICAL MONITORING OF DAMS AND BARRIERS

Abstract. Design of electrical monitoring of dams and barriersis an actual task in geophysics. A primary purpose is an exposure of change of structure, erosion, cracks and losses of weir on the early stages. Then it is important to remove and repair a weir and prevent destructions of dike overall. For mathematical modeling of electrical monitoring of dams and barriers, the authors consider the method of ERT. The paper shows a mathematical model of the electrical survey of dams and barriers based on the method of integral equations and the Fourier transform. Numerical calculations for this model are performed. The simulation results for studying the influence of the location of the water-dam boundary with respect to the sounding array are presented. For the purposes of mathematical modeling, two extreme cases were considered: a) a fluid is assumed to be infinitely conductive, b) a fluid is not conductive, i.e. distilled. The effect of a change in the position of the supply electrode at a fixed water level was also studied. The simulation results are presented in the form of apparent resistivity curves, as it is customary in geophysical practice. Distribution of density of secondary charges is also shown for the cases of infinitely conducting and distilledwater.

Key words: method of integral equations, Fourier transform, apparent resistivity, electrical monitoring of dams and barriers, electrical tomography, resistivity method.

Introduction

Mathematical modeling is currently an indispensable tool for geophysical research. In particular, modeling of electrical monitoring of dams and barriers is one of the important tasks in geophysics. Modeling the influence of changes in the dam structure, the detection of leakage zones, the appearance of erosion, changes in water levels at the upper and lower pools, dam breaks and much more associated direct and inverse problems interest many scientists [1] – [10]. In order to prevent the damage of the dam and the destruction its structure, it is necessary to identify problems of leakage and erosion in the early stages by timely monitoring. In this case, it is desirable that the measurements were carried out on the same profiles and the same grounded electrodes along seasonal and annual monitoring. One of the powerful methods for monitoring dams and barriers is the Electrical Resistivity Tomography (ERT) method. In many cases of dam monitoring, electrical tomography is performed along the dam crest and different longitudinal levels of the dam body [1] – [5]. This is due to the influence of the shape of the dam and its complex structure on the anomalies of apparent resistivities and the lack of reliable interpretation methods for profiles located across the body of the dam. However, with longitudinal soundings of the foot of the dam, where there may be leaks, and even flushing the dam, electrical tomography becomes problematic. A change in the water level at the upstream also affects the results of tomography. To solve such problems, modeling the electrical tomography of a dam across its body comes to the fore. In this paper, the authors simulate the electrical sounding of a dam across its body, using the quasi-three-dimensional model [11] based on the integral equation method [12] – [18] and the Fourier transform [11]. Studies were carried out for the following two cases: a) when the water is infinitely conductive and distilled for different water levels; b) the influence of the position of the supply electrode is studied at a constant water level. For both cases, curves of apparent resistivity are computed.

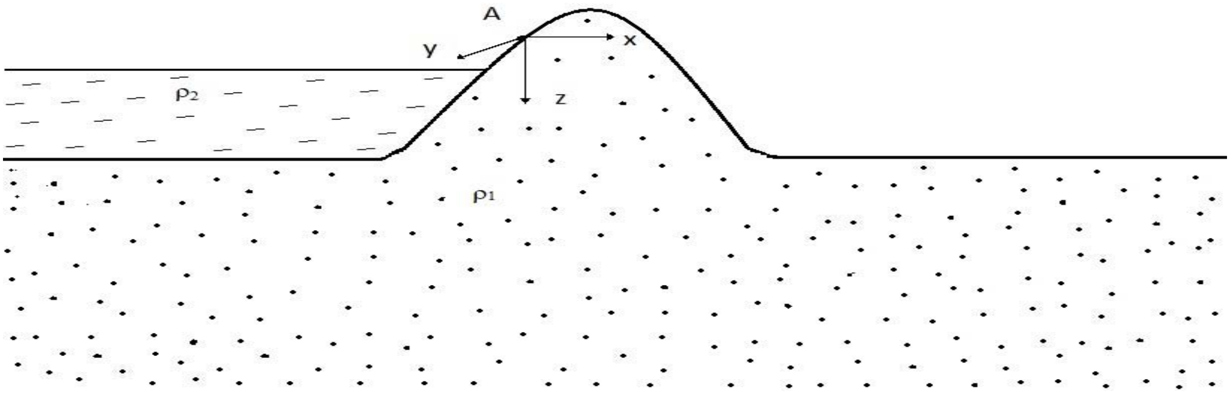

Figure 1 – The dam model

Mathematical model. Integral Equation and Fourier Transform

The dam has the shape of a single shaft, to the left of which is water (Figure 1). It has been shown in the monograph [11] that for the case of homogeneous media with non-flat surface, the most adequate and computationally low-cost method is the Integral Equation Method (IEM). It has been also shown in [11] that for the case of 2D media with step-wise constant resistivity distribution, the corresponding integral equation can be reduced to series of 1D integral equations in the spectral space. After solving the problem for spectral data, the spatial distribution of the electric field is calculated using the inverse Fourier transform. The described approach significantly reduces computational costs for the 3D electric field of a point source in two-dimensional media [11].The novelty of our approach consists of application of the IEM and subsequent Fourier transform method to the media with non-flat surface, causethis case is not considered before.

Let us apply the above-mentioned methods to the considered problem. The field is excited by the direct current flowing down from the electrode $A(x_A, 0{,}0)$. The dam is elongated along the y axis, the direction of the normal depends only on the x and z coordinates of the point $M(x, y, z)$. The point P with coordinates $P(x', y', z')$ belong to the surface of integration. As shown in the monograph [11], the problem of electrical monitoring is reduced to a system of integral equations for the density of secondary sources (simple layer) distributed along the boundaries of contacting media. Let $q_0(x,y,z)$ and $q_{12}(x,y,z)$ be the densities of a simple layer of secondary charges distributed along the dam-air surface and along the water-dam boundary. Under the assumption that the electrical conductivity of water is much greater than the conductivity of the dam body, and literally applyingthe method of the monograph [11], we write the following integral equations:

$$q_0(x,y,z) = -\frac{1}{2\pi}\iint_{\Gamma^0} q_0(x',y',z')\frac{\partial}{\partial n_M^0} G\left(\frac{1}{(xx',yy',zz')}\right) d\Gamma_p^0 + \frac{\partial}{\partial n^0} G\left(\frac{1}{2\pi(xx_A,yy_A,zz_A)}\right) \tag{1}$$

$$q_{12}(x,y,z) = -æ_{12}\frac{1}{2\pi}\iint_{\Gamma^{12}} q_{12}(x',y',z')\frac{\partial}{\partial n_M^{12}} G\frac{d\Gamma^{12}}{(xx',yy',zz')} -$$

$$æ_{12}\frac{1}{2\pi}\iint_{\Gamma^0} q_0(x',y',z')\frac{\partial}{\partial n_M^{12}} G\frac{\partial\Gamma^0}{(xx',yy',zz')} + æ_{12}\frac{\partial}{\partial n^{12}} G\left(\frac{1}{2\pi(xx_A,yy_A,zz_A)}\right) \tag{2}$$

Here $G(x,x',y,y',z,z')$ is is the Green's function of the problem, which depends on the following arguments $G(x,x',y-y',z,z')$. In formulas (1), (2), the functions are differentiated along the direction of the external normal to the boundary at the point $M(x,y,z)$.

Note that integration over the surfaces Γ^0и Γ^{12} can be represented as a sequential integration over a generator directed along the y axis, and then along the contours L_0 and L_{12} respectively. $L_0$is the contour of the surface Γ^0, and L_{12} s the contour of Γ^{12}. Since the dam is elongated along the y axis, formulas (1), (2) can be written in the following form:

$$q_0(x,y,z)=\frac{\partial}{\partial n^0}G\left(\frac{1}{2\pi(xx_A,y-y_A,zz_A)}\right)-\frac{1}{2\pi}\int_{L_0}\int_{-\infty}^{+\infty}q_0(x',y',z')\frac{\partial}{\partial n_M^0}G\left(\frac{1}{(xx'',y-y',zz')}\right)dy'dL_0 \quad (3)$$

$$q_{12}(x,y,z)=\frac{æ_{12}}{2\pi}\frac{\partial}{\partial n^{12}}G\left(\frac{1}{(xx_A,y-y_A,zz_A)}\right)-æ_{12}\frac{1}{2\pi}\iint_{L_T-\infty}^{+\infty}q_{12}(x',y',z')\frac{\partial}{\partial n_M^{12}}G\frac{dy'dL_T}{(xx',y-y',zz')}$$
$$+æ_{12}\frac{1}{2\pi}\iint_{L_1-\infty}^{+\infty}q_0(x',y',z')\frac{\partial}{\partial n_M^0}G\left(\frac{1}{(xx_A,y-y_A,zz_A)}\right)dy'dL_s \quad (4)$$

The internal integrals in equations (3), (4) are the convolution integrals of the function $q_0(x',y',z')$ and $\frac{\partial}{\partial n_M^0}G\left(\frac{1}{(xx',y-y',zz')}\right)$with respect to the coordinate y. The coefficient $æ_{12}$ depends on the resistivities of the dam and the water, and is equal to +1 or -1 for a conductive and non-conductive fluid, respectively.

Next, we move to the spectral space. Since the functions $q_0(x,y,z)$, $q_0(x',y',z')$, $\frac{\partial}{\partial n_M^0}G\left(\frac{1}{(xx',y-y',zz')}\right)$ and $\frac{\partial}{\partial n^0}G\left(\frac{1}{(xx_A,y-y_A,zz_A)}\right)$ are even functions with respect to the variable y, we use the partial cosine Fourier transform [11]:

$$\tilde{q}_0(x,k_y,z)=$$
$$=2\int_0^{\infty}q_0(x,y,z)\cos\cos(k_y\cdot y)dy$$

$$\tilde{q}_0(x',k_y,z')=$$
$$=2\int_0^{\infty}q_0(x',y',z')\cos\cos(k_y\cdot y)dy$$

$$\frac{\tilde{\partial}}{\partial n_M^0}G\left(\frac{1}{(xx',k_y,zz')}\right)=2\int_0^{\infty}\frac{\partial}{\partial n_M^0}G\left(\frac{1}{(xx',y-y',zz')}\right)\cos\cos(k_y\cdot y)dy$$

$$\frac{\tilde{\partial}}{\partial n^0}G\left(\frac{1}{(xx_A,k_y,zz_A)}\right)=2\int_0^{\infty}\frac{\partial}{\partial n^0}G\left(\frac{1}{(xx_A,y-y_A,zz_A)}\right)\cos\cos(k_y\cdot y)dy$$

By virtue of the two-dimensional geometry of the medium, the normal **n** does not depend on the coordinate *y*; therefore, the Fourier transform and differentiation commute.

Spectra $\tilde{q}_0(x,k_y,z)$, $\tilde{q}_0(x',k_y,z')$, $\frac{\widetilde{\partial}}{\partial n_M^0}G\left(\frac{1}{(xx',k_y,zz')}\right)$ and $\frac{\widetilde{\partial}}{\partial n^0}G\left(\frac{1}{(xx_A,y-y_A,zz_A)}\right)$ are the amplitudes of spatial harmonics with respect to frequency. Then the integral equation (3) after the cosine Fourier transform takes the form:

$$\tilde{q}_0(x,k_y,z)=\frac{1}{2\pi}\frac{\partial}{\partial n^0}G\left(\frac{1}{(xx_A,k_y,zz_A)}\right)-$$
$$\frac{1}{2\pi}\iint_{L_s}^{\infty}\left[\int_{-\infty}^{+\infty} q_0(x',y',z')\frac{\partial}{\partial n_M^0}G\left(\frac{1}{(xx',y-y',zz')}\right)dy'\right]\cdot cos\,cos(k_y\cdot y')dy'dL_0 \quad (5)$$

$\int_0^{+\infty}\int_{-\infty}^{+\infty} q_0(x',y',z')\frac{\partial}{\partial n_M^0}G\left(\frac{1}{(xx',y-y',zz')}\right) cos\,cos(k_y y)dy'dy$ – is the product of the spectra of the functions under convolution. Hence,

$$\tilde{q}_0(x,k_y,z)=\frac{1}{2\pi}\frac{\partial}{\partial n^0}G\left(\frac{1}{(xx_A,y-y_A,zz_A)}\right)-\frac{1}{2\pi}\int_{L_0}\tilde{q}_0(x',k_y,z')\frac{\widetilde{\partial}}{\partial n_M^0}G\left(\frac{1}{(xx',k_y,zz')}\right)dL_0 \quad (6)$$

We perform the same procedure for the integral equation (4):

$$\tilde{q}_{12}(x,k_y,z)=2\int_0^{\infty} q_0(x,y,z)\,cos\,cos(k_y\cdot y)dy$$

$$\tilde{q}_{12}(x,k_y,z)=2\int_0^{\infty} q_{12}(x',y',z')\,cos\,cos(k_y\cdot y)dy$$

$$\frac{\tilde{\partial}}{\partial n_M^{12}}G\left(\frac{1}{(xx',k_y,zz')}\right)=2\int_0^{\infty}\frac{\partial}{\partial n_M^{12}}G\left(\frac{1}{(xx',y-y',zz')}\right)cos\,cos(k_y\cdot y)dy$$

$$\frac{\tilde{\partial}}{\partial n^{12}}G\left(\frac{1}{(xx_A,k_y,zz_A)}\right)=2\int_0^{\infty}\frac{\partial}{\partial n^{12}}G\left(\frac{1}{(xx_A,y-y',zz_A)}\right)cos\,cos(k_y\cdot y)dy$$

So, the equation (4) takes the form:

$$\tilde{q}_{12}(x,k_y,z)=\frac{æ_{12}}{2\pi}\frac{\tilde{\partial}}{\partial n^{12}}G\left(\frac{1}{xx_A,k_y,zz_A}\right)-\frac{æ_{12}}{2\pi}\int_{L_{12}}\tilde{q}_{12}(x',k_y,z')\frac{\tilde{\partial}}{\partial n_M^{12}}G\left(\frac{1}{xx',k_y,zz'}\right)dL_{12}+$$
$$+\frac{æ_{12}}{2\pi}\int_{L_0}\tilde{q}_0(x',y',z')\frac{\tilde{\partial}}{\partial n_M^{12}}G\left(\frac{1}{xx',k_y,zz'}\right)dL_0 \quad (7)$$

Integral equations (6), (7) is the cosine Fourier transform of the system of integral equations (1), (2).

For a homogeneous half-space the expression in the integral equation (6) is written as:

$$\frac{\partial}{\partial n_M^0}G(x,x',y-y',z,z')=\frac{\rho}{\pi r^3}\mathbf{rn}$$

$$\frac{\partial}{\partial n_M^0}G(x,x_A,y-y_A,z,z_A)=\frac{\rho}{\pi r^3}\mathbf{rn}$$

where **n** is the unit vector of the external normal to the surface Γ^0 at the point (x, y, z). Given by $(\mathbf{1}y\cdot n)=0$, for the spectra $\frac{\tilde{\partial}}{\partial n_M^0}G(x,x',k_y,z,z')$and $\frac{\tilde{\partial}}{\partial n_M^0}G(x,x_A,k_y,z,z_A)$ we obtain the following expressions:

$$\frac{\tilde{\partial}}{\partial n_M^0} G\left(\frac{1}{xx', k_y, zz'}\right) = \frac{1}{2\pi}[(x-x')\cdot(n_x) + (z-z')(n_z)] \int_0^\infty \frac{cos\, cos(k_y \cdot y)}{(R^2+y^2)^{\frac{3}{2}}} dy \tag{8}$$

$$\frac{\tilde{\partial}}{\partial n^0} G\left(\frac{1}{xx_A, k_y, zz_A}\right) = \frac{1}{2\pi}[(x-x_A)(n_x) + (z)(n_z)] \int_0^\infty \frac{cos\, cos(k_y \cdot y)}{(R_A^2+y^2)^{3/2}} dy \tag{9}$$

Here $R^2 = (x-x')^2 + (z-z')^2$, $R_A^2 = (x-x_A)^2 + (z-z_A)^2$. The values of the R,R_A represent projections of the distances r, $r_A$onto the plane xOz respectively.

For the second integral equation, we have similarly:

$$\frac{\partial}{\partial n_M^{12}} G(x, x', y-y', z, z') = \frac{\rho}{\pi r^3}\mathbf{rn}$$

$$\frac{\partial}{\partial n_M^{12}} G(x, x_A, y-y_A, z, z_A) = \frac{\rho}{\pi r^3}\mathbf{rn}$$

where $\mathbf{n} = (n_x, n_y, n_z)$ – is the unit vector of the external normal to the surface Γ^{12} also at the point $M(x,y,z)$. Take into account that $(\mathbf{1y} \cdot \mathbf{n}) = 0$:

$$\frac{\tilde{\partial}}{\partial n_M^{12}} G\left(\frac{1}{(xx', k_y, zz')}\right) = \frac{æ_{12}}{2\pi}[(x-x')\cdot(n_x) + (z-z')\cdot(n_z)] \int_0^\infty \frac{cos\, cos(k_y \cdot y')}{\left(R^2+y'^2\right)^{\frac{3}{2}}} dy' \tag{10}$$

$$\frac{\tilde{\partial}}{\partial n^{12}} G\left(\frac{1}{(xx_A, k_y,\ zz_A)}\right) = \frac{æ_{12}}{2\pi}[(x-x_A)\cdot(n_x) + (z-z_A)(n_z)] \int_0^\infty \frac{cos\, cos(k_y \cdot y')}{\left(R^2+y'^2\right)^{\frac{3}{2}}} dy' \tag{11}$$

In formulas (8)-(10) there is a cosine transformation of the functions of the form $\frac{I}{(a^2+y^2)^{\frac{3}{2}}}$ where $a = const$. For this transformation we have:

$$S(k_y, a) =$$

$$\int_0^\infty \frac{cos\, cos(k_y \cdot y)}{(a^2+y^2)^{\frac{3}{2}}} dy = \frac{k_y}{2a} K_1(a \cdot k_y)$$

where $K_1(x)$ – is the MacDonald function (modified Bessel function of the second kind) of the first order. In numerical solutions of integral equations (6), (7), standard libraries of Fortran for the function $K_1(x)$ are used to compute $\frac{\partial}{\partial n_M^0} G\left(\frac{1}{|PM|}\right)$ and $\frac{\partial}{\partial n_M^0} G\left(\frac{1}{|AM|}\right)$. In order to reduce (6), (7) to the system of linear algebraic equation (SLAE), the contours L_0 and L_{12} are divided into elements Δl_0 и Δl_{12} within which $q_0(x,y,z)$, $q_{12}(x',y',z')$ are considered constant. Having found the spectral density of secondary sources q_0, we pass to spatial variables using the inverse Fourier cosine transform:

$$q_0(x,y,z) = \frac{1}{\pi}\int_0^\infty \tilde{q}_0(x,k_y,z)\cos(k_y \cdot y)dk_y \tag{12}$$

Next, based on the computed density of the secondary charges, we calculate the electric field potential by integration over the corresponding surface.

Numerical implementation.

The numerical solution of the integral equations was carried out by discretizing formulas (6), (7) and (12) on a logarithmic grid with respect to frequency. To calculate the cosine – Fourier transform, we consider the finite part of the boundaries Γ_0 and Γ_{12}. Uniform grids are built at the boundaries of dam-air and dam-water. The shape of the boundaries are approximated by the radial basis function (RBF) method [19] – [22]. At the dam-air interface, we take into account that no current flows into the air; and at the water-dam boundary, the current flows down depending on the resistivity of the media. The supply electrode is located on the dam. In the calculations, the height of the water and the position of the supply electrode are varied. The field potential is computed at points corresponding to the location of the measuring electrodes. Then, through the potential differences of the field, the apparent resistivity of the medium are calculated by standard formulas.

Numerical solutions are made for the following cases:

1. The position of the water-dam boundary was changed when the water was supposed to be infinitely conductive and distilled. However, even the second case is quite rare in practice, it is interesting from the point of view of mathematical modeling. This will determine the nature of the anomalies of apparent resistivity if the resistivity of the dam material is significantly less than the resistivity of the liquid. Based on the calculated electric field, apparent resistivity curves are constructed.

2. The position of the source electrode is changed when the water level stays the same, and curves of apparent resistivity are also plotted.

Figures 2 a) and b) show the density distribution of a simple layer q (M) at the air-dam boundary Γ^0 when the water is infinitely conductive, the value is $æ_{12}$= +1 and when the water is distilled, with the value is $æ_{12}$= -1, respectively.

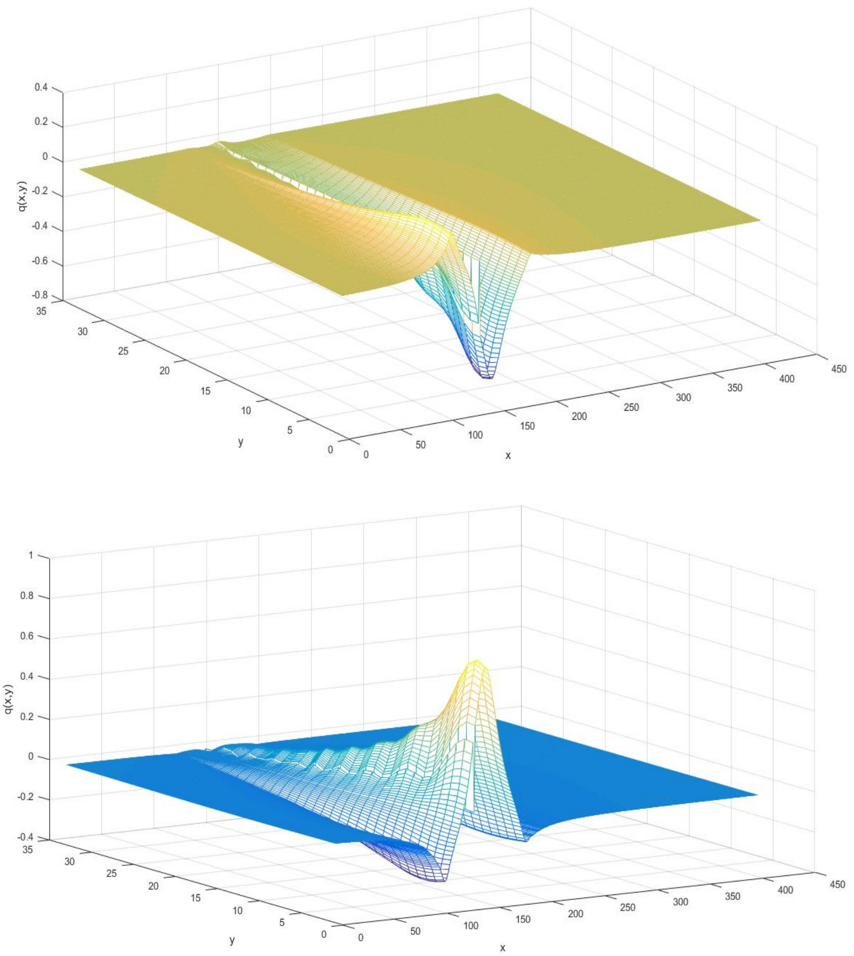

a)

b)

Figure 2 – The density distribution of a simple layer q (M) on the surface Γ^0, achieved using the Fourier transform method, when water is infinitely conductive(a), and for distilled water (b)

Figure 2 shows the distribution of the simple layer density q (M) on the surface Γ^0 obtained after the Fourier transform when the water is infinitely conductive (a), and when the water is distilled (b). In Figure 3 corresponding apparent resistivity curves are demonstrated also.

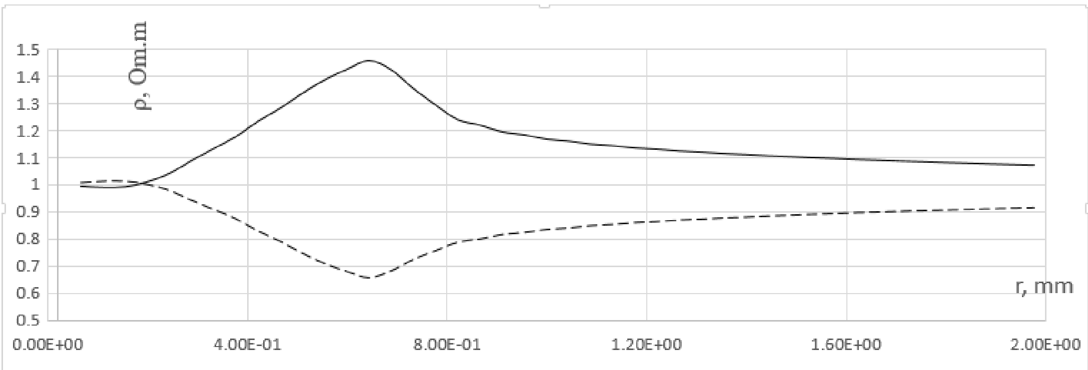

Figure 3 – Apparent resistivity curves
(-) – distilled water, (-) – infinitely conductive water

This test shows that for infinitely conductive water, the apparent resistivity curve is inverted with respect to the second case, as the current flows into the water.

The second test was conducted under conditions when the dam resistivity is ρ_1=10, and the water resistivity is ρ_2=100. The position of the supply electrode is changed: it was assumed that Apos = 16m, 18m, 20m from the origin, the water level does not change and is placed at the point at a distance of Cpos = 10m from the origin (Figure 4).

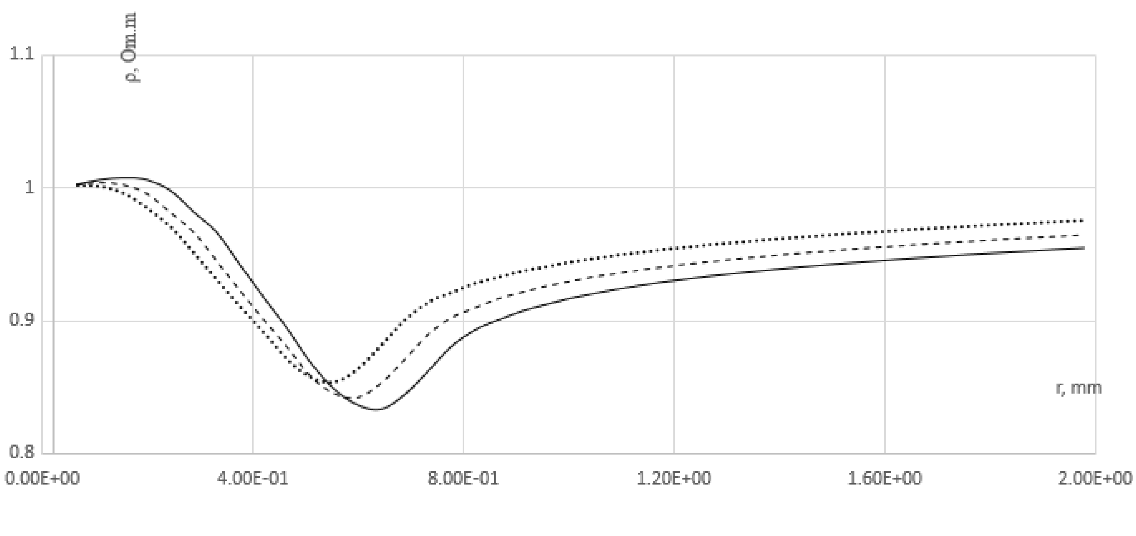

Figure 4 – Curves of apparent resistivity at the position of the source electrode
(-) Apos = 16m, (--) Apos = 18m, (…) Apos = 20m

Figure 4 illustrates the apparent resistivity curves at the positions of the source electrode Apos = 16m, Apos = 18m and Apos = 20m. It can be seen that the proximity of the liquid to the source electrode increases the amplitude of the anomaly in the apparent resistivity of the medium.

Conclusion

In a numerical solution, there is an investigation of the behavior of the apparent resistivity curves for infinitely conductive and distilled water. It is shown that in these cases the anomalies are of the opposite nature. These curves are in agreement with geophysical studies. It is also shown how the position of the source electrode affects the apparent resistivity curves at a constant water level.

Authors express their deep gratitude to the anonymous reviewer whose comments helped improve the presentation of the results.

References

1. Sjödahl P., Dahlin T., Johansson S., Loke M.H. «Resistivity monitoring for leakage and internal erosion detection at Hällby embankment dam», Journal of Applied Geophysics 65,2008, 155–164

2. Sjödahl P., Dahlin T., Johansson S. «Embankment dam seepage evaluation from resistivity monitoring data», Near Surface Geophysics, 2009, 463-474

3. Chih-Ping Lin, Yin-Chun Hung, Po-Lin Wu, Zen-Hung Yu «Performance of 2-D ERT in Investigation of Abnormal Seepage: A Case Study at the Hsin-Shan Earth Dam in Taiwan», Journal of Environmental and Engineering Geophysics 2017, p:101-112

4. In-Ky Cho, Ik-Soo Ha , Ki-Seog Kim , Hee-Yoon Ahn , Seunghee Lee, Hye-Jin Kang «3D effects on 2D resistivity monitoring in earth-fill dams», Near Surface Geophysics, 2014, 12, 73-81

5. Bolève A., Revil A., Janod F., Mattiuzzo J.L. and Fry J.-J. «Preferential fluid flow pathways in embankment dams imaged by self-potential tomography», Near Surface Geophysics, 2009, 447-462

6. Zerkal Evgeny «Interpretation of electrical resistivity tomography monitoring data of the Boguchan hydroelectric power plant rockfill dam», Proceedings of the 12th SEGJ International Symposium, 2015, 20-24

7. Shevnin V.A., Bobachev A.A., Ivanova S.V., «Rezultaty primeneniia metodov estestvennogo polia i elektrotomografii dlia izucheniia Aleksandrovskogo gorodishcha (Kaluzhskaia oblast)[The results of applying the methods of the natural field and electrotomography to study the Alexander settlement (Kaluga region)]», Notes of the Mining Institute. T.211 Petersburg 201, 35-42

8. Bolshakov D.K., Kozlov O.V., Modin I.N. «Vozmozhnosti elektrotomografii dlia monitoringa filtratsionnykh protsessov v tele kamenno-nabrosnoi plotiny vo vremia napolneniia vodokhranilishcha [Possibilities of electrotomography for monitoring filtration processes in the body of a rock-fill dam during reservoir filling]». VIII International Scientific and Practical Conference and Exhibition, " Engineering Geophysics - 2012", Moscow, Russia, 2012, 83-93

9. Pavlova A.M. «Primenenie maloglubinnoi elektrorazvedki dlia izucheniia trekhmerno neodnorodnykh sred [The use of shallow electrical exploration for the study of three-dimensionally inhomogeneous media]», The dissertation for the degree of candidate of technical sciences. Moscow – 2014

10. Kozlov O.V., Pavlova A.M. «Geoelektricheskii monitoring kamenno-nabrosnoi plotiny Boguchanskoi GES metodom elektrotomografii [Geoelectric monitoring of the rock-fill dam of the Boguchanskaya hydroelectric station]». Engineering survey, 12/2013, P. 40-47.

11. Mukanova B., Modin I., The Boundary Element Method in Geophysical Survey, Springer, t: 4, 2017

12. Balgaisha Mukanova, Tolkyn Mirgalikyzy and Dilyara Rakisheva, «Modelling the Influence of Ground Surface Relief on Electric Sounding Curves Using the Integral Equations Method», Mathematical Problems in Engineering.-Volume 2017, 210-215

13. Balgaisha Mukanova, A numerical solution to the well resistivity-sounding problem in the axi-symmetric case, Invers problems in science and engineering-Volume -21-5 Published -2012., 767-780

14. Mukanova B., Mirgalikyzy T. Modeling the impact of relief boundaries in solving the direct problem of direct current electrical sounding Communications in Computer and Information Science, Mathematical Modeling of Technological Processes: International Conference, CITech-2015. – Almaty: Proceedings, Springer, 2015. 117-123.

15. Mirgalikyzy T., Mukanova B., Modin I. Method of Integral Equations for the Problem of Electrical Tomography in a Medium with Ground Surface Relief, Journal of Applied Mathematics. – 2015

16. Mukanova B., Mirgalikyzy T. (2015) Modeling the Impact of Relief Boundaries in

Solving the Direct Problem of Direct Current Electrical Sounding. In: Danaev N., Shokin Y., Darkhan AZ. (eds) Mathematical Modeling of Technological Processes. Communications in Computer and Information Science, vol 549. Springer, Cham.

17. Mukanova B.G., Mirkaliqizi T, Rakisheva D.S., «Modelirovanie vliianiia relefa zemnoi poverkhnosti na krivye elektricheskogo zondirovaniia metodom integralnykh uravnenii [Modeling the effect of the earth's relief on electric sounding curves by the method of integral equations]», II International Scientific Conference «Informatics and Applied Mathematics» II. – Almaty, 2017. – P.352-366.

18. B. Mukanova, T. Mirgalikyzy, M. Turarova, Numerical aspects of the adaptive computational grid in solving the problems of electrical prospecting with direct current, International Journal of Mathematics and Physics 9, No2, 4 (2018), 4-12

19. Grady B. Wright Radial Basis Function Interpolation: Numerical and Analytical Developments, Doctoral Dissertation. - Colorado, 2003, 155

20. Nail A. Gumerov, Ramani Duraiswami Fast Radial Basis Function interpolation via preconditioned Krylov Iteration. - URL: http:// www.umiacs.umd.edu/ ~ramani/ pubs/ Gumerov Duraiswami IterativeRBF06.pdf

21. Xin Yin, Weiwei Xu, Ryo Akama and Hiromi T.Tanaka A Synthesis of 3-D Kabuki Face from Ancient 2-D Images Using Multilevel Radial Basis Function. - URL: http:// www.art-science.org/ journal/ v7n1/ v7n1pp14/ artsci-v7n1pp14.pdf

22. Rakisheva D.S., Mirgalikyzy T., Mukanova B.G., «Approksimatsiia poverkhnosti relefa dnevnoi poverkhnosti metodom RBF [Approximation of the surface relief of the surface by the RBF method]», Bulletin of the National Academy of Sciences of the Republic of Kazakhstan. V. 1, N. 365, Published 2017, 210-215

IRSTI 30.19.15; 30.19.21 https://doi.org/10.26577/ijmph.2020.v11.i1.02

D.A. Prikazchikov

School of Computing and Mathematics, Keele University, Staffordshire, UK
e-mail: d.prikazchikov@keele.ac.uk

EXPLICIT MODEL FOR SURFACE WAVES IN A PRE-STRESSED, COMPRESSIBLE ELASTIC HALF-SPACE

Abstract. The paper is concerned with the derivation of the hyperbolic-elliptic asymptotic model for surface wave in a pre-stressed, compressible, elastic half-space, within the framework of plane-strain assumption. The consideration extends the existing methodology of asymptotic theories for Rayleigh and Rayleigh-type waves induced by surface/edge loading, and oriented to extraction of the contribution of studied waves to the overall dynamic response. The methodology relies on the slow-time perturbation around the eigensolution, or, equivalently, accounting for the contribution of the poles of the studied wave. As a result, the vector problem of elasticity is reduced to a scalar one for the scaled Laplace equation in terms of the auxiliary function, with the boundary condition is formulated as a hyperbolic equation with the forcing terms. Moreover, hyperbolic equations for surface displacements are also presented. Scalar hyperbolic equations for surface displacements could potentially be beneficial for further development of methods of non-destructive evaluation.

Key words: surface wave; pre-stressed, compressible, elastic half-space; Rayleigh and Rayleigh-type waves.

Introduction and Literature Review

Mathematical modelling of dynamic problems of elasticity related to propagation of surface waves is an important problem having various applications in modern engineering and technology, including in particular areas of seismic protection, non-destructive testing, development of high-speed railway transport, etc., see e.g. [1-3] and references therein.

Studies of elastic surface waves originate from the classical work of Lord Rayleigh [4], followed by numerous contributions to the subject, see for example [5-8] to name a few. One of the important sub-areas is associated with propagation of surface waves in pre-stressed media [9,10], which becomes especially relevant for more accurate modelling of seismic vibrations in the near-surface domain. Some more recent advances in the area of Rayleigh wave include waves with transverse structure [11], representation through quasi-particles [12], as well as reciprocity approach [13].

A prospective methodology of hyperbolic-elliptic asymptotic models for surface waves (induced by prescribed surface loading) oriented to surface waves only has been developed in the last decade, see e.g. [14, 15] and references therein. This formulation relies on the representation of a surface wave field in terms of a single harmonic function [5, 16], with the decay over the interior governed by the Laplace equation. At the same time, the wave propagation is described by a hyperbolic equation on the surface, with the loading terms appearing in the right hand side. The results of the reduced model prove to be especially relevant in dynamic problems of elasticity, when the Rayleigh wave dominates, in particular, in the near-resonant regimes of moving loads, see e.g. [17]. The approach has also been extended to a special case of anisotropy associated with attenuation without oscillations in [18], as well as pre-stressed incompressible half-space [19]. A parallel parabolic-elliptic formulation for dispersive bending edge Rayleigh-type waves has been presented in [20]. Other recent developments include composite models for dispersion of waves in an elastic layer [21], application of the formulation to seismic meta-surfaces [22], as well as coated half-space with clamped surface and relatively soft coating layer [23].

In this paper, we extend the previous considerations to a pre-stressed compressible elastic half-space within the plane strain assumption, complementing the results in [19]. It is known that incorporation of compressibility may enrich the dynamics behaviour of pre-stressed material, see e.g. [24]. First, a slow-time perturbation procedure is constructed, revealing at leading order the eigensolution for surface waves, including the scaled Laplace equation for the auxiliary function following from the fourth order elliptic equation for one of the displacements. Then, at next order correction, a hyperbolic equation on the surface is established, implying hyperbolic equations for surface displacements. It is also noticed that in absence of the pre-stress, the results reduce to a known formulation for an isotropic elastic half-space. The results are also discussed within the framework of the known asymptotic models for Rayleigh and Rayleigh-type waves for other material properties.

Materials and Methods

Statement of the problem

Consider an elastic, isotropic, compressible body in three-dimensional Cartesian coordinate system in its natural unstressed state $\mathcal{B}_u$. The body is then subjected to a homogeneous static deformation $x_i\left(X_A\right)$, thus transforming to a finitely deformed equilibrium configuration $\mathcal{B}_e$. Then, small-amplitude motion $u_i\left(x_{j,}t\right)$ is super-imposed over $\mathcal{B}_e$, resulting in the current configuration $\mathcal{B}_t$. Thus, the current position vector is given by

$$\tilde{x}_i\left(X_A,t\right)=x_i\left(X_A\right)+u_i\left(x_{j,}t\right). \qquad (2.1)$$

Consider the elastic half-space $x_2 \geq 0$, with the coordinate axis directed along the principal directions of primary deformation. Throughout the paper we are focusing on two-dimensional super-imposed motions for which $u_3 = 0$, and u_j (j = 1, 2) are independent of x_3.

Following [10], the governing equations of motion may be written as

$$\begin{gathered} A_{1111}\frac{\partial^2 u_1}{\partial x_1^2}+A_{2121}\frac{\partial^2 u_1}{\partial x_2^2}+ \\ \left(A_{1122}+A_{1221}\right)\frac{\partial^2 u_2}{\partial x_1 \partial x_2}=\rho_e\frac{\partial^2 u_1}{\partial t^2}, \\ A_{1212}\frac{\partial^2 u_2}{\partial x_1^2}+A_{2222}\frac{\partial^2 u_2}{\partial x_2^2}+ \\ \left(A_{1122}+A_{1221}\right)\frac{\partial^2 u_1}{\partial x_1 \partial x_2}=\rho_e\frac{\partial^2 u_2}{\partial t^2}, \end{gathered} \qquad (2.2)$$

where

$$A_{ijkl}=J^{-1}\bar{F}_{iA}\bar{F}_{kC}\left.\frac{\partial^2 W}{\partial F_{jA}\partial F_{lC}}\right|_{F=\bar{F}}, \qquad (2.3)$$

are the components of the fourth-order elasticity tensor, with its non-zero elements defined by (see [25] for more detail)

$$\begin{aligned} A_{iijj}&=J^{-1}\lambda_i\lambda_j\frac{\partial^2 W}{\partial\lambda_i\partial\lambda_j}, \\ A_{ijij}&=\begin{cases}\left(\lambda_i\dfrac{\partial W}{\partial\lambda_i}-\lambda_j\dfrac{\partial W}{\partial\lambda_j}\right)\dfrac{\lambda_i^2}{J\left(\lambda_i^2-\lambda_j^2\right)}, & i\neq j,\quad \lambda_i\neq\lambda_j, \\ \dfrac{1}{2}\left(A_{iiii}-A_{iijj}+\dfrac{\lambda_i}{J}\dfrac{\partial W}{\partial\lambda_i}\right), & i\neq j,\quad \lambda_i\neq\lambda_j,\end{cases} \\ A_{ijji}&=A_{jiij}=A_{ijij}-\sigma_i. \end{aligned} \qquad (2.4)$$

In the above W is the strain-energy function,

$$W=W\left(I_1,I_2,J\right), \qquad (2.5)$$

depending on the invariants

$$I_1=\operatorname{tr}\mathrm{C},\quad I_2=\frac{1}{2}\left[\left(\operatorname{tr}\mathrm{C}\right)^2-\operatorname{tr}\left(\mathrm{C}^2\right)\right],\ \text{and}$$

$$J=\det F=\lambda_1\lambda_2\lambda_3=\frac{\rho_u}{\rho_e}, \qquad (2.6)$$

with F and $\bar{F}$ being the gradient deformation tensor associated with the mapping from $\mathcal{B}_u$ to $\mathcal{B}_t$, and $\mathcal{B}_u$ to $\mathcal{B}_e$, respectively, $C = FF^T$ denoting the right Cauchy-Green tensor, λ_1, λ_2 and λ_3 conventionally denoting the principal stretches, p_u and p_e stand for the material density in the configurations $\mathcal{B}_u$ and $\mathcal{B}_e$, respectively, whereas the principal Cauchy stresses σ_i are

$$\sigma_i = \frac{\lambda_i}{J}\frac{\partial W}{\partial \lambda_i}. \tag{2.7}$$

The linearised measure of the incremental traction is given by

$$\tau_j^{(n)} = A_{ijkl}\frac{\partial u_l}{\partial x_k} n_i, \tag{2.8}$$

for more detail see e.g. [24]. The boundary conditions at the surface $x_2 = 0$ are prescribed in the form of specified traction components, i.e.

$$A_{2121}\frac{\partial u_1}{\partial x_2} + \left(A_{2121} - \sigma_2\right)\frac{\partial u_2}{\partial x_1} = P_1, \quad A_{1122}\frac{\partial u_1}{\partial x_1} + A_{2222}\frac{\partial u_2}{\partial x_2} = P_2. \tag{2.9}$$

It should be noted that the material parameters are chosen within the range of stability of the material, i.e. strong ellipticity conditions are satisfied, see [10].

1.1. Explicit model for surface wave field

Following the procedure in [18], the following ansatz for displacement components may be adopted

$$u_i = u_i\left(\xi, x_2, \tau\right), \qquad i = 1, 2, \tag{2.10}$$

where $\xi = x_1 - ct$, and $\tau = \varepsilon t$ is slow time, with the physical meaning of the small parameter being the deviation of the phase speed from the surface wave speed. Then, the displacement components u_i are expanded as asymptotic series

$$u_i = \frac{1}{\varepsilon}\left(u_{i0} + \varepsilon u_{i1} + \ldots\right), \qquad i = 1, 2. \tag{2.11}$$

The leading order problem is then given by

$$\begin{gathered} A_{2121}\frac{\partial^2 u_{10}}{\partial x_2^2} + \left(A_{1111} - \hat{c}^2\right)\frac{\partial^2 u_{10}}{\partial \xi^2} + \left(A_{1122} + A_{1221}\right)\frac{\partial^2 u_{20}}{\partial x_2 \partial \xi} = 0, \\ A_{2222}\frac{\partial^2 u_{20}}{\partial x_2^2} + \left(A_{1212} - \hat{c}^2\right)\frac{\partial^2 u_{20}}{\partial \xi^2} + \left(A_{1122} + A_{1221}\right)\frac{\partial^2 u_{10}}{\partial x_2 \partial \xi} = 0, \end{gathered} \tag{2.12}$$

where $\hat{c}^2 = \rho_e c^2$, subject to the boundary conditions

$$\begin{gathered} A_{2121}\frac{\partial u_{10}}{\partial x_2} + \left(A_{2121} - \sigma_2\right)\frac{\partial u_{20}}{\partial \xi} = 0, \\ A_{1122}\frac{\partial u_{10}}{\partial \xi} + A_{2222}\frac{\partial u_{20}}{\partial x_2} = 0. \end{gathered} \tag{2.13}$$

Equations (2.12) may be transformed to a single fourth order PDE in respect of one displacement component, say, u_1, giving in operator form

$$\left[\partial_{22} + k_1^2 \partial_{\xi\xi}\right]\left[\partial_{22} + k_2^2 \partial_{\xi\xi}\right] u_{10} = 0, \tag{2.14}$$

where

$$k_1^2+k_2^2=\frac{\alpha_{22}\left(\alpha_{11}-\hat{c}^2\right)+\gamma_2\left(\gamma_1-\hat{c}^2\right)-\chi^2}{\alpha_{22}\gamma_2},$$

$$k_1^2k_2^2=\frac{\left(\alpha_{11}-\hat{c}^2\right)\left(\gamma_1-\hat{c}^2\right)}{\alpha_{22}\gamma_2},$$

$$\alpha_{ij}=A_{iijj},\quad \gamma_m=A_{mjmj},$$

$$\chi=\alpha_{12}+\gamma_2-\sigma_2,\quad i,j,m=1,2;\quad j\neq m.$$

The solution of (2.14) is given by

$$u_{10}\left(\xi,x_2,\tau\right)= =\varphi_{10}\left(\xi,k_1x_2,\tau\right)+\varphi_{20}\left(\xi,k_2x_2,\tau\right), \tag{2.15}$$

where φ_{10} and φ_{20} are arbitrary functions, harmonic in the first two arguments. Using (2.12) along with the Cauchy-Riemann identities, we deduce

$$u_{20}\left(\xi,x_2,\tau\right)=f\left(k_1\right)\varphi_{10}{}^*\left(\xi,k_1x_2,\tau\right)+ +f\left(k_2\right)\varphi_{20}{}^*\left(\xi,k_2x_2,\tau\right), \tag{2.16}$$

where the asterisk denotes the harmonic conjugate, and

$$f(k_i)=\frac{\gamma_2k_i{}^2-\left(\alpha_{11}-\hat{c}^2\right)}{k_i\chi},\quad i=1,2. \tag{2.17}$$

On substituting (2.15) and (2.16) into (1.62), the solvability of the system implies

$$\sqrt{\frac{\gamma_2\left(\alpha_{11}-\hat{c}^2\right)\left(\gamma_1-\hat{c}^2\right)}{\alpha_{22}}}\left[\alpha_{22}\left(\alpha_{11}-\hat{c}^2\right)-\alpha_{12}^2\right]+\left(\alpha_{11}-\hat{c}^2\right)\left[\gamma_2\left(\gamma_1-\hat{c}^2\right)-\left(\gamma_2-\sigma_2\right)^2\right]=0, \tag{2.18}$$

which coincides with the surface wave speed equation obtained in [10], hence the speed c in the definition of the moving co-ordinate ξ coincides with the surface wave speed c_R, being the unique root of (2.18). An addition, a relation between the functions φ_{10} and φ_{20} is established

$$\varphi_{20}\left(\xi,k_2x_2,\tau\right)=-\frac{g(k_1)}{g(k_2)}\varphi_{10}\left(\xi,k_2x_2,\tau\right), \tag{2.19}$$

with

$$g(k_i)=\gamma_2\alpha_{12}k_i+\frac{\left(\gamma_2-\sigma_2\right)\left(\alpha_{11}-\hat{c}^2\right)}{k_i},\quad i=1,2. \tag{2.20}$$

Thus, the leading order displacements u_{10} and u_{20} are expressed in terms of a single harmonic function as

$$u_{10}\left(\xi,x_2,\tau\right)=\varphi_{10}\left(\xi,k_1x_2,\tau\right)-\frac{g(k_1)}{g(k_2)}\varphi_{10}\left(\xi,k_2x_2,\tau\right), \tag{2.21}$$

$$u_{20}\left(\xi,x_2,\tau\right)=f\left(k_1\right)\varphi_{10}{}^*\left(\xi,k_1x_2,\tau\right)-\frac{f\left(k_2\right)g(k_1)}{g(k_2)}\varphi_{10}{}^*\left(\xi,k_2x_2,\tau\right). \tag{2.22}$$

Next order problem may now be formulated, involving the equations of motion

$$\begin{aligned}
&A_{2121}\frac{\partial^2u_{11}}{\partial x_2^2}+\left(A_{1111}-\hat{c}^2\right)\frac{\partial^2u_{11}}{\partial\xi^2}+\left(A_{1122}+A_{1221}\right)\frac{\partial^2u_{21}}{\partial x_2\partial\xi}=-2\rho_ec_R\frac{\partial^2u_{10}}{\partial\xi\partial\tau},\\
&A_{2222}\frac{\partial^2u_{21}}{\partial x_2^2}+\left(A_{1212}-\hat{c}^2\right)\frac{\partial^2u_{21}}{\partial\xi^2}+\left(A_{1122}+A_{1221}\right)\frac{\partial^2u_{11}}{\partial x_2\partial\xi}=-2\rho_ec_R\frac{\partial^2u_{20}}{\partial\xi\partial\tau},
\end{aligned} \tag{2.23}$$

subject to the boundary conditions

$$A_{2121}\frac{\partial u_{11}}{\partial x_2}+\left(A_{2121}-\sigma_2\right)\frac{\partial u_{21}}{\partial \xi}=P_1,$$
$$A_{1122}\frac{\partial u_{11}}{\partial \xi}+A_{2222}\frac{\partial u_{21}}{\partial x_2}=P_2. \tag{2.24}$$

The solutions of (2.23) may be found in a similar way to that employed in [18]. Furthermore, on substituting the latter into (2.24), from the solvability on the boundary $x_2=0$, a hyperbolic equation may be deduced for the auxiliary function $\varphi_1=\varepsilon^{-1}\varphi_{10}$, namely

$$\varphi_{1,11}-\frac{1}{c_R^2}\varphi_{1,tt}=A_{R1}P_{1,1}^{*}+A_{R2}P_{2,1} \text{ (at } x_2=0\text{)}. \tag{2.25}$$

Here the asterisk may be interpreted in the sense of the Hilbert transform, and the material constants A_{R1} and A_{R2} are given by

$$A_{Ri}=\frac{S_i}{\rho_e c_R^2 \vartheta\, R_1},\ i=1,2, \tag{2.26}$$

with

$$R_1=\eta\sqrt{\alpha_{22}\gamma_2}+\left(\alpha_{11}+\gamma_1-2\rho_e c_R^2\right)\left[\gamma_2+\frac{1}{2\eta}\sqrt{\frac{\gamma_2}{\alpha_{22}}}\left(\alpha_{22}(\alpha_{11}-\rho_e c_R^2)-\alpha_{12}^2\right)\right]-\left(\gamma_2-\sigma_2\right)^2,$$
$$S_1=\eta\sqrt{\alpha_{11}\alpha_{22}+\gamma_1\gamma_2-\beta^2+\left(\alpha_{22}+\gamma_2\right)\rho_e c_R^2+2\eta\sqrt{\alpha_{22}\gamma_2}},\qquad \vartheta=1-\frac{g(k_1)}{g(k_2)},$$
$$S_2=\left(\gamma_2-\sigma_2\right)\left(\alpha_{11}-\rho_e c_R^2\right)-\eta\alpha_{12}\sqrt{\frac{\gamma_2}{\alpha_{22}}},\qquad \eta=\sqrt{\left(\gamma_1-\rho_e c_R^2\right)\left(\alpha_{11}-\rho_e c_R^2\right)}.$$

Note, the hyperbolic equation (2.24) serves as a boundary condition to the elliptic equation

$$\varphi_{1,22}+k_1^2\varphi_{1,11}=0, \tag{2.27}$$

following from (2.14) and (2.15).

Results and Discussion

Thus, the hyperbolic-elliptic model for surface wave in a pre-stressed compressible elastic half-space under the plane-strain assumption has been derived, comprised of the hyperbolic equation (2.25) and elliptic equation (2.27). It should be noted that once the auxiliary function φ_1 is determined, the displacements follow from the expressions of (2.21) and (2.22). Moreover, displacements satisfy the following hyperbolic equations on the surface

$$x_2=0\quad u_{1,11}-\frac{1}{c_R^2}u_{1,tt}=\vartheta\left(A_{R1}P_{1,1}^{*}+A_{R2}P_{2,1}\right) \tag{3.1}$$

and

$$u_{2,11}-\frac{1}{c_R^2}u_{2,tt}=\left(f(k_1)-\frac{f(k_2)g(k_1)}{g(k_2)}\right)\left(-A_{R1}P_{1,1}+A_{R2}P_{2,1}^{*}\right). \tag{3.2}$$

It may be shown that in case of no pre-stress the obtained results simplify to the known results for classical Rayleigh waves in linearly elastic, isotropic media (cf., for example, equation (3.1) in absence of tangential load (P_1 = 0) with equation (98) in [15]).

Another observation which may be made is related to similarity of the derivation procedure between the orthorhombic case in [18] and the current problem, which is highlighting once again the formal parallels between anisotropy and pre-stress, having although an important difference related to symmetry/non-symmetry of the stress tensor.

Another remark can be made regarding the similarity of the slow-time perturbation procedures in the current problem with that for the dispersive bending edge wave on a semi-infinite Kirchhoff plate, presented in [20]. Indeed, both of the cases are dealing with the scaled bi-harmonic equation, in respect of the displacements. The auxiliary function φ_1 may be interpreted within the sense of a partial potential decomposition, since its analogue in the isotropic case would be a derivative of the longitudinal Lamé potential.

Conclusion

A hyperbolic-elliptic model for Rayleigh-type wave induced by prescribed load on the surface of a pre-stressed, compressible, elastic half-space has been formulated in terms of a single plane harmonic function. The decay over the interior is governed by a scaled Laplace equation, whereas wave propagation is modelled by a hyperbolic equation. The results complement existing ones for isotropic media [15], as well as particular type of orthorhombic media [18] and pre-stressed incompressible media [19]. Scalar hyperbolic equations for surface displacements could potentially be beneficial for further development of methods of non-destructive evaluation.

The advantage of the obtained formulation is clearly associated with a reduction of the vector problem of elasticity to a scalar problem for a Laplace equation, thus opening the path to a number of analytical solutions for prescribed forms of surface loading. At the same time, it is emphasised that the model is only accounting for surface wave contribution and would therefore be efficient in situations when the surface wave field is dominant, and the contribution of the bulk waves is negligible. Examples of such behaviour include the far-field analysis or near-resonant regimes of the moving load. Moreover, the proposed approach may be further developed for seismic meta-surfaces, see e.g. [22], [26], as well as for layered half-space [15], [23]. Finally, we mention a less obvious generalisation to inhomogeneous media, see e.g. [27].

References

1. Palermo, A., Krödel, S., Marzani, A., Daraio, C. “Engineered metabarrier as shield from seismic surface waves.” *Sci. Rep.* 6 (2016): 39356.
2. Cho, Y. S. “Non-destructive testing of high strength concrete using spectral analysis of surface waves.” *NDT & E Int.* 36 (2003): 229–235.
3. Krylov, V.V. *Noise and Vibration from High-Speed Trains*. London: Thomas Telford, 2001.
4. Lord Rayleigh. “On waves propagated along the plane surface of an elastic solid.” *Proc. R. Soc. Lond.* 17 (1885): 4–11.
5. Chadwick, P. “Surface and interfacial waves of arbitrary form in isotropic elastic media.” *J. Elast.* 6 (1976): 73–80.
6. Barnett, D.M., Lothe, J. “Consideration of the existence of surface wave (Rayleigh wave) solutions in anisotropic elastic crystals.” *J. Phys. F:* 4 (1974): 671-686.
7. Fu, Y.B., Mielke, A. “A new identity for the surface-impedance matrix and its application to the determination of surface-wave speeds.” *Proc. R. Soc. A* 458 (2002): 2523-2543.
8. Destrade, M. “Seismic Rayleigh waves on an exponentially graded, orthotropic half-space.” *Proc. R. Soc. A* 463 (2007): 495-502.
9. Hayes, M.A., Rivlin, R.S. “Surface waves in deformed elastic materials.” *Arch. Ration. Mech. Anal.* 8 (1961): 358–380.
10. Dowaikh, M. A., Ogden, R. W. “On surface waves and deformations in a compressible elastic half space.” *SAACM*, 1 (1991): 27–45.
11. Kiselev, A. P. “Rayleigh wave with a transverse structure.” *Proc. Roy. Soc. A* 460 (2004): 3059–3064.
12. Rousseau, M., Maugin, G.A. “Rayleigh surface waves and their canonically associated quasi-particles.” *Proc. Roy. Soc. A* 467 (2010): 495–507.
13. Phan H., Cho Y., Achenbach J.D. “Application of the reciprocity theorem to scattering of surface waves by a cavity.” *Int. J. Solids Struct*. 50 (2013): 4080–4088.
14. Kaplunov, J., Prikazchikov, D.A. “Explicit models for surface, interfacial and edge waves in elastic solids.” In *Dynamic Localization Phenomena in Elasticity, Acoustics and Electromagnetism*, edited by -Craster, R., Kaplunov, J. P. 73-114. CISM Lecture Notes, Vol 547. Berlin: Springer, 2013.
15. Kaplunov, J., Prikazchikov, D.A. “Asymptotic theory for Rayleigh and Rayleigh-type waves.” *Adv. Appl. Mech.* 50 (2017): 1–106.
16. Kiselev, A.P., Parker, D.F. “Omni-directional Rayleigh, Stoneley and Schölte waves with general time dependence.” *Proc. R. Soc. A* 466 (2010): 2241–2258.
17. Erbaş, B., Kaplunov J., Prikazchikov, D.A., Şahin, O. “The near-resonant regimes of a moving

load in a three-dimensional problem for a coated elastic half-space." *Math. Mech. Solids* 22 (2017): 89–100.

18. Nobili, A., Prikazchikov, D.A. "Explicit formulation for the Rayleigh wave field induced by surface stresses in an orthorhombic half-plane." *Europ. J. Mech. A. Solids* 70 (2018): 86–94.

19. Khajiyeva L.A., Prikazchikov, D.A., Prikazchikova L.A. "Hyperbolic-elliptic model for surface wave in a pre-stressed incompressible elastic half-space." *Mech. Res. Comm.* 92 (2018): 49–53.

20. Kaplunov, J., Prikazchikov, D.A., Rogerson, G.A. "Edge bending wave on a thin elastic plate resting on a Winkler foundation." *Proc. Roy. Soc. A* 472 (2016): 20160178

21. Erbaş, B., Kaplunov, J., Nolde, E., Palsü, M. "Composite wave models for elastic plates." *Proc. Roy. Soc. A* 474 (2018): 20180103.

22. Wootton, P.T., Kaplunov, J., Colquitt, D.J. "An asymptotic hyperbolic-elliptic model for flexural-seismic metasurfaces." *Proc. Roy. Soc. A* 475 (2019): 20190079.

23. Kaplunov, J., Prikazchikov, D., Sultanova, L. "Rayleigh-type waves on a coated elastic half-space with a clamped surface." *Phil. Trans. Roy. Soc. A*. 377 (2019): 20190111.

24. Nolde, E., Prikazchikova, L., Rogerson, G.A. "Dispersion of small amplitude waves in a pre-stressed compressible elastic plate." *J. Elast.* 75 (2004): 1–29.

25. Ogden R.W. *Non-Linear Elastic Deformations*. Dover: Ellis Horwood, 1984.

26. Colombi, A., Colquitt, D.J., Roux, P., Guenneau, S., Craster, R.V. "A seismic metamaterial: The resonant metawedge." *Sci. Rep.*, 6 (2016): 27717.

27. Argatov, I., Iantchenko, A. Rayleigh surface waves in functionally graded materials – long-wave limit. *Quart. J. Mech. Appl. Math.* 72 (2019): 197-211.

IRSTI 27.35.17 https://doi.org/10.26577/ijmph.2020.v11.i1.03

[1]A. Zadauly, [2]A.O. Beketaeva

[1]Institute of Mechanics and Engineering Science, Kazakhstan, Almaty
[21]Institute of Mathematics and Mathematical Modeling, Kazakhstan, Almaty,
e-mail: akerkeh_333@mail.ru

NUMERICAL SIMULATION OF A SUPERSONIC TURBULENT COMPRESSIBLE JET IN A CO-FLOW WITH STOCHASTIC SPECTRAL INFLOW BOUNDARY CONDITIONS

Abstract. A compressible supersonic turbulent jet of a perfect gas in a co-flow with the formulation of stochastic spectral inflow boundary conditions is numerically modeled. The base equations are the LES averaged Navier – Stokes equations closed by the Smagorinsky model, the solution of which is carried out by the ENO scheme of the third order of accuracy. The stochastic boundary conditions at the inlet are constructed on the basis of the spectral method of generating fluctuations of gas-dynamic variables to obtain an inhomogeneous anisotropic turbulent flow. The numerical results of turbulent characteristics are compared with experimental data for the shear layer problem. The thickness of the shear layer is obtained, in which the growth of the shear layer between the jet and the co-flow for three types of grid (coarse, medium and fine) is demonstrated. Coherent vortex structures appearing in the jet are constructed in dynamics, which made it possible to analyze in detail the growth and development of vortices over time.
Key words: supersonic jet, supersonic co-flow, LES, spectral boundary conditions, shear layer.

Introduction

Turbulent jet flows are of particular interest when considering many aerodynamic problems, such as turbulent mixing of a jet of fuel with co-flowing air in rocket combustion chambers, predicting the noise level of propulsion systems, the interaction of jets when launching space rocket technology with launch equipment. Turbulent jets were experimentally studied in the works of many authors [1-7,25]. The issue of numerical simulation of such flows is especially relevant today, and the application of the LES method (large eddy simulation) is justified, since it gives a more accurate description of turbulence, while, in contrast to the direct numerical simulation (DNS), without requiring large computational resources. The main problem of the LES method is the correct formulation of the inflow boundary conditions. Stochastic spectral boundary conditions are promising for this method, since they give the result closest to reality and do not require a large amount of information about the statistics of turbulent characteristics. The spectral boundary conditions use a set of random numbers that satisfies the given statistical turbulence data [8–13], and the key point in their formulation is the introduction of an anisotropic perturbation field. The ways of introducing anisotropy and inhomogeneity in the velocity field lead to a similarity between turbulence obtained numerically and natural real turbulence. In [14], using the spectral boundary conditions, an inhomogeneous anisotropic field of turbulence velocities with zero divergence was synthesized for a plane turbulent flow in a channel and for a circulation flow, and as a result, turbulent structures in the flow close to the real ones were obtained. In many works, spectral boundary conditions were used to solve actual physical problems, as, for example, in [15] the effect of wind on a tall steel building was studied. The authors found that the velocity profiles of the incoming wind flow mainly affect the average pressure coefficients of the building and the profiles of random turbulent intensities significantly affect the fluctuation forces of the wind. In [16], a comparison was made between the LES models with different boundary conditions, including spectral ones, as well as a comparison with experiment in order to determine the accuracy of the LES method when simulating flows in combustion chambers, using the example of particle distribution in circulating two-phase flows.

As a result, the authors simulated the characteristic fluctuation velocity fields, which gave a satisfactory agreement with the experiment. The authors of [17] studied the spread of atmospheric pollution on the streets of the city by modeling atmospheric flows with a boundary layer with obstacles. The study was conducted numerically using the RANS model and the LES model with spectral boundary conditions. Both methods were compared with each other and with experimental data. As a result, the LES method was able to detect both external and internal induced periodicities and, accordingly, pulsating and unstable fluctuations in the flow field, which made it possible to obtain the correct calculation of the transient process of mixing air with a pollutant using the example of city streets. This in turn led to a more accurate prediction of horizontal concentration diffusion, since it was the LES method with spectral boundary conditions that made it possible to reproduce unsteady concentration fluctuations. In [18], using the LES, turbulent combustion of methane and oxygen with preliminary mixing was simulated using spectral boundary conditions, a comparison was made with experiment, and a satisfactory agreement between the numerical and experimental calculations was obtained. The authors of [19] investigated the effect of oncoming turbulent structures in the air flow on the low-speed wing. Good results were obtained from the wing response to the effects of turbulent structures in both two-dimensional and three-dimensional modeling. In [20], a turbulent flow passing through a rotating wind turbine was simulated using the LES with spectral boundary conditions in order to study the formation and propagation of a wake behind a wind turbine. As a result, the structures obtained behind the wind turbine turned out to be a system of intense and stable rotating spiral vortices, which determined the dynamics of the wake. As a recommendation, the authors proposed the following: the boundary between the near and far wake should be defined as the initial location for the decay of the wake. Also, a comparison with experiment was made in the work, which gave good agreement on the time-averaged pressure coefficients.

The aim of this work is numerical simulation of a supersonic turbulent jet of a perfect gas in a co-flowing air stream using the LES method with stochastic spectral boundary conditions at the input. The schematic flow diagram is presented in Figure 1:

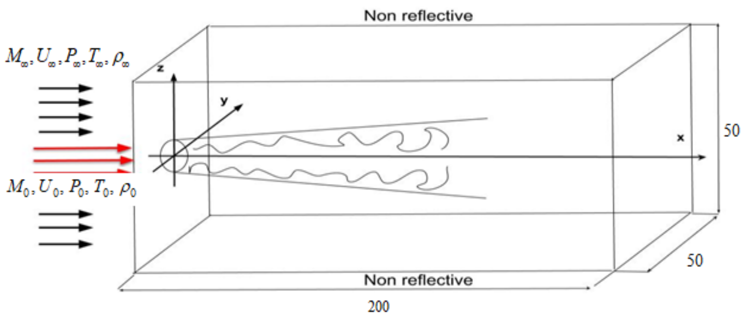

Figure 1 – Schematic flow diagram

Basic equations

The basic equations are a system of three-dimensional LES-filtered Navier-Stokes equations for a compressible turbulent perfect gas in a Cartesian coordinate system, written in a conservative form:

$$\frac{\partial \vec{U}}{\partial t} + \frac{\partial (\vec{E} - \vec{E}_v)}{\partial x} + \frac{\partial (\vec{F} - \vec{F}_v)}{\partial y} + \frac{\partial (\vec{G} - \vec{G}_v)}{\partial z} = 0 \qquad (1)$$

where vectors of dependent parameters and vectors of flow are defined as:

$$\vec{U} = (\rho, \rho u, \rho v, \rho w, E_t)^T$$
$$\vec{E} = (\rho u, \rho u^2 + P, \rho uv, \rho uw, (E_t + P)u)^T$$
$$\vec{F} = (\rho v, \rho uv, \rho v^2 + P, \rho vw, (E_t + P)v)^T$$
$$\vec{G} = (\rho w, \rho uw, \rho vw, \rho w^2 + P, (E_t + P)w)^T$$
$$\vec{E}_v = (0, \tau_{xx}, \tau_{xy}, \tau_{xz}, u\tau_{xx} + v\tau_{xy} + w\tau_{xz} - q_x)^T$$
$$\vec{F}_v = (0, \tau_{xy}, \tau_{yy}, \tau_{yz}, u\tau_{xy} + v\tau_{yy} + w\tau_{yz} - q_y)^T$$
$$\vec{G}_v = (0, \tau_{xz}, \tau_{yz}, \tau_{zz}, u\tau_{xz} + v\tau_{yz} + w\tau_{zz} - q_z)^T$$

The components of the viscous stress tensor are defined as follows:

$$\tau_{xx} = \frac{2\mu_{eff}}{3\mathrm{Re}}\left(2\mathrm{u}_x - v_y - w_z\right)$$
$$\tau_{yy} = \frac{2\mu_{eff}}{3\mathrm{Re}}\left(2\mathrm{v}_y - u_x - w_z\right)$$
$$\tau_{zz} = \frac{2\mu_{eff}}{3\mathrm{Re}}\left(2\mathrm{w}_z - u_x - v_y\right)$$
$$\tau_{xy} = \tau_{yx} = \frac{\mu_{eff}}{\mathrm{Re}}\left(u_y + v_x\right)$$
$$\tau_{xz} = \tau_{zx} = \frac{\mu_{eff}}{\mathrm{Re}}\left(u_z + w_x\right)$$
$$\tau_{yz} = \tau_{zy} = \frac{\mu_{eff}}{\mathrm{Re}}\left(v_z + w_y\right)$$

Heat flows are represented as:

$$q_x = -\frac{\mu_{eff}}{(\gamma-1)M_\infty^2 \mathrm{PrRe}} T_x$$
$$q_y = -\frac{\mu_{eff}}{(\gamma-1)M_\infty^2 \mathrm{PrRe}} T_y$$
$$q_z = -\frac{\mu_{eff}}{(\gamma-1)M_\infty^2 \mathrm{PrRe}} T_z$$

Effective viscosity is the sum of the dynamic and vortex viscosities: $\mu_{eff} = \mu_l + \mu_{sgs}$, where μ_l is obtained from the Sutherland's formulae, and μ_{sgs} is as follows:

$$\mu_{sgs} = \rho(C\Delta)^2 \sqrt{\widetilde{S}_{ij}\widetilde{S}_{ij}}, \tag{2}$$
$$\widetilde{S}_{ij} = \frac{1}{2}\left(\frac{\partial \widetilde{u}_i}{\partial x_j} + \frac{\partial \widetilde{u}_j}{\partial x_i}\right), i = 1,2,3,\ j = 1,2,3$$

where C is semi-empirical coefficient of the model, $\Delta = \Delta x \cdot \Delta y \cdot \Delta z$ is the width of the filter.

Pressure and temperature are set as follows:

$$P = (\gamma-1)\left[E_t - \frac{1}{2}\left(\rho u^2 + \rho w^2 + \rho v^2\right)\right]$$
$$T = \left(\frac{1}{\rho c_v}\right)\left[E_t - \frac{1}{2}\left(\rho u^2 + \rho w^2 + \rho v^2\right)\right] \tag{3}$$

$$c_v = \frac{1}{\gamma(\gamma-1)M_\infty^2}$$

In (1) u, w, v are the components of the velocity vector, ρ is the density, c_v is the specific heat at constant volume, γ is the specific heat ratio, M_∞ is the flow Mach number.

The system (1) is written in dimensionless form, where the flow parameters $u_\infty, \rho_\infty, T_\infty$ taken as a reference values; for the pressure P and the total energy E_t the reference values are $\rho_\infty u_\infty^2$, the length scale is the initial vorticity thickness of a mixing layer:

$$\delta_\theta(x) = \int_{-H/2}^{+H/2} (\overline{\rho}(\widetilde{u} - u_\infty)\cdot(u_0 - \widetilde{u})/(\rho_\infty \Delta u^2))dz$$

where $\widetilde{u} = (u - u_\infty)/\Delta u \quad \Delta u = u_0 - u_\infty$

Pr, Re are the Prandtl and the Reynolds numbers. Index 0 corresponds to the parameters of the jet and index ∞ corresponds to the parameters of the flow.

Boundary and Initial conditions

At the input, the initial conditions for the velocity profile are set in the form:

$$\vec{V}(x_i, t) = \vec{V}(x_i)^{base} + \vec{V}(x_i, t)^{natural} \tag{4}$$

where $\vec{V} = (u, v, w),\ (x_i) = (x, y, z)$

$\vec{V}(x_i)^{base}$ is the velocity field given as follows:

$$\vec{V}(x_i)^{base} = \begin{cases} u_\infty = 1, v_\infty = 0, w_\infty = 0, \\ for \quad x = 0, 0 \le y \le H_y, 0 \le z \le H_z \\ u_0 = \sqrt{T_0}\dfrac{M_0}{M_\infty}, v_0 = 0, w_0 = 0, \\ for \quad x = 0, \quad \left|z^2 + y^2\right| \le R \end{cases}$$

At the transition of two gas flows, the above physical variables are determined by the function of the hyperbolic tangent:

$$\phi(z) = 0.5(\phi_0 + \phi_\infty) + 0.5(\phi_0 - \phi_\infty)\tanh(0.5z/\delta_\theta) \quad (5)$$

where $\phi = (u, v, w)$.

Here H_x, H_y and H_z are length, width, and height of the computational domain, respectively, and R is the radius of the jet orifice.

The "natural" fluctuation velocity field at the entrance $\vec{V}(x_i, t)^{natural}$ from (4) is given by analogy as in [13] and the spectral boundary conditions at the entrance for this case are as follows:

$$\vec{V}'(x_i, t) = 0.5 \cdot \sum_{n=1}^{N} \sqrt{q^n}\left[\cos(k^n \cdot d \cdot x_i + \varphi_n)\right]$$

where d is the random frequency and φ_n is the random phase shift, both determined in the interval [0;1], here N is taken as $N = 100$ and q^n is the normalized amplitude:

$$q^n = \frac{E(k^n)\Delta k^n}{\sum_{n=1}^{N} E(k^n)\Delta k^n}, \qquad \sum_{n=1}^{N} q^n = 1$$

where *E(k)* is the modified von Karman energy spectrum:

$$E(k) = \frac{(k/k_e)^4}{[1 + 2.4(k/k_e)^2]^{17/6}} \quad (7)$$

where

$$k^n = k^{\min} \cdot (1+\alpha)^{n-1}, \quad n = 1 \div N, \quad \alpha = 0.01$$

$$k^{\min} = \beta \cdot k_e^{\min}, \beta \le 1, k_e^{\min} = 2\pi / l_e^{\max},$$

$$l_e^{\max} = \max(h_x, h_z, h_y)$$

In the output and the lateral boundaries the non reflective boundary conditions are specified [21].

Method of solution

Preliminary, at the level of the jet injection, a thickening of the grid is introduced for a more accurate numerical solution. Then the system (1) in the transformed coordinate system is written in the form:

$$\frac{\partial \tilde{U}}{\partial t} + \frac{\partial \tilde{E}}{\partial \xi} + \frac{\partial \tilde{F}}{\partial \zeta} + \frac{\partial \tilde{G}}{\partial \eta} = \frac{\partial \tilde{E}_v}{\partial \xi} + \frac{\partial \tilde{F}_v}{\partial \zeta} + \frac{\partial \tilde{G}_v}{\partial \eta} \quad (9)$$

where $\tilde{U} = \vec{U}/J$, $\tilde{E} = \xi_x \vec{E}/J$, $\tilde{F} = \zeta_y \vec{F}/J$, $\tilde{G} = \eta_z \vec{G}/J$, $\tilde{E}_v = \xi_x \vec{E}_v/J$, $\tilde{F}_v = \zeta_y \vec{F}_v/J$, $\tilde{G} = \eta_z \vec{G}_v/J$ и $J = \partial(\xi, \zeta, \eta)/\partial(x, y, z)$ is the Jacobian transform.

The solution of the system (9) is performed with semi-implicit method proposed in [22, 23].

Firstly, the linearization procedure is applied to the equations (9). Then, the factored scheme of the linearized system is written. This form reduced the three-dimensional matrix inversion problem to the three one-dimensional problems in directions ξ, ζ, η. Secondly, the obtained one-dimensional problems are solved implicitly with matrix sweep method for the vector $\tilde{U}$. Here, the advective terms are approximated using the third-order ENO scheme in detail represented by authors in [22, 23]. The central differences of the second order accuracy are used for approximation of diffusion terms.

Results

The verification of the numerical model is conducted by the comparison of the computational results with the experimental data of [24] for the shear layer problem. Schematic diagram of the flow is presented in Figure 2:

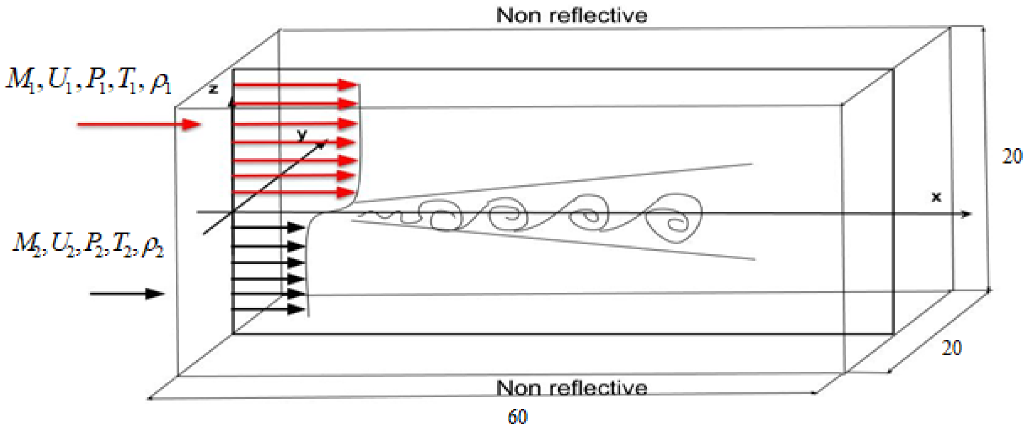

Figure 2 – Schematic diagram of the shear layer problem

Two parallel flows with different Mach numbers are defined by the following parameters:

M_1	M_2	M_c	U_1 / U_2	ρ_1 / ρ_2	T	p
1.80	0.51	0.51	0.36	0.64	291K	1 *atm.*

where $M_c = (U_1 - U_c) / a_1, (a_1 U_2 + a_2 U_1) / (a_1 + a_2)$ is the convective Mach number and U_1, U_2 are velocities of the upper (indexed by 1) and lower flows (indexed by 2), and a_1, a_2 are the local sound velocities of flows. The pressure at the input remains constant. The simulation is made for three types of grids: coarse (75x25x25 nodes), middle (135x51x51 nodes), fine (271x101x101 nodes). This is made in purpose for the grid independence analysis which shows that the simulation with the computational grid of 301x131x131 nodes gives the same results as for the 271x101x101 nodes simulations. And this is the cause why there is no need of using more computational resources with finer grid and here the grid of 271x101x101 nodes is in use. At the input, the spectral boundary conditions are used.

The results of comparing turbulent characteristics with experiment are shown in Figure 3-5 for $x = 180$ cross-section. For stream wise and lateral turbulence intensities and for Reynolds stress profiles a satisfactory agreement with experiment is obtained (grid of 271x101x101 nodes). This result confirms the validity and correctness of the selected spectral boundary conditions at the input.

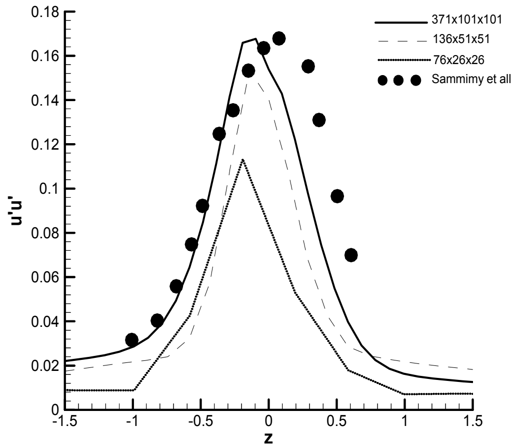

Figure 3 – Streamwise turbulence intensities

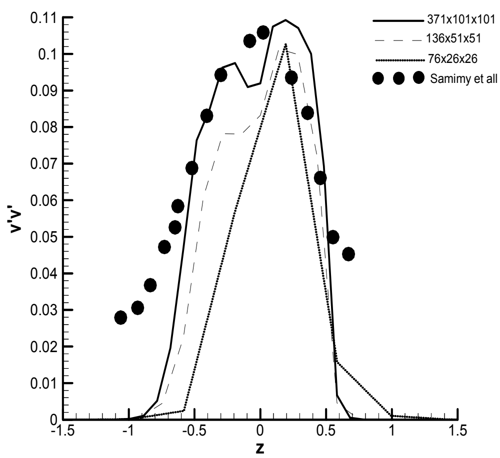

Figure 4 – Lateral turbulence intensities

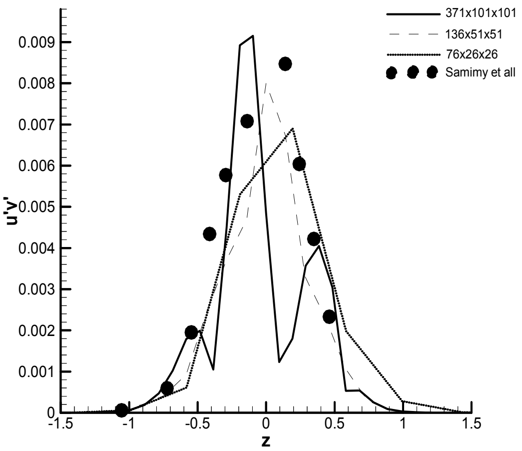

Figure 5 – The Reynolds stress profiles

The following are the results of numerical modeling of the problem with the following parameters: $M_\infty = 1$, $M_0 = 2$, $\mathrm{Re} = 10^5$, $d = 6$ is the diameter of the orifice, $P = 1atm$ is the pressure which is constant. The sizes of the domain are next $H_x = 200$, $H_y = 200$, $H_z = 30$ and $y_0 = 25$, $z_0 = 25$ are coordinates of the center of the jet.

In Figure 6 showing the vorticity thickness $\delta_\omega = \dfrac{u_\infty - u_0}{(\partial u / \partial z)_{\max}}$ of the shear layer, shows the results of calculations with three types of grids for comparison. In the case of a fine mesh (black solid line), the vorticity thickness increases from 4.7 to 8.5.

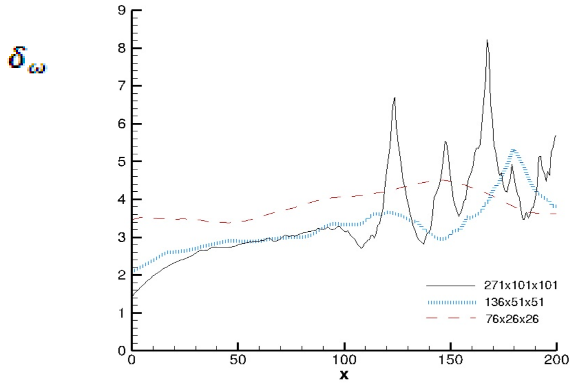

Figure 6 – Vorticity thickness for three types of grids.

Figure 7 (a) presents instantaneous isosurfaces for densities and vorticity, and Figure 7 (b) shows isolines of density and vorticity in a cross section *y=25* for natural jet in co-flow:

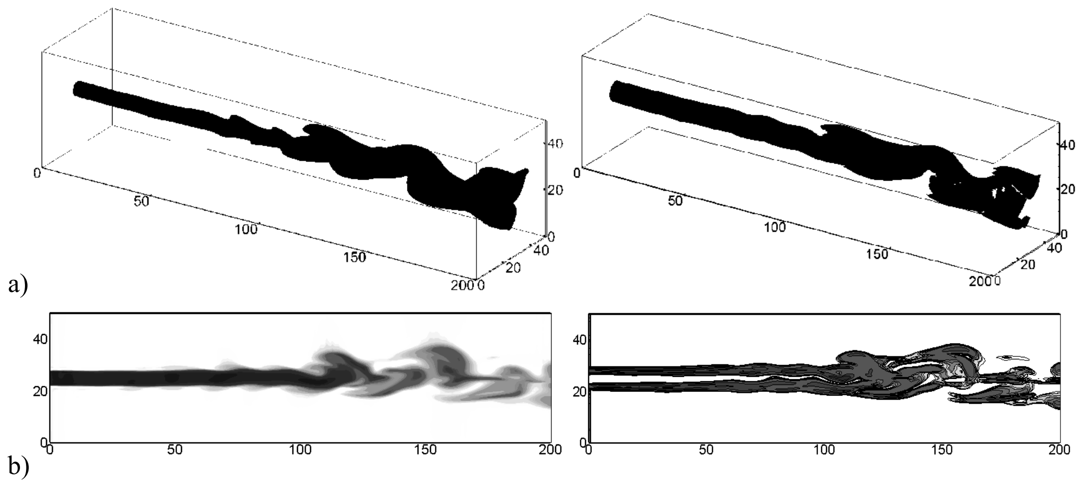

Figure 7 – Instantaneous isosurface for densities and vorticity (a) , isolines of density and vorticity in cross section *y=25* (b) for natural jet in co-flow

The results on Figure 7 show that with spectral boundary conditions taken at the input the obtained turbulence is close to the real one. As it is seen there are 6 vortices appeared starting from the point x = 55 which is seems to be a good result for this kind of flows. The main problem in all supersonic flows is in making the starting point (where the vortices start to form) distance as shorter as possible. Solving this problem leads to beneficial improvements in construction of the combustion chambers, namely the reduced size of combustors. More detailed analysis of the formation of vortices is shown on Figure 8 where the dynamic of the vortices structures in the shear layer between jet and co-flow is demonstrated:

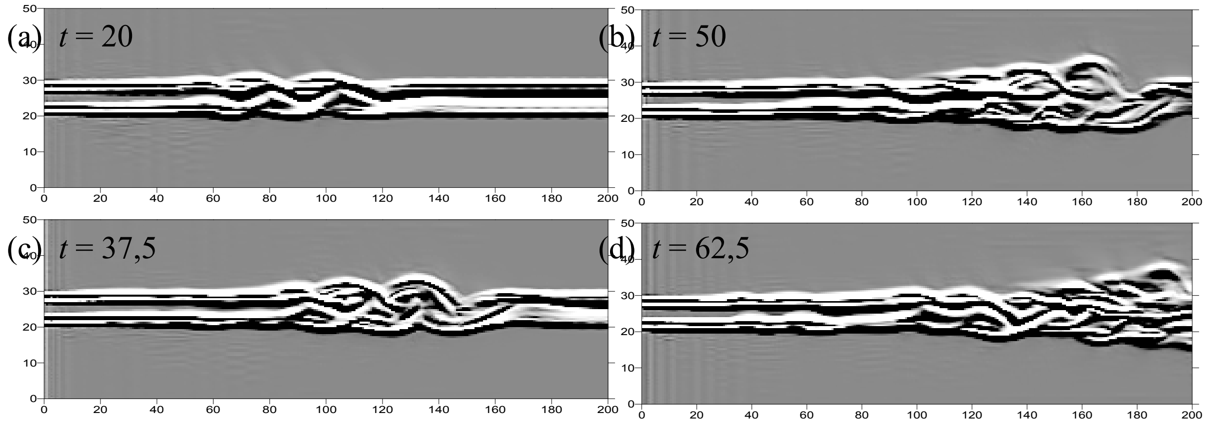

Figure 8 – Evolution of vorticity isolines at various times for natural jet in co-flow

It shows that to the time t = 37.5 the vortices are started forming and they are moving downstream (Fig. 8 (b)). Pairing of the adjacent vortices with forming the larger ones is demonstrated in Fig. 8 (c). And the relatively stable turbulence occurs to the time t = 62,5 (Fig. 8 (d)).

Conclusion

Stochastic boundary conditions at the entrance are presented based on the spectral method of generating fluctuations of gas-dynamic variables to obtain an inhomogeneous anisotropic turbulent flow. Based on them, the problem of injecting the compressible supersonic turbulent jet into a co-flowing stream is numerically solved. The analysis of grid independence for computational grids is carried out, which gave the most suitable number of nodes for the grid. Comparison of the results of obtained turbulent characteristics with experiment showed satisfactory agreement. It was also revealed that the far region of the jet in the shear layer is characterized by a developed turbulent structure. Thus, the formulation of stochastic spectral boundary conditions made it possible to obtain anisotropic inhomogeneous turbulence close to real.

References

1. M.R. Davis. Measurements in a subsonic turbulent jet using a quantitative schlieren technique // J. Fluid Mech. – 1971. – Vol. 46, part 4. – P. 631-656.

2. M.R. Davis. Quantitative schlieren measurements in a supersonic turbulent jet // J. Fluid Mech. – 1972. – Vol. 51, part 3. – P. 435-447.

3. R.A. Antonia and R.W. Bilger. An experimental investigation of an axisymmetric jet in a co-flowing air stream // J. Fluid Mech. – 1973. – Vol. 61, part 4. – P. 805-822.

4. J.-L. Borean, D. Huilier, H. Burnage. On the effect of a co-flowing stream on the structure of an axisymetric turbulent jet // Experimental Thermal and Fluid Science. – 1998. – Vol. 17. – P. 10-17.

5. L.P. Xia, K.M. Lam. Velocity and concentration measurements in initial region of submerged round jets in stagnant environment and in coflow // Journal of Hydro-environment Research. – 2009. – Vol. 3. – P. 21-34.

6. J.J. Charonko and K. Prestridge. Variable-density mixing in turbulent jets with coflow // J. Fluid Mech. – 2017. – Vol. 825. – P. 887-921.

7. F. De Gregorio, F. Albano. Free compressible jet nozzle investigation // 16th Int.

Symp. on Applications of Laser Techniques to Fluid Mechanics, Lisbon, Portugal. – 9-12 July, 2012.

8. A. Smirnov, S. Shi and I. Celik. Random Flow Generation Technique for Large Eddy Simulations and Particle-Dynamics Modeling // Journal of Fluids Engineering. – 2001. – Vol. 123, No. 2. – P. 359–371.

9. P. Batten, U. Goldberg and S. Chakravarthy. Interfacing Statistical Turbulence Closures with Large-Eddy Simulation // AIAA Journal. – 2004. – Vol. 42, No. 3. – P. 485–492.

10. L. Davidson. Hybrid LES-RANS: Inlet Boundary Conditions for Flows Including Recirculation // Proceedings of the 5th International Symposium on Turbulence and Shear Flow Phenomena. – 2007. – Vol. 2. – P. 689–694.

11. S. Huang, Q. Li and J. Wu. A General Inflow Turbulence Generator for Large Eddy Simulation // Journal of Wind Engineering and Industrial Aerodynamics. – 2010. – Vol. 98, No. 10–11. – P. 600–617.

12. H.G. Castro and R.R. Paz. A Time and Space Correlated Turbulence Synthesis Method for Large Eddy Simulation // Journal of Computational Physics. – 2013. – Vol. 235. – P.742–763.

13. D. Yu. Adamyan, M.H., Strelets and A.K. Travin. An efficient method of generation of synthetic turbulence at the entrance boundaries of the LES region within the framework of combined RANS-LES approaches to the calculation of turbulent flows // Mathematical Modeling. – 2011. – Vol. 23, No. 7. – P. 3-19.

14. R.Yu and X.-S. Bai. A Fully Divergence-Free Method for Generation of Inhomogeneous and Anisotropic Turbulence with Large Spatial Variation // Journal of Computational Physics. – 2014. – Vol. 256. – P. 234–253.

15. S. Huang, Q. Li and S. Xu. Numerical Evaluation of Wind Effects on a Tall Steel Building by CFD // Journal of Constructional Steel Research. – 2007. – Vol. 63, No. 5. – P. 612–627.

16. E. Riber, V. Moureau, M. Garcia, T. Poinsot and O. Simonin. Evaluation of Numerical Strategies for Large Eddy Simulation of Particulate Two-Phase Recirculating Flows // Journal of Computational Physics. – 2009. – Vol. 228, No. 2. – P. 539–564.

17. S. M. Salim, R. Buccolieri, A. Chan and S.D. Sabatino. Numerical Simulation of Atmospheric Pollutant Dispersion in an Urban Street Canyon: Comparison Between RANS and LES // Journal of Wind Engineering and Industrial Aerodynamics. – 2011. – Vol. 99, No. 2–3. – P.103–113.

18. G. Wang, M. Boileau and D.Veynante. Implementation of a Dynamic Thickened Flame Model for Large Eddy Simulations of Turbulent Premixed Combustion // Combustion and Flame. – 2011. –Vol. 158, No. 11. – P. 2199–2213.

19. V. Golubev, J. Brodnick, L. Nguyen, J. Dudley and M. Visbal. High-Fidelity Simulations of Airfoil Interaction with Upstream Turbulence // 42nd AIAA Fluid Dynamics Conference and Exhibit, AIAA Paper 2012-3071. – June 2012.

20. J. Mo, A. Choudhry, M. Arjomandi and Y. Lee. Large Eddy Simulation of the Wind Turbine Wake Characteristics in the Numerical Wind Tunnel Model // Journal of Wind Engineering and Industrial Aerodynamics. – 2013. – Vol. 112. – P. 11–24.

21. T.J. Poinsot, S.K. Lele. Boundary Conditions for Direct Simulation of Compressible Viscous Flows // Journal of Computational Physics. – 1992. – Vol. 101. – P.104-129.

22. A. Beketaeva, A. Naimanova. Flow structure of the transverse jet interaction with supersonic flow for moderate to high pressure ratios // International journal of mechanics. – 2018. – Vol.12. – P. 88-95.

23. A. Beketaeva, P. Bruel and A. Naimanova. Vortical structures behind a transverse jet in a supersonic flow at high jet to crossflow pressure ratios // J. Appl. Mech. and Tech. Phys. – 2015. – Vol. 56, No 5. – P. 777-788.

24. M. Samimy and G.S. Elliott. Effects of compressibility on the characteristics of free shear layers // AIAA Journal. – 1990. – Vol. 28, No. 3. – P. 439-445.

25. A. Zadauly , A. Beketaeva Influence of slit sizes on the interaction structure of supersonic turbulent air flow with a multi-component injection je in a channel // International Journal of Mathematics and Physics – 2018 – V.9, № 2. – P.72-85.

IRSTI 27.31.15; 27.31.17; 27.33.15 https://doi.org/10.26577/ijmph.2020.v11.i1.04

A.D. Abildayeva, A.T. Assanova, B.B. Minglibayeva

Institute of Mathematics and Mathematical Modeling, Almaty, Kazakhstan,
e-mail: azizakz@mail.ru, assanova@math.kz, bayan_math@mail.ru

AN EXISTENCE SOLUTION TO AN IDENTIFICATION PARAMETER PROBLEM FOR HIGHER-ORDER PARTIAL DIFFERENTIAL EQUATIONS

Abstract. The initial-boundary value problem with parameter for higher-order partial differential equations is considered. We study the existence of its solution and also propose a method for finding approximate solutions. We are established a sufficient conditions for the existence and uniqueness of the solution to the identification parameter problem under consideration. Introducing new unknown functions, we reduce the considered problem to an equivalent problem consisting of a nonlocal problem for second-order hyperbolic equations with functional parameters and integral relations. An algorithm for finding an approximate solution to the problem under study is proposed and its convergence is proved. Sufficient conditions for the existence of a unique solution to an equivalent problem with parameters are established. The conditions for the unique solvability of the initial-boundary value problem with parameter for higher-order partial differential equations are obtained in terms of the initial data. Unique solvability to the initial-boundary value problem with parameter for higher-order partial differential equations is interconnected with unique solvability to the nonlocal problem with parameter for second-order hyperbolic equations.

Key words: higher-order partial differential equations, identification parameter problem, nonlocal problem with parameters, hyperbolic equations of second order, solvability.

Introduction

An initial-boundary value problems with and without parameters for higher-order partial differential equations belong to one of the most important classes of problems in mathematical physics [1-14]. For studying of various problems with and without parameters for higher-order partial differential equations, along with classical methods of mathematical physics, such as the Fourier method, the Green's function method, the Poincare metric concept, the method of differential inequalities, and other methods of the qualitative theory of ordinary differential equations are also often applied. Based on these methods, the solvability conditions of the considered problems with and without parameters were established and ways to solve them were offered in [15-33]. However, the search for effective criteria of the unique solvability of initial-boundary value problems with parameters still remains relevant.

It is known that an ordinary differential equation of higher order can be reduced to a system of ordinary differential equations of the first order by special substitution. Using the methods of the qualitative theory of ordinary differential equations, the solvability conditions for the obtaining system can be formulated in the terms of the fundamental matrix of the differential part or the right side of the system. An analogous approach can be applied to higher-order hyperbolic equations with two independent variables and their can be reduced to a system of second order hyperbolic equations with mixed derivatives by replacement. Further, using well-known methods for solving problems for systems of hyperbolic equations with mixed derivatives, the solvability conditions can be established in different terms.

Mathematical modeling of many problems of physics, mechanics, chemistry, biology, and other sciences has resulted into the necessity of studying initial-boundary value problems with parameter for higher-order partial differential equations of hyperbolic type. Applying the methods of the qualitative theory of differential equations directly to these problems, we can establish the conditions for their solvability [1, 7, 8, 14, 23, 27-30]. Nonlocal problems with parameter for higher-order partial differential equations of hyperbolic type by replacement are reduced to nonlocal problems with parameter for system of second-order hyperbolic equations. The theory of nonlocal problems with parameter for system of second-order hyperbolic equations has been developed in many papers. To date, various solvability conditions for nonlocal problems with parameter for hyperbolic equations have been obtained.

The criteria for the unique solvability of some classes of linear nonlocal problems for hyperbolic equations with variable coefficients were obtained relatively recently [34-36]. In [34], a nonlocal problem with an integral condition for systems of hyperbolic equations by introducing new unknown functions is reduced to a problem consisting of a family of boundary value problems with an integral condition for systems of ordinary differential equations and functional relations. It is established that the well-posedness of a nonlocal problem with an integral condition for systems of hyperbolic equations is equivalent to the well-posedness of a family of two-point boundary value problems for a system of ordinary differential equations. In terms of the initial data, a criterion is established for the well-posedness of a nonlocal problem with an integral condition for systems of hyperbolic equations.

In present paper, we consider a higher-order partial differential equation defined in a rectangular domain. The boundary conditions for the time variable are specified as a combination of values from the partial derivatives of the desired solution in rows t = 0, t = T and $t=\theta$. We also study the existence and uniqueness of the solution to the initial-boundary value problem with parameter for a higher-order partial differential equation and its applications.

To solve the problem under consideration, we use the method of introducing additional functional parameters [34-36] and reduce the original problem to an equivalent problem consisting of a nonlocal problem with parameter for a second-order hyperbolic equation with functional parameters and integral relations. We establish sufficient conditions for the unique solvability of the considered problem in the terms of unique solvability of nonlocal problem with parameter for a second-order hyperbolic equation. Algorithms for finding a solution to an equivalent problem are constructed. The conditions for the unique solvability of the initial-boundary-value problem with parameter for the higher-order partial differential equations are established in the terms of the coefficients of the system and the boundary matrices.

Statement of problem and scheme of method introduction functional parameters

At the domain $\Omega=[0,T]\times[0,\omega]$, we consider the initial-boundary value problem with parameter for the higher-order partial differential equation of the following form:

$$\frac{\partial^{m+1}u}{\partial t\partial x^m}=\sum_{i=1}^{m}\left\{A_i(t,x)\frac{\partial^i u}{\partial x^i}+B_i(t,x)\frac{\partial^i u}{\partial t\partial x^{i-1}}\right\}+C(t,x)u+D(t,x)\mu(x)+f(t,x),\ (t,x)\in\Omega, \tag{1}$$

$$\sum_{j=0}^{1}\sum_{i=1}^{m}\left\{P_{ij}(x)\frac{\partial^i u(t,x)}{\partial x^i}+S_{ij}(x)\frac{\partial^i u(t,x)}{\partial t\partial x^{i-1}}\right\}\Big|_{t=t_j}=\varphi(x),\ x\in[0,\omega], \tag{2}$$

$$u(t,0)=\psi_0(t),\ \frac{\partial u(t,x)}{\partial x}\Big|_{x=0}=\psi_1(t),\ \ldots,\ \frac{\partial^{m-1}u(t,x)}{\partial x^{m-1}}\Big|_{x=0}=\psi_{m-1}(t),\ t\in[0,T], \tag{3}$$

$$L(x)\frac{\partial^m u(\theta,x)}{\partial x^m}+M(x)\mu(x)=\varphi_1(x),\ x\in[0,\omega], \tag{4}$$

where $u(t,x)$ and $\mu(x)$ are an unknown functions, the functions $A_i(t,x)$, $B_i(t,x)$, $i=\overline{1,m}$, $C(t,x)$, and $f(t,x)$ are continuous on Ω, the functions $P_{ij}(x)$, $S_{ij}(x)$, $i=\overline{1,m}$, $j=0,1$, and $\varphi(x)$ are continuous on $[0,\omega]$, $0=t_0<t_1=T$, the functions $\psi_s(t)$, $s=\overline{0,m-1}$, are continuously

differentiable on $[0,T]$, the functions $L(x)$, $M(x)$, and $\varphi_1(x)$ are continuous on $[0,\omega]$, and $0<\theta<T$. Relation (4) is additional condition for determining unknown functional parameter $\mu(x)$. The initial data satisfy the matching condition.

A pair of functions $(u(t,x),\mu(x))$, with component $u(t,x)\in C(\Omega,R)$, $\mu(x)\in C([0,\omega],R)$ having partial derivatives $\dfrac{\partial^{p+r}u(t,x)}{\partial t^r \partial x^p}\in C(\Omega,R)$, $p=\overline{1,m}$, $r=0,1$, is called a solution to problem with parameter (1) – (4) if it satisfies equation (1) for all $(t,x)\in\Omega$, the initial-boundary conditions (2), (3) and additional condition (4).

We will investigate the questions of the existence and uniqueness of solutions to the initial-boundary value problem with parameter for a higher-order partial differential equation (1) – (4) and the construction of its approximate solutions. For these purposes, we apply the method of introducing additional functional parameters proposed in [34–36] for solving various nonlocal problems for systems of hyperbolic equations with mixed derivatives. The considered problem is reduced to a nonlocal problem with parameter for second-order hyperbolic equations, including additional functions, and integral relations. An algorithm for finding an approximate solution to the problem under study is proposed and its convergence is proved. Sufficient conditions for the existence of a unique solution to problem with parameter (1) – (4) are obtained in terms of the initial data.

Scheme of the method and reduction to equivalent problem.

We introduce new unknown functions

$$v(t,x)=\frac{\partial^{m-1}u(t,x)}{\partial x^{m-1}},\ v_1(t,x)=u(t,x),$$
$$v_2(t,x)=\frac{\partial u(t,x)}{\partial x},\ \ldots,\ v_{m-1}(t,x)=\frac{\partial^{m-2}u(t,x)}{\partial x^{m-2}} \quad (5)$$

and re-write problem with parameter (1)-(4) in the following form:

$$\frac{\partial^2 v}{\partial t\partial x}=A_m(t,x)\frac{\partial v}{\partial x}+B_m(t,x)\frac{\partial v}{\partial t}+A_{m-1}(t,x)v+f(t,x)+D(t,x)\mu(x)+$$
$$+\sum_{r=1}^{m-2}A_r(t,x)v_{r+1}(t,x)+\sum_{s=1}^{m-1}B_r(t,x)\frac{\partial v_r(t,x)}{\partial t}+C(t,x)v_1(t,x),\quad (t,x)\in\Omega \quad (6)$$

$$\sum_{j=0}^{1}\left\{P_{m,j}(x)\frac{\partial v(t,x)}{\partial x}+S_{m,j}(x)\frac{\partial v(t,x)}{\partial t}+P_{m-1,j}(x)v(t,x)\right\}\Big|_{t=t_j}=\phi(x)-$$
$$+\sum_{j=0}^{1}\left\{\sum_{r=1}^{m-2}P_{r,j}(x)v_{r+1}(t,x)+\sum_{s=1}^{m-1}S_{s,j}(x)\frac{\partial v_s(t,x)}{\partial t}\right\}\Big|_{t=t_j},\quad x\in[0,\omega] \quad (7)$$

$$v(t,0)=\psi_{m-1}(t),\ t\in[0,T], \quad (8)$$

$$L(x)\frac{\partial v(\theta,x)}{\partial x}+M(x)\mu(x)=\varphi_1(x),\ x\in[0,\omega], \quad (9)$$

$$v_s(t,x)=\sum_{p=0}^{s-1}\psi_k(t)\frac{x^p}{p!}+\int_0^x\frac{(x-\xi)^{m-1-s}}{(m-1-s)!}v(t,\xi)d\xi,\ s=\overline{1,m-1},\ (t,x)\in\Omega. \quad (10)$$

Here the conditions (3) are taken into account in (10).
Differentiating (10) by t, we obtain

$$\frac{\partial v_s(t,x)}{\partial t}=\sum_{p=0}^{s-1}\dot{\psi}_k(t)\frac{x^p}{p!}+\int_0^x\frac{(x-\xi)^{m-1-s}}{(m-1-s)!}\frac{\partial v(t,\xi)}{\partial t}d\xi\,,\ s=\overline{1,m-1},\ (t,x)\in\Omega\,. \tag{11}$$

A system of functions $(v(t,x),\mu(x),v_1(t,x),$ $v_2(t,x),...,v_{m-1}(t,x))$, where the function $v(t,x)\in C(\Omega,R)$ has partial derivatives $\frac{\partial v(t,x)}{\partial x}\in C(\Omega,R)$, $\frac{\partial v(t,x)}{\partial t}\in C(\Omega,R)$, and $\frac{\partial^2 v(t,x)}{\partial t\partial x}\in C(\Omega,R^n)$, the function $\mu(x)\in C([0,\omega],R)$, the functions $v_s(t,x)\in C(\Omega,R)$ have partial derivatives $\frac{\partial v_s(t,x)}{\partial t}\in C(\Omega,R)$, $s=\overline{1,m-1}$, is called a solution to problem with parameters (6)-(10), if it satisfies the second-order hyperbolic equation (6) for all $(t,x)\in\Omega$, boundary conditions (7) and (8), additional condition (9) and integral relations (10).

For fixed $v_s(t,x)$, $s=\overline{1,m-1}$, problem (6)--(9) is a nonlocal problem with parameter for the hyperbolic equation with respect to $v(t,x)$ and $\mu(x)$ on Ω. Integral relations (10) allow us to determine unknown functions $v_s(t,x)$, $s=\overline{1,m-1}$ for all $(t,x)\in\Omega$.

Algorithm

We determine the unknown function $v(t,x)$ from the nonlocal problem with parameter for hyperbolic equations (6)-(9). Unknown functions $v_s(t,x)$, $s=\overline{1,m-1}$, will be found from integral relations (10).

If we know the functions $v_s(t,x)$, $s=\overline{1,m-1}$, then from the nonlocal problem with parameter (6)--(9) we find the functions $v(t,x)$ and $\mu(x)$. And, conversely, if we know the functions $v(t,x)$ and $\mu(x)$, then from the integral conditions (10) we find the functions $v_s(t,x)$, $s=\overline{1,m-1}$. Since both functions $v(t,x)$, $\mu(x)$, $v_s(t,x)$, $s=\overline{1,m-1}$, are unknown, then to find a solution to problem (6)--(10) we use an iterative method.

The solution to problem with parameters (6)--(10) is the system of functions $(v^*(t,x),\mu^*(x),$ $v_1^*(t,x),v_2^*(t,x),...,v_{m-1}^*(t,x))$, which we defined as the limit of the sequence of systems $(v^{(k)}(t,x),\mu^{(k)}(x),v_1^{(k)}(t,x),v_2^{(k)}(t,x),...,v_{m-1}^{(k)}(t,x))$, $k=0,1,2,...$, according to the following algorithm:

Step 0. 1) Suppose in the right-hand side of equation (6) we have $v_s(t,x)=\sum_{p=0}^{s-1}\psi_k(t)\frac{x^p}{p!}$ and $\frac{\partial v_s(t,x)}{\partial t}=\sum_{p=0}^{s-1}\dot{\psi}_k(t)\frac{x^p}{p!}$, $s=\overline{1,m-1}$. From nonlocal problem with parameter (6)-(9) we find the initial approximations $v^{(0)}(t,x)$ and $\mu^{(0)}(x)$, and partial derivatives $\frac{\partial v^{(0)}(t,x)}{\partial x}$ and $\frac{\partial v^{(0)}(t,x)}{\partial t}$ for all $(t,x)\in\Omega$;

2) From integral relations (10) and (11) under $v(t,x)=v^{(0)}(t,x)$ and $\frac{\partial v(t,x)}{\partial t}=\frac{\partial v^{(0)}(t,x)}{\partial t}$, respectively, we find the functions $v_s^{(0)}(t,x)$ and $\frac{\partial v_s^{(0)}(t,x)}{\partial t}$, $s=\overline{1,m-1}$, for all $(t,x)\in\Omega$.

Step 1. 1) Suppose in the right-hand side of equation (6) we have $v_s(t,x)=v_s^{(0)}(t,x)$ and $\frac{\partial v_s(t,x)}{\partial t}=\frac{\partial v_s^{(0)}(t,x)}{\partial t}$, $s=\overline{1,m-1}$. From nonlocal problem with parameter (6)-(9) we find the first approximations $v^{(1)}(t,x)$ and $\mu^{(1)}(x)$, and partial derivatives $\frac{\partial v^{(1)}(t,x)}{\partial x}$ and $\frac{\partial v^{(1)}(t,x)}{\partial t}$ for all $(t,x)\in\Omega$.

2) From integral relations (9) and (10) under $v(t,x)=v^{(1)}(t,x)$ and $\frac{\partial v(t,x)}{\partial t}=\frac{\partial v^{(1)}(t,x)}{\partial t}$, respectively, we find the functions $v_s^{(1)}(t,x)$ and $\frac{\partial v_s^{(1)}(t,x)}{\partial t}$, $s=\overline{1,m-1}$, for all $(t,x)\in\Omega$.

And so on.

Step k. 1) Suppose in the right-hand side of equation (6) we have $v_s(t,x)=v_s^{(k-1)}(t,x)$ and $\frac{\partial v_s(t,x)}{\partial t}=\frac{\partial v_s^{(k-1)}(t,x)}{\partial t}$, $s=\overline{1,m-1}$. From nonlocal problem with parameter (6)-(9) we find the k-th approximations $v^{(k)}(t,x)$ and $\mu^{(k)}(x)$, and partial derivatives $\frac{\partial v^{(k)}(t,x)}{\partial x}$ and $\frac{\partial v^{(k)}(t,x)}{\partial t}$ for all $(t,x)\in\Omega$:

$$\begin{aligned}\frac{\partial^2 v^{(k)}}{\partial t\partial x}&=A_m(t,x)\frac{\partial v^{(k)}}{\partial x}+B_m(t,x)\frac{\partial v^{(k)}}{\partial t}+A_{m-1}(t,x)v^{(k)}+f(t,x)+D(t,x)\mu^{(k)}(x)+\\&+\sum_{r=1}^{m-2}A_r(t,x)v_{r+1}^{(k-1)}(t,x)+\sum_{s=1}^{m-1}B_r(t,x)\frac{\partial v_r^{(k-1)}(t,x)}{\partial t}+C(t,x)v_1^{(k-1)}(t,x),\quad (t,x)\in\Omega\end{aligned}\tag{12}$$

$$\begin{aligned}&\sum_{j=0}^{1}\left\{P_{m,j}(x)\frac{\partial v^{(k)}(t,x)}{\partial x}+S_{m,j}(x)\frac{\partial v^{(k)}(t,x)}{\partial t}+P_{m-1,j}(x)v^{(k)}(t,x)\right\}\Big|_{t=t_j}=\phi(x)-\\&+\sum_{j=0}^{1}\left\{\sum_{r=1}^{m-2}P_{r,j}(x)v_{r+1}^{(k-1)}(t,x)+\sum_{s=1}^{m-1}S_{s,j}(x)\frac{\partial v_s^{(k-1)}(t,x)}{\partial t}\right\}\Big|_{t=t_j},\quad x\in[0,\omega]\end{aligned}\tag{13}$$

$$v^{(k)}(t,0)=\psi_{m-1}(t),\ t\in[0,T],\tag{14}$$

$$L(x)\frac{\partial v^{(k)}(\theta,x)}{\partial x}+M(x)\mu^{(k)}(x)=\varphi_1(x),\ x\in[0,\omega].\tag{15}$$

2) From integral relations (10) and (11) under $v(t,x)=v^{(k)}(t,x)$ and $\frac{\partial v(t,x)}{\partial t}=\frac{\partial v^{(k)}(t,x)}{\partial t}$, respectively, we find the functions $v_s^{(k)}(t,x)$ and $\frac{\partial v_s^{(k)}(t,x)}{\partial t}$, $s=\overline{1,m-1}$, for all $(t,x)\in\Omega$:

$$v_s^{(k)}(t,x)=\sum_{p=0}^{s-1}\psi_k(t)\frac{x^p}{p!}+\int_0^x\frac{(x-\xi)^{m-1-s}}{(m-1-s)!}v^{(k)}(t,\xi)d\xi,\ s=\overline{1,m-1},\ (t,x)\in\Omega.\tag{16}$$

$$\frac{\partial v_s^{(k)}(t,x)}{\partial t}=\sum_{p=0}^{s-1}\dot\psi_k(t)\frac{x^p}{p!}+\int_0^x\frac{(x-\xi)^{m-1-s}}{(m-1-s)!}\frac{\partial v^{(k)}(t,\xi)}{\partial t}d\xi,\ s=\overline{1,m-1},\ (t,x)\in\Omega.\tag{17}$$

Here $k=1,2,3,\ldots$.

The main results

Consider auxiliary nonlocal problem with parameter

$$\frac{\partial^2 v}{\partial t\partial x}=A_m(t,x)\frac{\partial v}{\partial x}+B_m(t,x)\frac{\partial v}{\partial t}+A_{m-1}(t,x)v+f(t,x)+D(t,x)\mu(x),\ (t,x)\in\Omega,\tag{18}$$

$$\sum_{j=0}^{1}\left\{P_{m,j}(x)\frac{\partial v(t,x)}{\partial x}+S_{m,j}(x)\frac{\partial v(t,x)}{\partial t}+P_{m-1,j}(x)v(t,x)\right\}\Big|_{t=t_j}=\varphi(x),\ x\in[0,\omega], \tag{19}$$

$$v(t,0)=\psi_{m-1}(t),\ t\in[0,T], \tag{20}$$

$$L(x)\frac{\partial v(\theta,x)}{\partial x}+M(x)\mu(x)=\varphi_1(x),\ x\in[0,\omega]. \tag{21}$$

The following theorem provides conditions for the feasibility and convergence of the constructed algorithm, as well as conditions for the existence of a unique solution to problem with parameter (6)--(10). The functions functions $A_i(t,x)$, $B_i(t,x)$, $i=\overline{1,m}$, $C(t,x)$, and $f(t,x)$ are continuous on Ω, the functions $P_{ij}(x)$, $S_{ij}(x)$, $i=\overline{1,m}$, $j=0,1$, and $\varphi(x)$ are continuous on $[0,\omega]$, the functions $\psi_s(t)$, $s=\overline{0,m-1}$, are continuously differentiable on $[0,T]$, the functions $L(x)$, $M(x)$, and $\varphi_1(x)$ are continuous on $[0,\omega]$.

Theorem 1. *Let*

i) the functions $A_i(t,x)$, $B_i(t,x)$, $i=\overline{1,m}$, $C(t,x)$, *and* $f(t,x)$ *be continuous on* Ω;

ii) the functions $P_{ij}(x)$, $S_{ij}(x)$, $i=\overline{1,m}$, $j=0,1$, and $\varphi(x)$ *be continuous on* $[0,\omega]$;

iii) the functions $\psi_s(t)$, $s=\overline{0,m-1}$, *be continuously differentiable on* $[0,T]$;

iv) th nonlocal problem with parameter has a unique solution.

Then the nonlocal problem for the hyperbolic equation with parameters and integral conditions (6)--(10) has a unique solution $(v^*(t,x),\mu^*(x),$ $v_1^*(t,x),v_2^*(t,x),...,v_{m-1}^*(t,x))$ *as a limit of sequences* $(v^{(k)}(t,x),\mu^{(k)}(x),v_1^{(k)}(t,x),$ $v_2^{(k)}(t,x),...,v_{m-1}^{(k)}(t,x))$ *determined by the algorithm proposed above for* $k=0,1,2,...$.

The proof of Theorem 1 is similar to the proof of Theorem 1 in [35].

Then the unique solution $(u^*(t,x),\mu^*(x))$ to problem with parameter (1)-(4) determines as $u^*(t,x)=v_1^*(t,x)$ and $\mu^*(x)$.

The equivalence of problems (6)-(10) and (1)-(4) implies

Theorem 2. *Let conditions i) – iv) of Theorem 1 be fulfilled.*

Then the initial-boundary value problem with parameter for the higher-order partial differential equation (1)--(4) has a unique classical solution $(u^*(t,x),\mu^*(x))$.

Introduce the following notation:

$$\alpha(x,t,\tau)=\int_\tau^t A_m(\tau_1,x)d\tau_1,$$

$$Q(x,T,\theta)=\begin{bmatrix} P_{m,1}(x)+S_{m,1}(x)e^{\alpha(x,T,0)} & S_{m,1}(x)\int_0^T e^{\alpha(x,T,\tau)}D(\tau,x)d\tau \\ L(x)e^{\alpha(x,\theta,0)} & L(x)\int_0^\theta e^{\alpha(x,\theta,\tau)}D(\tau,x)d\tau+M(x)\end{bmatrix},\ x\in[0,\omega].$$

Theorem 3. *Let*

a) conditions i) – iii) of Theorem 1 be fulfilled;

b) the (2x2)- matrix $Q(x,T,\theta)$ *is invertible for all* $x\in[0,\omega]$.

Then the initial-boundary value problem with parameter for the higher-order partial differential equation (1)--(4) has a unique classical solution $(u^*(t,x),\mu^*(x))$.

Conclusion

Therefore, we are studied the identification parameter problem for higher-order partial differential equations with two variables. We are established the sufficient conditions for the existence and uniqueness of the solution to the considered identification parameter problem. We are reduced this problem to the equivalent problem consisting of the nonlocal problem for second-order hyperbolic equations with functional parameters and integral relations by introducing new unknown functions. An algorithm for finding an approximate solution to the equivalent problem with parameters is proposed and its convergence is proved. Sufficient conditions for the existence of the unique solution to the equivalent problem with parameters are established. The conditions for the unique solvability of the initial-boundary value problem with parameter for higher-order partial differential equations are obtained in terms of the initial data. Unique solvability to the identification parameter problem for higher-order partial differential equations is interconnected with unique solvability to the identification parameter problem for second-order hyperbolic equations. These results will be developed to various initial-boundary value problems with parameters for the higher-order system of partial differential equations and control problems for second-order system of hyperbolic equations.

Acknowledgement

The research is partially supported by grant AP05131220 of Ministry of Education and Science of the Republic of Kazakhstan (2018-2020).

References

1. Ptashnyck B.I. "Ill-posed boundary value problems for partial differential equations", *Naukova Dumka*, Kiev (1984) (in Russ.).
2. Ptashnyk B.Yo., Il'kiv V.S., Kmit' I. Ya., Polishchuk V.M. "Nonlocal boundary value problems for partial differential equations", *Naukova Dumka*, Kyiv, Ukraine (2002). (in Ukrain.)
3. Kiguradze T., Lakshmikantham V. "On Dirichlet problem in a characteristic rectangle for higher order linear hyperbolic equations", *Nonlinear Anal.*, 50 (2002): 1153–1178.
4. Kiguradze T.I., Kusano T. "Well-posedness of initial-boundary value problems for higher-order linear hyperbolic equations with two independent variables", *Differ. Equ.*, 39 (2003): 553-563.
5. Kiguradze T., Kusano T. "On ill-posed initial-boundary value problems for higher order linear hyperbolic equations with two independent variables", *Differ. Equ.,* 39 (2003): 1379–1394.
6. Dzhokhadze O.M. "The Riemann function for higher-order hyperbolic equations and systems with dominated lower terms", *Differ. Equ.,* 39 (2003): 1440–1453.
7. Nakhushev A.M. "Problems with shift for a partial differential equations", *Nauka*, Moskow (2006). (in Russ.).
8. Kiguradze I., Kiguradze T. "On solvability of boundary value problems for higher order nonlinear hyperbolic equations", *Nonlinear Analysis*, 69 (2008): 1914-1933.
9. Kiguradze T. "The Valle-Poussin problem for higher order nonlinear hyperbolic equations", *Computers & Math. with Appl.*, 59 (2010): 994-1002.
10. Kong L., Wong J.S.W. "Positive solutions for higher order multi-point boundary value problems with nonhomogeneous boundary conditions", *J. Math. Anal. Appl.,* 367(2010): 588-611.
11. Henderson J., Luca R. "Existence of positive solutions for a system of higher-order multi-point boundary value problems", *Appl. Math. Comp.,* 219 (2012): 3709-3720.
12. Kuz' A.M., Ptashnyk B.I. "A problem with integral conditions with respect to time for Gårding hyperbolic equations", *Ukr. Math. J.* 65 (2013): 277-293.
13. Il'kiv V.S., Nytrebych Z.M., Pukach P.Y. "Boundary-value problems with integral conditions for a system of Lamé equations in the space of almost periodic functions", *Electr. J. Differ. Equ.,* 2016, 304 (2016): 1-12.
14. Kiguradze I.T., Kiguradze T.I. "Analog of the first Fredholm theorem for higher-order nonlinear differential equations", *Differ. Equ.,* 53 (2017): 996-1004.
15. Dzhumabaev D.S. "Multi-iterative method of solving of the two boundary-value problems for semi-explicit differential equations with parameter in Banach spaces", *Izvestia AN Kazakhs-koi SSR. Ser. fiz.-matem.,* 3 (1978): 9-15. (in Russ.)
16. Dzhumabaev D.S. "The necessary and sufficient conditions of existence solutions to boundary-value problems with parameter", *Izvestia AN Kazakhskoi SSR. Ser. fiz.-matem.,* 3 (1979): 5-12. (in Russ.)
17. Kurpel N.S., Marusiak A.G. "About one multi-point boundary-value problem for differential

equation with parameters", Ukr. Math. J., 32 (1980): 223-226. (in Russ.)

18. Kiguradze I.T. "Boundary value problems for systems of ordinary differential equations". *Sovremennye problemy matematiki. Noveishie dostizhenia.* (Itogi nauki i techniki. VINITI AN SSSR), Moscow, 30 (1987): 3-103 (in Russ.).

19. Luchka A.Yu. "Application of iterative processes to boundary value problems for differential equations with parameters", *Doklady AN Ukr. SSR. Ser. A. fiz.-matem. i tekhn. nauki,* 10 (1989): 22-27. (in Russ.)

20. Ronto M., Samoilenko A.M. "Numerical-analytic methods in the theory of boundary-value problems". *World Scientific*, River Edge, NJ, USA (2000).

21. Minglibaeva B.B. "The coefficients conditions of unique solvability of linear two-point boundary value problems with parameter", *Mathem. J.,* 3, 2 (2003): 55-62. (in Russ.)

22. Dzhumabaev D.S., Minglibaeva B.B. "The well-posed solvability of linear two-point boundary value problem with parameter", Mathem.J., 4, 1 (2004): 41-51. (in Russ.)

23. Boichuk A.A., Samoilenko A.M. "Generalized inverse operators and Fredholm boundary-value problems". *VSP*, Utrecht, Boston (2004).

24. Kugler P. "Online parameter identification in time-dependent differential equations as a non-linear inverse problem", *European J. Appl. Math*. 19, (2008): 479-506.

25. Loreti P., Sforza D. "Control problems for weakly coupled systems with memory". *J. Diff. Equat.,* 257 (2014): 1879-1938.

26. Volpert V. "Elliptic partial differential equations Vol. 2: Reaction-Diffusing Equations". *Birkhauser Springer*, Basel etc. (2014).

27. Yuldashev T.K. "Inverse problem for a nonlinear Benney-Luke type integro-differential equations with degenerate kernel", *Russian Math.* 60, 9 (2016): 53-60.

28. Yuldashev T.K. "Determination of the coefficient and boundary regime in boundary value problem for integro-differential equation with degenerate kernel", *Lobachevskii J. Math.* 38, 3 (2017): 547–553.

29. Yuldashev T.K. "On inverse boundary value problem for a Fredholm integro-differential equation with degenerate kernel and spectral parameter", *Lobachevskii J. Math.* 40,2 (2019): 230-239.

30. Dzhumabaev D.S. Bakirova E.A., Kadirbayeva Zh.M. "An algorithm for solving a control problem for a differential equation with a parameter", *News of the NAS RK. Phys.-Math. Series,* 5, 321(2018): 25-32.

31. Assanova A.T., Bakirova E.A., Kadirbayeva Zh.M. "Numerical implementation of solving a boundary value problem for a system of loaded differential equations with parameter". *News of the NAS RK. Phys.-Math. Series*. 3, 325(2019): 77-84.

32. Assanova A.T., Bakirova E.A., Kadirbayeva Zh.M. "Numerical solution of a control problem for ordinary differential equations with multipoint integral condition", *International Journal of Mathematics and Physics* 10, 2, 4 (2019): 4-10.

33. Assanova A.T., Bakirova E.A., Kadirbayeva Z.M. "Numerical solution to a control problem for integro-differential equations", *Comput. Math. and Math. Phys*. 60, 2 (2020): 203–221

34. Asanova A.T., Dzhumabaev D.S. "Well-posedness of nonlocal boundary value problems with integral condition for the system of hyperbolic equations", J. Math. Anal. Appl., 402, 1 (2013): 167-178.

35. Assanova A.T. "An integral-boundary value problem for a partial differential equation of second order", *Turkish J. Math*., 43, 4 (2019): 1967-1978.

36. Assanova A.T., Iskakova N.B., Orumbayeva N.T. "On the well-posedness of periodic problems for the system of hyperbolic equations with finite time delay", *Mathematical Methods in the Applied Sciences*, 43, 2 (2020): 881-902.

IRSTI 27.31.44,27.35.21,27.35.59 https://doi.org/10.26577/ijmph.2020.v11.i1.05

Zh.K. Dzhobulaeva

Institute of Mathematics and Mathematical Modeling,
Almaty, Kazakhstan, e-mail: zhanat-78@mail.ru

AN IRREGULAR CONJUGATIONPROBLEM FOR THE SYSTEM OF THE PARABOLICE QUATIONS IN THE HOLDER SPACE

Abstract. We consider the conjugation problem for the system of parabolicequations with two small parameters $\kappa > 0$, $\varepsilon > 0$ in the boundary conditions.There are proved the existence, uniqueness and uniform coercive estimates ofthe solution with respect to the small parameters in the Holder space. Thisproblem is linearized one of the nonlinear problem with the free boundary ofFlorin type and it is in the base of the proof of the solidified of this nonlinearproblem in the Holder space.We study the problem with the free boundary of the Florin type in the Holder space $\overset{\circ}{C}{}_{x\ \ t}^{2+l,1+l/2}(\overline{\Omega}_{jT})$, $j=1,2,$ where $l-$ is non-integer positive number. Existence, uniqueness, estimates for solution of the problem with constants independent of small parameters in the Holder space areproved. It gives us the opportunity to establish the existence, uniqueness and estimates of the solution of the problem without loss of smoothness of given functions for $\kappa = 0$, $\varepsilon > 0$; $\kappa > 0$; $\varepsilon = 0$ and $\kappa = 0$, $\varepsilon = 0$.

Key words :parabolic equations, existence, uniqueness of the solution, coercive estimates, Holder space.

1 Introduction

In the work the problem of Florin type is studied for the system of parabolicequations in the Holder spaces. This problem is a mathematical model describingfiltration of liquids and gases in the porous medium. Linear problems with smallparameters with time derivatives functions of the free boundary were studied in [1]-[7]. In this article the problem is studied without time derivatives functionsof the free boundaries $\psi(t)$ in the right-hand sides of the conditions (6), (7), whichcorresponds to a degenerate nonlinear the free boundary problem of melting binaryalloys and in which free boundary is set as an implicit function. In contrast fromproblems in [1]$-$[7], where free border is set explicitly.

Let$\Omega_1 = (0,\rho_0)$, $\Omega_2 = (\rho_0, b), 0 < \rho_0 < b$, $b > 0$, $\Omega_{jT} = \Omega_j \times (0,T)$, $j = 1,2$, $\sigma_T = (0,T)$, $\chi(\lambda)$ be a smooth shear function, equal to one at$|\lambda| \le \delta_0$andzero for$|\lambda| \ge 2\delta_0$and having the rating$|d^m\chi/dx^m| \le C_m\delta_0^{-m}, \delta_0 = const > 0$.

Define second order elliptic operators

$$A_j(x,t;\partial_x)v_j := a_j(x,t)\partial_x^2 v_j + \\ +b_j(x,t)\partial_x v_j + d_j(x,t)v_j,$$

$$A_{j+2}(x,t;\partial_x)z_j := a_{j+2}(x,t)\partial_x^2 z_j + \\ +b_{j+2}(x,t)\partial_x z_j + d_{j+2}(x,t)z_j,$$

where $a_j(x,t), a_{j+2}(x,t) \ge a_0 = const > 0$ in $\overline{\Omega}_{jT}$, $j = 1,2$.

It is required to find functions $v_j(x,t)$, $z_j(x,t)$, $j = 1,2$, and $\psi(t)$ satisfyingparabolic equations

$$\partial_t v_j - A_j(x,t;\partial_x)v_j - \alpha_j(x,t)\chi(x-\rho_0)D_t\psi = \\ = f_j(x,t)\text{in}\overline{\Omega}_{jT},\ \ j = 1,2, \tag{1}$$

$$\partial_t z_j - A_{j+2}(x,t;\partial_x)z_j - \beta_j(x,t)\chi(x-\rho_0)D_t\psi = \\ = f_{j+2}(x,t)\text{in}\overline{\Omega}_{jT},\ \ j = 1,2, \tag{2}$$

and initial conditions

$$\psi|_{t=0} = 0,\ \ v_j|_{t=0} = v_{oj}, \\ z_j|_{t=0} = z_{oj},\ \text{in}\Omega,\ \ j = 1,2, \tag{3}$$

boundary conditions

$$v_1|_{x=0} = p_1(t),\ v_2|_{x=b} = p_2(t),\quad t \in \sigma_T, \tag{4}$$

$$z_1|_{x=0} = q_1(t),\ z_2|_{x=b} = q_2(t),\quad t \in \sigma_T, \tag{5}$$

and conjugation conditions on the border $x = \rho_0$

$$(v_1 - v_2)|_{x=\rho_0} = \eta_0(t), \quad t \in \sigma_T, \qquad (6)$$

$$\big(z_j - \gamma_j(x,t)v_j\big)|_{x=\rho_0} = \eta_j(t), \quad j = 1,2, \quad t \in \sigma_T, \qquad (7)$$

$$(\lambda_1(x,t)\partial_x v_1 - \kappa\lambda_2(x,t)\partial_x v_2)|_{x=\rho_0} = g_1(t) + \kappa g_2(t), \quad t \in \sigma_T, \qquad (8)$$

$$(k_1(x,t)\partial_x z_1 - \varepsilon k_2(x,t)\partial_x z_2)|_{x=\rho_0} = g_3(t) + \varepsilon g_4(t), \quad t \in \sigma_T, \qquad (9)$$

where $\gamma_j(x,t) \geq d_1 = const > 0$, $\lambda_j(x,t) \geq d_2 = const > 0$, $k_j(x,t) \geq d_3 = const > 0, j = 1,2$, $\kappa > 0, \varepsilon > 0$ −small parameters, $\partial_t = \partial/\partial_t$, $\partial_x = \partial/\partial_x, D_t = d/dt$.

Problem (1)-(9) is a linearized problem of the Florintype nonlinear problem, which describes the process of filtering liquids and gases in the porous medium.

This problem will be studied in Holder spaces. Let l be a noninteger positivenumber, $\alpha = l - [l] \in (0,1)$.

Under $C_{x\ t}^{l,l/2}(\overline{\Omega}_T)$, $C_t^{l/2}(\overline{\sigma}_T)$, we will understand Banach spaces of functions$u(x,t)$and $\psi(t)$,with thenorms

$$|u|_{D_T}^{(l)} := \sum_{2m_0+m=0}^{[l]} |\partial_t^{m_0}\partial_x^m u|_{\Omega_T} + \sum_{2m_0+m=[l]} \left([\partial_t^{m_0}\partial_x^m u]_{x,\Omega_T}^{(\alpha)} + [\partial_t^{m_0}\partial_x^m u]_{t,\Omega_T}^{(\alpha/2)}\right) + $$

$$+ \sum_{2m_0+m=[l]} [\partial_t^{m_0}\partial_x^m u]_{t,\Omega_T}^{((1+\alpha)/2)},$$

$$|\psi|_{\sigma_T}^{(l/2)} := \sum_{m_0=0}^{[l/2]} |D_t^{m_0}\psi|_{\sigma_T} + [D_t^{[l/2]}\psi]_{\sigma_T}^{(l/2-[l/2])}, \qquad (10)$$

$$\Omega_T = \Omega \times (0,T), \qquad |v|_{\Omega_T} = \sup_{(x,t)\in\Omega_T} |v|,$$

$$[v]_{x,\Omega_T}^{(\alpha)} = \sup_{(x,t),(z,t)\in\Omega_T} \frac{|v(x,t) - v(z,t)|}{|x-z|^\alpha}, \ [v]_{t,\Omega_T}^{(\alpha)} = \sup_{(x,t),(x,t_1)\in\Omega_T} \frac{|v(x,t) - v(x,t_1)|}{|t-t_1|^\alpha}.$$

Through $\overset{\circ}{C}{}_{x\,t}^{l,l/2}(\overline{\Omega}_T)$, we denote the subspaces of functions $u(x,t)$ belonging to $C_{x\,t}^{l,l/2}(\overline{\Omega}_T)$ and satisfying the conditions

$$\partial_t^k u|_{t=0}, \ k = 0, \dots, [l/2].$$

The following lemma holds.

Lemma 1. In the space $\overset{\circ}{C}{}_t^{\frac{(1+l)}{2}}(\overline{\sigma}_T)$, $l-$ is a non-integer positive number, the norm $|\psi|_{\overline{\sigma}_T}^{(1+l/2)}$, defined by the formula (10), is equivalent to the norm

$$\|\psi\|_{\overline{\sigma}_T}^{\left(\frac{1+l}{2}\right)} = \sup_{t\in\sigma_T} t^{-\frac{1+l}{2}} |\psi|_{\overline{\sigma}_T} + $$

$$+ \left[D_t^{[(1+l)/2]}\psi\right]_{\overline{\sigma}_T}^{\left(\frac{1+l}{2} - \left[\frac{1+l}{2}\right]\right)}.$$

We define function of Banach spaces for solving the problem. Let

$$B(\Omega_T) := \overset{\circ}{C}{}_{x\ \ t}^{2+l,1+l/2}(\overline{\Omega}_{1T}) \times$$

$$\times \overset{\circ}{C}{}_{x\ \ t}^{2+l,1+l/2}(\overline{\Omega}_{2T}) \times \overset{\circ}{C}{}_{x\ \ t}^{2+l,1+l/2}(\overline{\Omega}_{1T}) \times$$

$$\times \overset{\circ}{C}{}_{x\ \ t}^{2+l,1+l/2}(\overline{\Omega}_{2T}) \times \overset{\circ}{C}{}_t^{1+l/2}(\overline{\sigma}_T)$$

be the space of vector-functions $w=(v_1,v_2,z_1,z_2,\psi)$ with the norm

$$\|w\|_{B(\Omega_T)}= = \sum_{j=1}^{2}\left(|v_j|_{\Omega_{jT}}^{(2+l)}+|z_j|_{\Omega_{jT}}^{(2+l)}\right)+|\psi|_{\sigma_T}^{(1+l/2)}, \quad (11)$$

$$:= \overset{\circ}{C}{}_{x\,t}^{\,l,l/2}(\overline{\Omega_{1T}})\times \overset{\circ}{C}{}_{x\,t}^{\,l,l/2}(\overline{\Omega_{1T}})\times \overset{\circ}{C}{}_{x\,t}^{\,l,l/2}(\overline{\Omega_{1T}})\times \overset{\circ}{C}{}_{x\,t}^{\,l,l/2}(\overline{\Omega_{1T}})\times \overset{\circ}{C}{}_{t}^{\,1+l/2}(\overline{\sigma_T})\times \overset{\circ}{C}{}_{t}^{\,1+l/2}(\overline{\sigma_T})\times$$

$$\times \overset{\circ}{C}{}_{t}^{\,1+l/2}(\overline{\sigma_T})\times \overset{\circ}{C}{}_{t}^{\,1+l/2}(\overline{\sigma_T})\times \overset{\circ}{C}{}_{t}^{\,1+l/2}(\overline{\sigma_T})\times$$

$$\times \overset{\circ}{C}{}_{t}^{\,1+l/2}(\overline{\sigma_T})\times \overset{\circ}{C}{}_{t}^{\,1+l/2}(\overline{\sigma_T})\times \overset{\circ}{C}{}_{t}^{\,\frac{(1+l)}{2}}(\overline{\sigma_T})\times$$

$$\times \overset{\circ}{C}{}_{t}^{\,\frac{(1+l)}{2}}(\overline{\sigma_T})\times \overset{\circ}{C}{}_{t}^{\,\frac{(1+l)}{2}}(\overline{\sigma_T})\times \overset{\circ}{C}{}_{t}^{\,\frac{(1+l)}{2}}(\overline{\sigma_T})$$

$$H(\Omega_T)$$

is the space of vector-functions $h=(f_1, f_2, f_3, f_4, p_1, p_2, q_1, q_2, \eta_0, \eta_1, \eta_2, g_1, \kappa g_2, g_3, \varepsilon g_4)$wit h the norm

$$\|h\|_{H(\Omega_T)}=\sum_{j=1}^{2}\left(|f_j|_{\Omega_{jT}}^{(l)}+|f_{j+2}|_{\Omega_{jT}}^{(l)}+|p_j|_{\sigma_T}^{\left(1+\frac{l}{2}\right)}+|q_j|_{\sigma_T}^{\left(1+\frac{l}{2}\right)}\right)+$$
$$+\sum_{k=0}^{2}|\eta_k|_{\sigma_T}^{\left(1+\frac{l}{2}\right)}+|g_1|_{\sigma_T}^{\frac{1+l}{2}}+\kappa|g_2|_{\sigma_T}^{\frac{1+l}{2}}+|g_3|_{\sigma_T}^{\frac{1+l}{2}}+\varepsilon|g_4|_{\sigma_T}^{(1+l)/2}. \quad (12)$$

It is required fulfillment of the conditions for matching the initial and boundarydata for solving boundary value problems for parabolic equations in a Holder space.

We define these conditions for the problem (1)–(9) [8]. They are found from the boundary conditions (4)–(9) by differentiating them by t, excluding thederivatives $\partial_t^p v_j, \partial_t^p z_j, j=1,2, p=0,1,\dots,$ found from the equations (1), (2), and using the initial conditions (3). Find them.

From the equations (1), (2) we find the time derivatives

$$\partial_t v_j = A_j(x,t;\partial_x)v_j+\alpha_j(x,t)\chi(x-\rho_0)D_t\psi+ +f_j(x,t),\ \ j=1,2, \quad (13)$$

$$\partial_t z_j = A_{j+2}(x,t;\partial_x)z_j+\beta_j(x,t)\chi(x-\rho_0)D_t\psi+ +f_{j+2}(x,t),\ \ j=1,2, \quad (14)$$

we substitute them into the boundary and conjugation conditions (4)–(7).

By virtue of the initial conditions (3) we have

$$\partial_x^2 v(x,t)|_{t=0}=v_0''(x),$$
$$\partial_x v(x,t)|_{t=0}=v_0'(x),$$
$$v(x,t)=|_{t=0}=v_0(x).$$

The zero order matching conditions will be

$$v_{01}(0,0)=p_1(0), \qquad z_{01}(0,0)=q_1(0),$$
$$v_{02}(b,0)=p_2(0), \qquad z_{02}(b,0)=q_2(0),$$

for$x=0,\ x=b$and

$$v_{01}(\rho_0,0)-v_{02}(\rho_0,0)=\eta_0(0),$$

$$z_{0j}(\rho_0,0)-\gamma_{0j}(\rho_0,0)(\rho_0,0)v_{0j}(\rho_0,0)= =\eta_j(0),\ \ j=1,2,$$

$$\begin{pmatrix}\lambda_1(\rho_0,0)\partial_x v_{01}(x,0)-\\ -\kappa\lambda_2(\rho_0,0)\partial_x v_{02}(x,0)\end{pmatrix}|_{x=\rho_0}= =g_1(0)+\kappa g_2(0),$$

$$\begin{pmatrix}k_1(\rho_0,0)\partial_x z_{01}(x,0)-\\ \backslash -\varepsilon k_2(\rho_0,0)\partial_x z_{02}(x,0)\end{pmatrix}|_{x=\rho_0}= =g_3(0)+\varepsilon g_4(0)$$

for$x=\rho_0$.

To obtain the first order matching condition, let us differentiate the boundary and conjugation conditions (4)–(7) with respect to the variable t, taking intoaccount (13), (14).

The first order matching conditions for $x=\rho_0$ are

$$\big(A_1v_{01}(x,0)-A_2v_{02}(x,0)\big)|_{x=\rho_0}+ +\big(\alpha_1(\rho_0,0)-\alpha_2(\rho_0,0)\big)D_t\psi|_{t=0}+ +f_1(\rho_0,0)-f_2(\rho_0,0)=D_t\eta_0(0), \quad (15)$$

$$A_{j+2}z_{0j}(x,0)|_{x=\rho_0}+\beta_j(\rho_0,0)D_t\psi|_{t=0}+ +f_{j+2}(\rho_0,0)-\gamma_j(\rho_0,0)(A_jv_{0j}(x,0)|_{x=\rho_0}+ +\alpha_j(\rho_0,0)D_t\psi|_{t=0}+f_j(\rho_0,0))= =D_t\eta_j(0),\ j=1,2. \quad (16)$$

Find the $D_t\psi|_{t=0}$from formulas (15) and (16)

$$D_t\psi|_{t=0} := \frac{D_t\eta_0(0) - \left(A_1 v_{01}(x,0) - A_2 v_{02}(x,0)\right)|_{x=\rho_0} - f_1(\rho_0,0) + f_2(\rho_0,0)}{\alpha_1(\rho_0,0) - \alpha_2(\rho_0,0)}, \qquad (17)$$

and

$$D_t\psi|_{t=0} := \frac{D_t\eta_j(0) - A_{j+2} z_{0j}(x,0)|_{x=\rho_0} - f_{j+2}(\rho_0,0) + \gamma_j(\rho_0,0)(A_j v_{0j}(x,0)|_{x=\rho_0} - f_j(\rho_0,0)}{\beta_j(\rho_0,0) - \gamma_j(\rho_0,0)\alpha_j(\rho_0,0)}, \qquad (18)$$

where $|\alpha_1(\rho_0,0) - \alpha_2(\rho_0,0)| > 0, \left|\beta_j(\rho_0,0) - \gamma_j(\rho_0,0)\alpha_j(\rho_0,0)\right| > 0,\ j = 1,2.$

Equating the found derivatives (17), (18) , we get the matching condition

$$D_t\psi|_{t=0} \equiv \frac{D_t\eta_0(0) - \left(A_1 v_{01}(x,0) - A_2 v_{02}(x,0)\right)|_{x=\rho_0} - f_1(\rho_0,0) + f_2(\rho_0,0)}{\alpha_1(\rho_0,0) - \alpha_2(\rho_0,0)} =$$

$$= \frac{D_t\eta_j(0) - A_{j+2} z_{0j}(x,0)|_{x=\rho_0} - f_{j+2}(\rho_0,0) + \gamma_j(\rho_0,0)(A_j v_{0j}(x,0)|_{x=\rho_0} - f_j(\rho_0,0)}{\beta_j(\rho_0,0) - \gamma_j(\rho_0,0)\alpha_j(\rho_0,0)}, j = 1,2.$$

We say that for the problem (4)−(7) the conditions for matching the order of$p$ are satisfied if the equalities

$$\partial_t^p v_1(x,t)|_{x=0,t=0} = D_t^{(p)} p_1(0),$$
$$\partial_t^p z_1(x,t)|_{x=0,t=0} = D_t^{(p)} q_1(0),$$

$$\partial_t^p v_2(x,t)|_{x=b,t=0} = D_t^{(p)} p_2(0),$$
$$\partial_t^p z_2(x,t)|_{x=b,t=0} = D_t^{(p)} q_2(0),$$

$$\left(\partial_t^p v_1(x,t) - \partial_t^p v_2(x,t)\right)|_{x=\rho_0,t=0} = D_t^{(p)}\eta_0(0),$$
$$p = 0, \dots, 1 + [l/2],$$

$$\left(\partial_t^p z_j(x,t) - \gamma_j(x,t)\partial_t^p v_j(x,t)\right)|_{x=\rho_0,t=0}$$
$$= D_t^{(p)}\eta_j(0), j = 1,2, p = 0, \dots, 1 + [l/2]$$

take place.

Here the derivatives $\partial_t^p v_j$, $\partial_t^p z_j, j = 1,2$, are determined by the recurrence formulas:

$$\partial_t v_j = A_j(x,t;\partial_x)v_j$$
$$+\alpha_j(x,t)\chi(x-\rho_0)D_t\psi + f_j(x,t),$$

$$\partial_t^2 v_j = \partial_t\left(\partial_t v_j\right) = \partial_t A_j v_j + A_j\partial_t v_j +$$
$$+ \partial_t\alpha_j(x,t)\chi(x-\rho_0)D_t\psi(t) +$$

$$+\alpha_j(x,t)\chi(x-\rho_0)D_t^2\psi(t) + \partial_t f_j(x,t),$$

$$\dots$$

$$\partial_t^p v_j = \partial_t\left(\partial_t^{p-1}v_j\right) = \partial_t^{p-1}A_j v_j +$$
$$+(p-1)\partial_t^{p-2}A_j\partial_t v_j + \dots + A_j\partial_t^{p-1}v_j +$$
$$+\partial_t^{p-1}\alpha_j(x,t)\chi(x-\rho_0)D_t\psi +$$
$$+(p-1)\partial_t^{p-2}\alpha_j(x,t)\chi(x-\rho_0)D_t^2\psi(t) + \dots +$$
$$+\alpha_j(x,t)\chi(x-\rho_0)D_t^p\psi(t) + \partial_t^{p-1}f_j(x,t),$$

$$\partial_t^p z_j = \partial_t\left(\partial_t^{p-1}z_j\right) = \partial_t^{p-1}A_{j+2}z_j +$$
$$+(p-1)\partial_t^{p-2}A_{j+2}\partial_t z_j + \dots + A_{j+2}\partial_t^{p-1}z_j +$$
$$+\partial_t^{p-1}\beta_j(x,t)\chi(x-\rho_0)D_t\psi +$$
$$+(p-1)\partial_t^{p-2}\beta_j(x,t)\chi(x-\rho_0)D_t^2\psi(t) + \dots +$$
$$+\beta_j(x,t)\chi(x-\rho_0)D_t^p\psi(t) + \partial_t^{p-1}f_{j+2}(x,t).$$

We rewrite the problem (1)−(9) in the operator form

$$Aw = h, \qquad (19)$$

where the operator A is defined by the expressions in the left parts of the equationsand conjugation conditions problem (1)−(9).

We will assume that the following conditions:

$$a) a_j(x,t), a_{j+2}(x,t), b_j(x,t), b_{j+2}(x,t),$$
$$d_j(x,t), d_{j+2}(x,t), \alpha_j(x,t), \beta_j(x,t)$$
$$\in C_{x\,t}^{l,l/2}(\overline{\Omega}_{jT}), \gamma_j(x,t) \in C_{x\,t}^{1+l/2}(\overline{\sigma}_T),$$
$$\lambda_j(x,t), k_j(x,t) \in C_{x\,t}^{(1+l)/2}(\overline{\sigma}_T),$$
$$j = 1,2, \alpha = l - [l] \in (0,1);$$

$b)$ $(\alpha_1(x,t)-\alpha_2(x,t))|_{x=\rho_0} \geq d_4 = const >$ $> 0, t \in \bar{\sigma}_T, (\beta_j(x,t)-\gamma_j(x,t)\alpha_j(x,t))|_{x=\rho_0} \geq$ $\geq d_5 = const > 0, j = 1,2, t \in \bar{\sigma}_T, (\beta_{3-j}(x,t) -$ $-\gamma_{3-j}(x,t)\alpha_j(x,t))|_{x=\rho_0} \geq d_6 = const >$ $> 0, j = 1,2, t \in \bar{\sigma}_T$ are fulfilled.

2 Main results

Theorem 1. Let$0 \leq \kappa \leq \kappa_0, 0 < \varepsilon \leq \varepsilon_0$ or $0 < \kappa \leq \kappa_0, 0 \leq \varepsilon \leq \varepsilon_0$ and conditions $a)$, $b)$ are fulfilled.

For any functions $f_j(x,t) \in \overset{\circ}{C}{}^{l,l/2}_{x\,t}(\overline{\Omega}_{jT})$, $f_{j+2}(x,t) \in \overset{\circ}{C}{}^{l,l/2}_{x\,t}(\overline{\Omega}_{jT})$, $v_{0j}(x) \in \overset{\circ}{C}{}^{2+l}_{x}(\overline{\Omega}_j)$, $z_{0j}(x) \in \overset{\circ}{C}{}^{2+l}_{x}(\overline{\Omega}_j)$, $p_j(t)$, $q_j(t) \in \overset{\circ}{C}{}^{1+l/2}_{t}(\overline{\sigma}_T)$, $j = 1,2$, $\eta_k(t) \in \overset{\circ}{C}{}^{1+l/2}_{t}(\overline{\sigma}_T)$, $k = 0,1,2; g_1(t)$, $\kappa g_2(t), g_3(t), \varepsilon g_4(t) \in C^{(1+l)/2}_{x\,t}(\overline{\sigma}_T)$, problem (1)-(9) has a unique solution $v_j(x,t) \in \overset{\circ}{C}{}^{2+l,1+l/2}_{x\quad t}(\overline{\Omega}_{jT})$, $z_j(x,t) \in \overset{\circ}{C}{}^{2+l,1+l/2}_{x\quad t}(\overline{\Omega}_{jT})$, $\psi(t) \in \overset{\circ}{C}{}^{1+l/2}_{t}(\overline{\sigma}_T)$ and following estimate is true

$$\|w\|_{B(\Omega_T)} \equiv \sum_{j=1}^{2}\left(|v_j|^{(2+l)}_{\Omega_{jT}} + |z_j|^{(2+l)}_{\Omega_{jT}}\right) + |\psi|^{\left(1+\frac{l}{2}\right)}_{\sigma_T} \leq$$
$$\leq C_1\left(\sum_{j=1}^{2}\left(|f_j|^{(l)}_{\Omega_{jT}} + |f_{j+2}|^{(l)}_{\Omega_{jT}} + |v_{0j}|^{(2+l)}_{\Omega_j} + |z_{0j}|^{(2+l)}_{\Omega_j} + |p_j|^{(1+l/2)}_{\sigma_T} + |q_j|^{(1+l/2)}_{\sigma_T}\right) + \right.$$
$$\left. + \sum_{k=0}^{2}|\eta_k|^{(1+l/2)}_{\sigma_T} + |g_1|^{(1+l)/2}_{\sigma_T} + \kappa|g_2|^{(1+l)/2}_{\sigma_T} + |g_3|^{(1+l)/2}_{\sigma_T} + \varepsilon|g_4|^{(1+l)/2}_{\sigma_T}\right), \tag{20}$$

where C_1 does not depend on κ and ε.

Proof. The existence of the solution is proved by constructing the regularizer [8], and the estimate (20) is proved by the Schauder method.

We cover the domain Ω with intervals $K^{(i)}_{\delta}, K^{(i)}_{2\delta}$ with common center ξ_i.Let $\zeta_i(x)$, $\mu_i(x)$ be smooth shear functions subject to the covering domains Ωsuch that $\zeta_i(x) = 1$, if $|x-\xi_i| \leq \delta$ and $\zeta_i(x) = 0$, if $|x-\xi_i| \geq 2\delta$, and with properties $\sum_i \zeta_i(x)\ \mu_i(x) = 1$ and $|D_m\zeta_i|$, $|D_m\mu_i| \leq C_{m,i}\delta^{-m}$. Denote the intervals asfollows: for$i \in \aleph_1$ intervals $K^{(i)}_{\delta}$contain a point ρ_0, for$i \in \aleph_2$ and $i \in \aleph_3$ intervals $K^{(i)}_{2\delta}$ adjoin the boundary of the domain $x = 0$ and $x = l$ accordingly, with $i \in \aleph_4$ intervals $K^{(i)}_{2\delta}$ are entirely contained in $\Omega_1 \cup \Omega_2$.

Note that for the equations (1), (2) $\chi(x-\rho_0) = 1$, $i \in \aleph_1$ and $\chi(x-\rho_0) = 0$ at $i \in \aleph_2 \cup \aleph_3$, $\delta_0 \leq \delta$.

We define the regularizer $\mathfrak{R}$ by formula

$$\mathfrak{R}h = \{\mathfrak{R}_1 h, \mathfrak{R}_2 h, \mathfrak{R}_3 h, \mathfrak{R}_4 h, \mathfrak{R}_5 h\} =$$
$$= \left\{\sum_{i\in\aleph}\mu_i(x)v_{1,i}(x,t), \sum_{i\in\aleph}\mu_i(x)v_{2,i}(x,t), \sum_{i\in\aleph}\mu_i(x)z_{1,i}(x,t), \sum_{i\in\aleph}\mu_i(x)z_{2,i}(x,t), \sum_{i\in\aleph_1}\mu_i(x)\psi_i(t)\right\},$$

where $\aleph := \aleph_1 \cup \aleph_2 \cup \aleph_3 \cup \aleph_4$, are functions $v_{j,i}(x,t), z_{j,i}(x,t), j = 1,2, \psi_i(t)$ satisfy zero initial data and are defined as solutions model conjugation problem for$i \in \aleph_1$, the first boundary value problem for$i \in \aleph_2 \cup \aleph_3$ and Cauchy problem with$i \in \aleph_4$.

Let

$$D_{jT}^{(i)} = D_j^{(i)} \times (0,T), K_{2\delta T}^{(i)} = \\ = \left(K_{2\delta}^{(i)} \cap (\Omega_1 \cup \Omega_2)\right) \times (0,T).$$

1. Let $i \in \aleph_1$. Perform a coordinate transformation $x = Y_i^{-1}(y): x = y + \rho_0$. This conversion translates areas $x < \rho_0, D_1^{(i)} = \{y \mid y < 0\}$ and $x > \rho_0$ into $D_2^{(i)} = \{y \mid y > 0\}$.

Set $\zeta_i(x) f_j(x,t),\ \zeta_i(x) g_j(x,t)|_{x=Y_i^{-1}(y)} =$

$$= f_{j,i}(y,t), f_{j+2,i}(y,t);\ \zeta_i(x)p_1(t)|_{x=0}, \\ \zeta_i(x)p_2(t)|_{x=l}, \zeta_i(x)q_1(t)|_{x=0}, \\ \zeta_i(x)q_2(t)|_{x=l} = p_{j,i}(t), q_{j,i}(t), \\ \zeta_i(x)\eta_j(t)|_{x=\rho_0} = \eta_{j,i}(t), j = 1,2, \zeta_i(x)g_1(t), \\ \zeta_i(x)\kappa g_2(t), \zeta_i(x)g_3(t), \zeta_i(x)\varepsilon g_4(t) = \\ = g_{1,i}(t), \kappa g_{2,i}(t), g_{3,i}(t), \varepsilon g_{4,i}(t)$$

and continue the functions$f_{j,i}, f_{j+2,i}$zero in$D_j^{(i)}$.

We define the functions $v'_{j,i}(y,t), z'_{j,i}(y,t)$, $j = 1,2$, $\psi_i(t)$ as a solution to thefollowing conjugation problem:

$$\partial_t v'_{j,i} - a_j(\xi_i,0)\partial_y^2 v'_{j,i} - \\ -\alpha_j(\xi_i,0)\chi(\xi_i)D_t\psi_i == f_{j,i}(y,t) \text{in} D_{jT}^{(i)}, \\ j = 1,2, \tag{21}$$

$$\partial_t z'_{j,i} - a_{j+2}(\xi_i,0)\partial_y^2 z'_{j,i} - \\ -\beta_j(\xi_i,0)\chi(\xi_i)D_t\psi_i = f_{j+2,i}(y,t) \text{in} D_{jT}^{(i)}, \\ j = 1,2, \tag{22}$$

$$\left(z'_{j,i} - \gamma_j(\xi_i,0)v'_{j,i}\right)|_{y=0} = \eta_{j,i}(t),\ j = 1,2, \tag{23}$$

$$\left(\lambda_1(\xi_i,0)\partial_x v'_{1,i} - \kappa\lambda_2(\xi_i,0)\partial_x v'_{2,i}\right)|_{y=0} = \\ = g_{1,i}(t) + \kappa g_{2,i}(t), \tag{24}$$

$$\left(k_1(\xi_i,0)\partial_x z'_{1,i} - \varepsilon k_2(\xi_i,0)\partial_x z'_{2,i}\right)|_{y=0} = \\ = g_{3,i}(t) + \varepsilon g_{4,i}(t). \tag{25}$$

In [1], Theorem was proved.

Theorem 2. Let$0 < \kappa \le \kappa_0, 0 < \varepsilon \le \varepsilon_0$ and be executed conditions $a), b)$.

For any functions $f_{j,i}(y,t) \in \overset{\circ}{C}{}_{x\,t}^{\,l,l/2}(\overline{D}_{jT}^{(i)})$,

$$f_{j+2,i}(x,t) \in \overset{\circ}{C}{}_{x\,t}^{\,l,l/2}(\overline{D}_{jT}^{(i)}), \\ \eta_{j,i}(t) \in \overset{\circ}{C}{}_{t}^{\,1+l/2}(\overline{\sigma}_T), \\ j = 1,2, g_{1,i}(t) \in \overset{\circ}{C}{}_{t}^{\,(1+l)/2}(\overline{\sigma}_T), \\ \kappa g_2(t) \in \overset{\circ}{C}{}_{t}^{\,(1+l)/2}(\overline{\sigma}_T), g_3(t) \in \overset{\circ}{C}{}_{t}^{\,(1+l)/2}(\overline{\sigma}_T), \\ \varepsilon g_4(t) \in \overset{\circ}{C}{}_{t}^{\,(1+l)/2}(\overline{\sigma}_T),$$

problem (21)-(25) has a unique solution $v'_{j,i} \in \overset{\circ}{C}{}_{x\ \ t}^{\,2+l,1+l/2}(\overline{D}_{jT}^{(i)}), z'_{j,i} \in \overset{\circ}{C}{}_{x\ \ t}^{\,2+l,1+l/2}(\overline{D}_{jT}^{(i)})$, $\psi_i(t) \in \overset{\circ}{C}{}_{t}^{\,1+l/2}(\overline{\sigma}_T)$, and following estimate is true

$$\sum_{j=1}^{2}\left(\left|v'_{j,i}\right|_{D_{jT}^{(i)}}^{(2+l)} + \left|z'_{j,i}\right|_{D_{jT}^{(i)}}^{(2+l)}\right) + |\psi_i|_{\sigma_T}^{\left(1+\frac{l}{2}\right)} \le C_2 \sum_{j=1}^{2}\left(\left|f_{j,i}\right|_{D_{jT}^{(i)}}^{(l)} + \left|f_{j+2,i}\right|_{D_{jT}^{(i)}}^{(l)} + \left|\eta_{j,i}\right|_{\sigma_T}^{\left(1+\frac{l}{2}\right)} + \left|g_{1,i}\right|_{\sigma_T}^{\frac{1+l}{2}} + \right. \\ \left. + \kappa\left|g_{2,i}\right|_{\sigma_T}^{(1+l)/2} + \left|g_{3,i}\right|_{\sigma_T}^{(1+l)/2} + \varepsilon\left|g_{4,i}\right|_{\sigma_T}^{(1+l)/2}\right), \tag{26}$$

where C_2 does not depend on κ and ε.

The functions $v'_{j,i}(y,t), z'_{j,i}(y,t), j = 1,2$, are defined as asolution of the first boundaryvalue problems $i \in \aleph_2 \cup \aleph_3$, and functions $v_{j,i}(y,t), z_{j,i}(y,t), j = 1,2$ with $i \in \aleph_4$ are solution of Cauchy problem. Each of these problems under the conditions of the Theorem 2has a unique solution and it is subject to estimates (27), (28) [8]

$$\left|v_{j,i}\right|_{K_{2\delta T}^{(i)}}^{(2+l)} \le C_3\left(\left|\zeta_i(x)f_j\right|_{K_{2\delta T}^{(i)}}^{(l)} + \left|\zeta_i(x)p_j\right|_{\sigma_T}^{\left(1+\frac{l}{2}\right)}\right), \\ i \in \aleph_2 \cup \aleph_3, j = 1,2,$$

$$\left|z_{j,i}\right|_{K_{2\delta T}^{(i)}}^{(2+l)} \le C_4\left(\left|\zeta_i(x)g_j\right|_{K_{2\delta T}^{(i)}}^{(l)} + \left|\zeta_i(x)q_j\right|_{\sigma_T}^{\left(1+\frac{l}{2}\right)}\right), \\ i \in \aleph_2 \cup \aleph_3, j = 1,2, \tag{27}$$

$$\left|v_{j,i}\right|^{(2+l)}_{K^{(i)}_{2\delta T}} \le C_5\left|\zeta_i(x)f_j\right|^{(l)}_{K^{(i)}_{2\delta T}},$$
$$\left|z_{j,i}\right|^{(2+l)}_{K^{(i)}_{2\delta T}} \le C_6\left|\zeta_i(x)f_{j+2}\right|^{(l)}_{K^{(i)}_{2\delta T}},$$
$$i \in \aleph_4,\ j = 1,2. \tag{28}$$

We introduce the norm [1]

$$\{w\}_{B(\Omega_T)} = \sup_i \|w\|_{B\left(K^{(i)}_{2\delta T}\right)},$$
$$\{h\}_{H(\Omega_T)} = \sup_i \|h\|_{H(K^{(i)}_{2\delta T})}, \tag{29}$$

where $K^{(i)}_{2\delta T} = (K^{(i)}_{2\delta} \cap (\Omega_1 \cup \Omega_2)) \times (0,T)$. The norms of $\{w\}_{B(\Omega_T)}, \{h\}_{H(\Omega_T)}$ are defined by formulas (11), (12). Note that the norms (29) are equivalent to the norms $\|w\|_{B(\Omega_T)}, \|h\|_{H(\Omega_T)}$[8].

Lemma 2. The operator $\Re := H(\Omega_T) \to B(\Omega_T)$ is bounded: $\{\Re h\}_{B(\Omega_T)} \le C_7\{h\}_{H(\Omega_T)}$.

Let us turn to the problem (1)-(9), which we recorded in operator form (19) $Aw = h$. Obviously, $A: B(\Omega_T) \to H(\Omega_T)$.

Lemma 3. For any $h \in H(\Omega_T)$, the equality $A\Re h = h + Ph$, takes place. Here $Ph = \{P_1h, P_2h, P_3h, P_4h, 0,0,0,0,0, P_5h, P_6h, P_7h, P_8h\}$, $P_jh, P_{j+2}h, P_{4+j}h, j = 1,2, P_7h, P_8h$ contain lower terms or higher terms with small coefficients.

Forexample,

$$P_jh = -\sum_{i\in\aleph} \mu_i(x)\big(b_j(x,t)\partial_x v_j + d_j(x,t)v_j\big) - a_j(x,t)\sum_{i\in\aleph}\left(\partial_x^2\,\mu_i(x)v_{j,i}(x,t) + 2\partial_x\mu_i(x)\partial_x v_{j,i}(x,t)\right) -$$
$$-\sum_{i\in\aleph} \mu_i(x)\left[a_j(x,t) - a_j(\xi_i,0)\right]\partial_x^2 v'_{j,i}(x,t) - \sum_{i\in\aleph_1}\mu_i(x)\left[a_j(x,t)\chi(x-\rho_0) - a_j(\xi_i,0)\chi(\xi_i-\rho_0)\right]D_t\psi_i,$$
$$j = 1,2.$$

Lemma 4. Under the conditions of the Theorem 1 for $t \le T_0$estimate

$$\{Ph\}_{H(\Omega_T)} \le æ\{h\}_{H(\Omega_T)} \tag{30}$$

is fulfilled, where $æ \in (0,1)$.

Lemma 5. Under the conditions of the Theorem 2 there exists for $t \le T_0$ bounded right inverse operator $A_r^{-1} = \Re(E+P)^{-1}: H(\Omega_{T_0}) \to B(\Omega_{T_0})$, where E is the unit operator.

Proof. We have the problem $Aw = h$. Substituting $\Re h$ instead of w, we get $A\Re h = h + Ph \equiv (E+P)h$. Let $(E+P)h = h_1$, where $h_1 \in H(\Omega_{T_0})$. Accordingto the assessment (30) this equation has a unique solution $h \in H(\Omega_{T_0})$, which is subject to estimate $\{h\}_{H(\Omega_{T_0})} \le \frac{1}{1-æ}\{h_1\}_{H(\Omega_{T_0})}$ for anyone vector $h_1 \in H(\Omega_{T_0})$. Then there is a limited the inverse operator $(E+P)^{-1}$ in the space $H(\Omega_{T_0})$. Substituting $h = (E+P)^{-1}h_1$ into the equation $A\Re h = h_1 \equiv h + Ph$, we get the identity $A\Re(E+P)^{-1}h_1 = h_1$ for any $h_1 \in H(\Omega_{T_0})$ or $A\Re(E+P)^{-1} = E$. According to the definition implies that the operator A has the right inverse of the bounded operator $A_r^{-1} = \Re(E+P)^{-1}$, and the problem $Aw = h$ has the solution $w = (v_1, v_2, z_1, z_2, \psi) \in B(\Omega_{T_0})$ for any vector $h \in H(\Omega_{T_0})$.

We obtain an estimate for the solution of the problem (1)-(9) using the Schauder method. Consider the functions of $v_{j,i}(x,t) = \mu_i(x)v_j(x,t), z_{j,i}(x,t) = \mu_i(x)z_j(x,t)$, $j = 1,2, \psi_i(t) = \mu_i(x)\,\psi(t)$, which are defined in $K^{(i)}_{2\delta} \times (0,T_0)$ and extend them by zero outside this area. Depending on the location of the interval $K^{(i)}_{2\delta}$ in Ω for functions $v_{j,i}(x,t), z_j(x,t), j = 1,2, \psi_i(t)$ from the problem (1)−(9) the model pairing problem, the first boundary value problem, and the Cauchyproblem can be obtained.

Multiply parabolic equations and problem conditions (1)−(9) on the cutting function $\mu_i(x)$. In the equations and conditions we will make transformations coordinates $x = Y_i^{-1}(y): x = y + \rho_0$ as $i \in \aleph_1$ for functions $v'_{j,i}(y,t) = v_{j,i}(x,t)|_{x=Y_i^{-1}(y)}, z'_{j,i}(y,t) = z_{j,i}(x,t)|_{x=Y_i^{-1}(y)}$, $j = 1,2, \psi_i(t)$ we get the conjugation problem with zero initial data in $D^{(i)}_{jT}, j = 1,2,$

$$\partial_t v'_{j,i} - a_j(\xi_i,0)\partial_y^2 v'_{j,i} - \alpha_j(\xi_i,0)\chi(\xi_i)D_t\psi_i = f'_{j,i}(y,t) + Y_i^{-1}(y)F_{j,i}(x,t),$$

$$\partial_t z'_{j,i} - a_{j+2}(\xi_i,0)\partial_y^2 z'_{j,i} - \beta_j(\xi_i,0)\chi(\xi_i)D_t\psi_i = f'_{j+2,i}(y,t) + Y_i^{-1}(y)F_{j,i}(x,t),$$

$$\left(z'_{j,i} - \gamma_j(\xi_i,0)v'_{j,i}\right)|_{y=0} = \eta_{j,i}(t) + Y_i^{-1}(y)H_{j,i}(x,t),\ j=1,2, \tag{31}$$

$$\left(\lambda_1(\xi_i,0)\partial_y v'_{1,i} - \kappa\lambda_2(\xi_i,0)\partial_y v'_{2,i}\right)|_{y=0} = g_{1,i}(t) + \kappa g_{2,i}(t) + Y_i^{-1}(y)H_{3,i}(x,t),$$

$$\left(k_1(\xi_i,0)\partial_x z'_{1,i} - \varepsilon k_2(\xi_i,0)\partial_x z'_{2,i}\right)|_{y=0} = g_{3,i}(t) + \varepsilon g_{4,i}(t) + Y_i^{-1}(y)H_{4,i}(x,t),$$

where $f'_{j,i}(y,t) = f_{j,i}(x,t)|_{x=Y_i^{-1}(y)}$, $f'_{j+2,i}(y,t) = f_{j+2,i}(x,t)|_{x=Y_i^{-1}(y)}$, $F_{j,i}(x,t)$, $F_{j+2,i}(x,t)$, $j=1,2, H_{j,i}(x,t)$, $H_{3,i}(x,t)$, $H_{4,i}(x,t)$, contain smallest coefficients or leading coefficients with small coefficients.

The conjugation problem (31), according to Theorem 2, uniquely solvable and for it's solution estimate (26) holds. Therefore, solutionof the problem (31)obeys the inequality

$$\sum_{j=1}^{2}\left(|v'_{j,i}|_{K_{2\delta T}^{(i)}}^{(2+l)} + |z'_{j,i}|_{K_{2\delta T}^{(i)}}^{(2+l)}\right) + |\psi_i|_{\sigma_T}^{\left(1+\frac{l}{2}\right)} \le C_8 \sum_{j=1}^{2}\Bigg(|f_{j,i}|_{K_{2\delta T}^{(i)}}^{(l)} + |f_{j+2,i}|_{K_{2\delta T}^{(i)}}^{(l)} + |\eta_{j,i}|_{\sigma_T}^{\left(1+\frac{l}{2}\right)} + |g_{1,i}|_{\sigma_T}^{\left(\frac{1+l}{2}\right)} +$$

$$+\kappa|g_{2,i}|_{\sigma_T}^{(1+l)/2} + |g_{3,i}|_{\sigma_T}^{(1+l)/2} + \varepsilon|g_{4,i}|_{\sigma_T}^{(1+l)/2} + |F_{j,i}|_{K_{2\delta T}^{(i)}}^{(l)} + |F_{j+2,i}|_{K_{2\delta T}^{(i)}}^{(l)} +$$

$$+|H_{j,i}(x,t)|_{\sigma_T}^{\left(1+\frac{l}{2}\right)} + |H_{j+2,i}(x,t)|_{\sigma_T}^{\left(1+\frac{l}{2}\right)}\Bigg), j=1,2, \tag{32}$$

where C_8 does not depend on κ and ε.

We also get the functions $v'_{j,i}(y,t)$, $z'_{j,i}(y,t), j=1,2$ as solutions of the firstboundary value problems for $i \in \aleph_2 \cup \aleph_3$, and functions $v_{j,i}(x,t), z_j(x,t), j=1,2$ for $i \in \aleph_4$ as the is solution of the Cauchy problems. Based on [1], the firstboundary problem and the Cauchy problem are uniquely solvable. To solve the first boundary problem and the problem Cauchy valid estimates similar to those

estimated. (27), (28) and (32), as well as similar functions arising in right partsof the equations of the first boundary value problems and the Cauchy problem.

The norms of the functions $F_{j,i}(x,t)$, $F_{j+2,i}(x,t)$, $H_{j,i}(x,t)$, $H_{j+2,i}(x,t)$, $j=1,2,$ are estimated the same way as with the proof of Lemma 3 norms of operators $P_j h, P_{j+2}h, P_{4+j}h, j=1,2, P_7 h, P_8 h$. Moreover, if note that in the interval $K_\delta^{(i)}$ the cutoff function $\mu_i(x)=1$, then in $K_\delta^{(i)} \times (0,T), v_{j,i} := \mu_i v_j = v_j, z_{j,i} := \mu_i z_j = z_j, \psi_i := \mu_i\psi = \psi$.

Using estimates of solutions of the conjugation problem (32), the first boundaryproblems and Cauchy problems we will have inequality

$$\|\mu_i w\|_{B\left(K_{2\delta t}^{(i)}\right)} \le C_9\|\mu_i h\|_{H\left(K_{2\delta t}^{(i)}\right)} + \\ +æ_1\|\mu_i w\|_{B\left(K_{2\delta t}^{(i)}\right)},$$

$$K_{2\delta t}^{(i)} = \left(K_{2\delta}^{(i)} \cap (\Omega_1 \cap \Omega_2)\right) \times (0,t), æ_1 \in (0,1).$$

Hence, we get

$$\|\mu_i w\|_{B\left(K_{2\delta t}^{(i)}\right)} \le \frac{C_9}{1-æ_1}\|\mu_i h\|_{H\left(K_{2\delta t}^{(i)}\right)}, \\ æ_1 \in (0,1), \tag{33}$$

where $K_{\delta t}^{(i)} = \left(K_\delta^{(i)} \cap (\Omega_1 \cap \Omega_2)\right) \times (0,t)$.

We proceed in the inequality (33) to the supremum on i, taking into accountthe definitions of the norms $\{w\}_{B(\Omega_{T_1})}$ and $\{h\}_{H(\Omega_{T_1})}$ in (29), as a result get anestimate

$$\{w\}_{B(\Omega_{T_1})} \leq C_{10}\{h\}_{H(\Omega_{T_1})}.$$

From this inequality, by virtue of the equivalence of norms $\{w\}_{B(\Omega_{T_1})}, \{h\}_{H(\Omega_{T_1})}$ and $\|w\|_{B(\Omega_{T_1})}, \|h\|_{H(\Omega_{T_1})}$, follows the evaluation of the solution to the problem (1)−(9)

$$\|w\|_{B(\Omega_{T_1})} \leq C_{11}\|h\|_{H(\Omega_{T_1})}. \quad (34)$$

The problem (1)−(9) is linear problem. The uniqueness of the solution followsfrom the evaluation (34). We proved the existence and uniqueness of the solutionof the problem (1)−(9) for $t \leq \min(T_0, T_1)$. Continuing the solution by t as in [8], we obtain Theorem 1 for $T > 0$.

References

1. Dzhobulaeva Zh.K. The estimates of the solution of the model problem for the system ofthe parabolic equations in the Holder space, *Matem. zhurnal*, 18, 2 (2018), 71-86 (inrussian).

2. Rodrigues J.F., Solonnikov V.A., Yi F.On a parabolic system with time derivative in theboundary conditions and related free boundary problems, *Math. Ann.,* 315 (1999), 61-95.

3. BizhanovaG.I. On the Stefan problem with the small parameter, *Banach Center Publications,*81 (2008), 43-63.

4. Bizhanova G.I. On the solutions of the linear free boundary problems of Stefan type with a small parameter. II, *Matem. zhurnal,*1 (2012), 70-86.

5. Alimzhanov E.S. The solution of the *Verigin model problem with a small parameter in the Holder space, KazNU* Bulletin, ser. mat., fiz., inf., 3, 78 (2013), 19-32 (inrussian).

6. Bizhanova G.I. Solution of a model problem *related to singularly perturbed, free boubdary, Stefan type problems, Zapiski*nauchn.semin. POMI, 362 (2008), 64-91.

7. Bizhanova G.I. On the solutions of the linear free boundary problems of Stefan type with a small parameter I, *Matem. zhurnal*, 12, 1 (2012), 24-37.

8. Ladyzhenskaya O.A., Solonnikov V.A., Ural'tseva N.N. Linear and Quasilinear Equationsof Parabolic Type, *Nauka, Moscow*, (1967).

IRSTI 89.57.35 89.25.00 https://doi.org/10.26577/ijmph.2020.v11.i1.06

[1]Z.B. Rakisheva, [2] N. Delpeche-Ellmann, [1] A.K. Sakhayeva

[1]Al-Farabi Kazakh National University, Almaty, Kazakhstan,
e-mail: zaure.rakisheva@kaznu.
[2] Institute of Cybernetics at Tallinn University of Technology, Tallinn, Estonia,
e-mail: nicole.delpeche@gmail.com

STUDYING UPWELLING PHASES IN THE KAZAKHSTAN PART OF THE CASPIAN SEA

Abstract. The process of upwelling is the rise of cold water masses to the surface of the reservoir and is the subject of study around the world, because this process affects many water parameters. Upwelling increases biological productivity and provides nutrients to marine fauna, partially causes changes in the mass of coastal waters, and the influx of cold water can affect local changes in the climate cycle.

In open and closed reservoirs, the process occurs in different ways. The Caspian Sea is a closed reservoir where the upwelling process is observed in the summer. In the article, based on satellite data of sea surface temperature, as well as local data on wind speed and direction, the phases of upwelling in the Kazakh part of the Caspian Sea, which occurred in the period from June 5 to August 22, 2017, are determined. The influence of constant North and North-East winds on the stages of upwelling development is shown, the spatial and temporal scales of the process development are determine.

Key words: process of upwelling, mass of coastal waters, satellite data, Ekman transfer, SNAP program.

Introduction

The upwelling process is the lifting of nutrient-rich colder waters from the depth to the upper layers [1]. The process occurs in coastal and open areas of the oceans and seas [2, 3, 4].

A strong constant horizontal wind creates tension in the surface layer of the reservoir, which is transmitted to the lower layers. A surface force occurs, is balanced by the Coriolis force of the next layer, and an Ekman spiral is formed, along which water masses are transferred from the depth to the surface. This effect was first physically explained by the Swedish oceanographer Vagn Walfrid Ekman and is called Ekman transfer [5].

The upwelling process can consist of two phases: the active phase and the relaxation phase. In the active phase, there is a strong constant horizontal wind, which causes the transfer of Ekman. The relaxation phase occurs when the wind force decreases, while the Ekman transfer is also observed, strong temperature changes persist, but the process gradually fades. According to [6], these phases can be divided into three stages depending on the wind speed: the first stage reflects the active phase with Ekman transfer, the second stage describes an intermediate state covering the end of the active phase and the beginning of the relaxation phase, and the third stage characterizes the end of the upwelling process.

There are generally accepted classifications of the following types of upwelling: Equatorial, coastal, neoceanic, artificial, etc.

The largest Equatorial upwelling of the open ocean is located near the equator in the Eastern Pacific ocean [2].

Coastal upwelling have been well studied off the North-West coast of Africa near the Canary Islands, in the southern regions of the African coast at latitudes 5-30^0, in the Gulf of Guinea, on the Pacific coast of South America in the area of the Peruvian current, etc. In General, stable coastal upwelling are observed mainly at the Eastern edges of the oceans and seas.

The process of coastal upwelling occurs differently in open and closed reservoirs. Coastal upwelling in the Eastern part of the Baltic Sea regularly affects the Gulf of Finland, which is about 400 km long and 100 km wide [7]. A group of Estonian scientists is actively working on the problems of wave dynamics of closed reservoirs. They regularly conduct measurements to track currents in the upper water layer at a test site located near the southern coast of the Gulf of Finland and the Baltic Sea. They have obtained interesting results that can be used in the study of similar processes in the Caspian Sea, similar in type to the Baltic Sea.

In the Caspian Sea in the summer, wind-induced upwelling results in a noticeable decrease in temperature and an increase in biomass in the upper layer of the Eastern part of the reservoir [8, 9, 10, 11, 12]. A number of Russian scientists have studied and recorded changes in the surface temperature of the Northern part of the Caspian Sea using a very high resolution radiometer (AVHRR). In addition to instrumental measurements of water flow velocity, the dynamics of the Caspian Sea can be studied with high accuracy using remote sensing data from space (satellite altimetry) [13, 14,15,16,17]. Iranian scientists are exploring the southern part of the Caspian Sea using the optical flow (OF) method, or the so-called Horn-Shunk method. This method makes it possible to study small-scale processes in small regions, providing information about the intensity of movements in each pixel with high spatial resolution [18]. But the disadvantage of this method is that the optical flow looks smooth on all images, and to determine the temperature difference, you need to enter parameters for the size of the smoothness, which must be selected accordingly, which is quite a time-consuming task [19].

Mesoscale dynamics of the Caspian Sea is also analyzed using SET satellite data to record fast submesoscale currents. Thus, in [20] to better understand the process of mixing and transport at mesoscales, the seasonal circulation of the Caspian Sea caused by wind was studied.

Statement of the problem

The Caspian Sea is characterized by the phenomenon of upwelling, which is most clearly expressed near the coast of the Middle Caspian. The main cause of the process is constant North and North-easterly winds. The process of upwelling in June-August 2017 is investigated. SST data from the Earth observation satellite system (EOS) is used to obtain moderate resolution images (MODIS) Aqua level 2 (MODIS heat bands 31 (11 μ) and 32 (12 μ)) from the NASA OceanColor open access website (http: //oceancolor.gsfc.nasa.gov/).

Adequate information on wind data is needed to account for atmospheric impacts. For this purpose, we use local data on sea wind measured at the Fort Shevchenko station. Station Fort Shevchenko is located on the Eastern shore of the Caspian Sea in Bucinskas Bay, which is part of the Tyub-Karagan Bay, and is located on the sandy Tyub-Karagan spit that separates the Bay from the sea. The zero mark of the post is 28.00 m BS (Baltic system). Coordinates of the post: latitude 44°33', longitude 50°15'. Since there was no reliable information about the stability of the air flow during the study interval, a constant correction factor of 0.85 was applied. This coefficient was chosen because it was calculated for similar conditions of a closed reservoir [12].

Results

SST maps do not allow you to determine the start of the upwelling process when cold water has not yet reached the sea surface. According to SST, upwelling becomes apparent when cold water reaches the surface layer. The data was processed in the SNAP (Sentinel Application Platform) program developed by the European space Agency (ESA). The program allows you to quickly create images taking into account atmospheric phenomena and displaying error areas, and determine the location of an object with convenient graphical processing (GPF). Advanced level management allows you to add and process new overlays, such as images from other bands, images from WMS servers, or ESRI shapefiles. ESA toolboxes support the scientific operation of ERS-ENVISAT and Sentinels 1/2/3 missions.

The obtained research results are shown in figures 1-3. Figure 1 shows the results of processing SST data in the SNAP program. Figure 2 shows a graph of wind speed and direction using local data, and figure 3 shows a calculation of temperature propagation depending on the distance from the coast using satellite data. Figure 2 and figure 3 were obtained using the MatLab program.

The SST maps (Fig.1) show that upwelling was caused by constant North and North-westerly winds that blew from 1-4 June 2017 at an average speed of 4.25 m/s (Fig. 2). According to satellite data, since June 5, 2017, the SST has decreased from 18° C to 15°C (Fig.1, a). By mid-June 2017, cold water filled a 300 km long coastal zone along the Eastern coast of Kazakhstan (Fig.1, b-d). This water soon formed jets (Fig.1, e-g), which reached a distance of 50 -55 km from the coast, as shown in Fig.3. The legend indicates the month / date. At the last stage 3 of upwelling, starting from July 28, the average wind speed fell below 5 m/s (Fig.2).

For consistency, the daily rate of temperature change was calculated from SST data. During the first phase of the rise of colder water to the surface layer (stage 1), the temperature dropped by about 1°C per day.

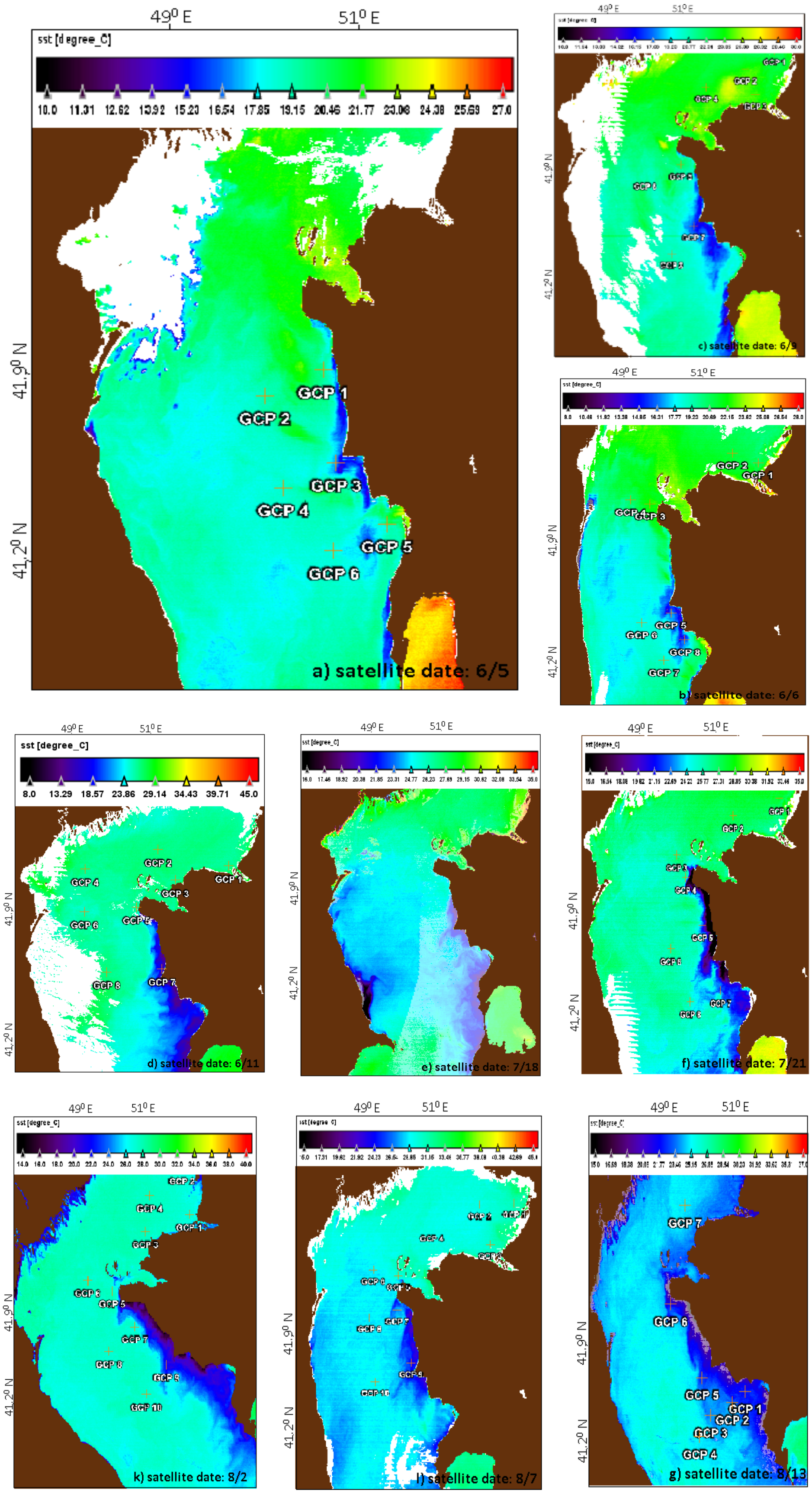

Figure 1 – SST maps of the Caspian Sea, cold-water distribution on the surface

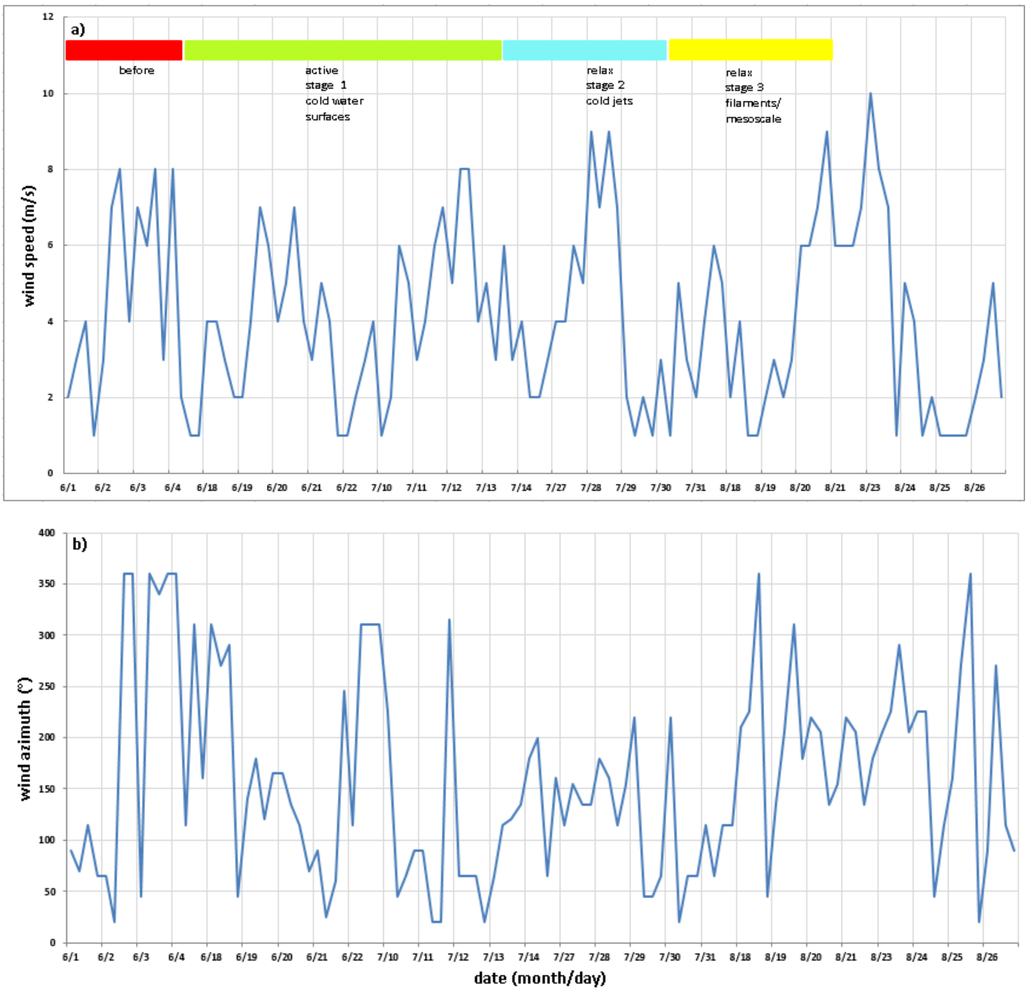

Figure 2. Values of wind speed (a) and wind azimuth
(b) according to the Fort Shevchenko station at various stages of upwelling

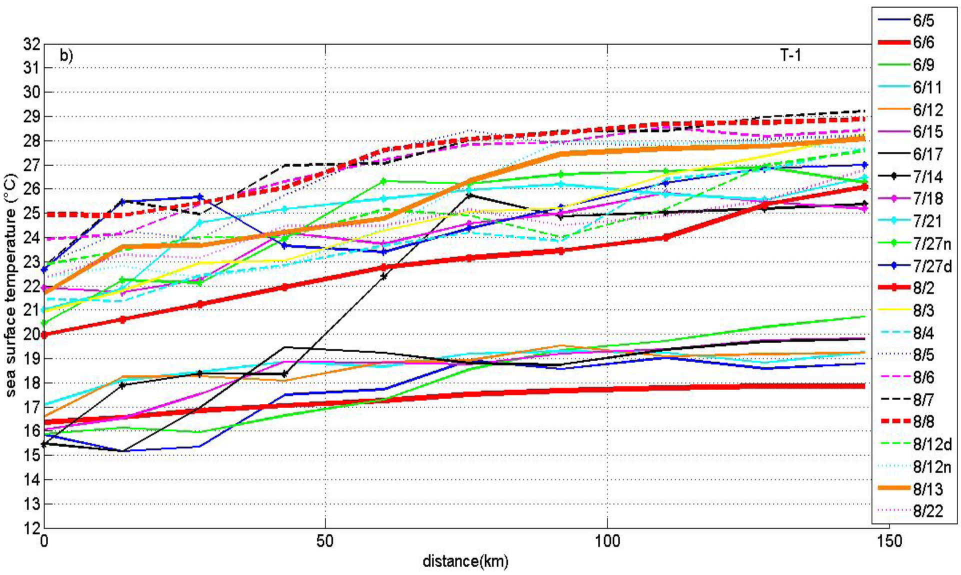

Figure 3 – Graph of temperature changes depending on the distance from the coast

This decrease was most intense at a distance of 50 km from the coastline and was significantly less away from the coast. During the next period of relatively strong winds (stage 2), the SST gradually increased, on average, by about 0.5°C per day. The subsequent relaxation phase (stage 3, June 11-15) was characterized by a decrease in wind speed. A much faster increase in SST (by 0.5-1°C per day) indicates the presence of intense mixing, which is most noticeable at a distance of 50-100 km from the coast.

Upwelling begins in June, but it reaches its highest intensity in July and August. As a result, there is a decrease in temperature on the water surface (by 13-15 C^0). SST data at the time of their explicit presentation on June 5-August 22 as clearly distinguishable sections of colder water on the surface of the sea allowed us to determine its spatial and temporal scales and study the spatial distribution of waters.

Thus, on SST maps, the upwelling process is clearly visible in the Eastern part of the Caspian Sea. Using local wind data and SST data, the temperature changes relative to the distance from the coast were calculated and the upwelling phases were determined, when cold water reaches the sea surface, forms water jets with low mixing intensity, and then the water jets mix intensively in weak winds.

Conclusion

The phases of the upwelling process that took place in the Middle part of the Caspian Sea in the period from June 5 to August 22, 2017, as well as the spatial and temporal scales of the process development were Determined.

It was found that the nature of movements in the surface layer of the sea strongly depends on the wind speed. For moderate (6-10 m / s) and strong (>10 m / s) winds, the Ekman transfer is formed. For a weak wind (<5 m/s), intensive mixing of different temperature waters occurs, which leads to the last stage of the process.

In the areas under consideration, upwelling reaches its highest intensity in July-August, with a temperature drop of 13-15 C0 observed on the water surface.

Acknowledgement like this:

Work has been supported financially by the research project *No AP*05132939 “Control system design of the satellite formation motion for remote sensing of the Earth”, for 2018-2020 of the al-Farabi Kazakh National University, which is gratefully acknowledged by the authors.

References

1. Bakun, A., 1990. Global climate change and intensification of coastal ocean upwelling. Science 247 (4939), 198–201.
2. Bondarenko, A.L. The Caspian Sea coastal upwelling (1998) Water Resources, 25 (4), pp. 467-469.
3. Knysh V. V., Ibrayev R. A., Korotaev G. K., and Inyushina N. V.. Seasonal Variability of Climatic Currents in the Caspian Sea Reconstructed by Assimilation of Climatic Temperature and Salinity into the Model of Water Circulation. Izvestiya, Atmospheric and Oceanic Physics, 2008, Vol. 44, No. 2, pp. 236–249.
4. Monakhova Galina Anatolyevna, Akhmedova Gulnara Akhmedovna. The rise of deep waters off the Western coast of the middle Caspian. The scientific journal of the Kuban state agrarian University, №63(09), 2010.
5. Gill A., Dynamics of the atmosphere and ocean, 2 (1988) 8-12 p.
6. Zhurbas, V., Laanemets, J., Vahtera, E., 2008. Modeling of the mesoscale structure of coupled upwelling/downwelling events and the related input of nutrients to the upper mixed layer in the Gulf of Finland, Baltic Sea. J. Geophys. Res. Oceans 113 (Art. No. C05004).
7. Nicole Delpeche-Ellmann a, Toma Mingelaitė, Tarmo Soomere. Examining Lagrangian surface transport during a coastal upwelling in the Gulf of Finland, Baltic Sea. Journal of Marine Systems 171 (2017) 21–30.
8. Halil J. Sur, Emin Ozsoy, Rashit Ibrayev. Satellite-derived flow characteristics of the Caspian Sea. Satellites, Oceanography and Society edited by David Halpern. 2000 Elsevier Science B.V. 289-297.
9. Asghar Bohlulya, Fariba Sadat Esfahani , Masoud Montazeri Namin, Fatemeh Chegini. Evaluation of wind induced currents modeling along the Southern Caspian Sea. Continental Shelf Research 153 (2018) 50–63.
10. Ivkina N. I. Features of coastal upwelling in the Eastern part of the middle Caspian. Hydrometeorology and ecology. 2 (65). 2012. 81-87. UDC: 556.536
11. Rivo Uiboupin, Jaan Laanemets. Upwelling characteristics derived from satellite sea surface temperature data in the Gulf of Finland, Baltic Sea. Boreal Environment research 14: 297-304. 2009.
12. Shiea, M., Bidokhti, A.A. The study of upwelling in the eastern coast of the Caspian Sea using numerical simulation (2015) Journal of the Earth and Space Physics, 41 (3), pp. 535-545.

13. 13Gurova, G., Lehmann, A., Ivanov, A., 2013. Upwelling dynamics in the Baltic Sea studied by a combined SAR/infrared satellite data and circulation model analysis. Oceanologia 55, 687–707.

14. Lebedev S. A., Kostyanoy A. G., Ginzburg A. I. Dynamics of the Caspian Sea based on instrumental measurements, modeling results and remote sensing data. May 2015. https://www.researchgate.net/publication/280254971

15. Abutalieva I. R. Oil and gas Content and main sources of hydrocarbon pollution of the Northern Caspian Sea. // Bulletin of the Astrakhan state technical University. 2005, 158-162 p.

16. Daisuke Kitazawa, Jing Yang. Numerical analysis of water circulation and thermohaline structures in the Caspian Sea. J Mar Sci Technol 17(2012) 168–180

17. Rakisheva Z. B., Kuzembayev K. K. On the problem of studying the wave climate of the Caspian Sea using satellite altimetry. / / «Bulletin of KazNPU» 2017. 2-vol. №2, 7p.

18. Emad Ghalenoei, Mahdi Hasanlou, Mohammad Ali Sharifi, Stefano Vignudelli, Ismael Foroughi. Spatiotemporal monitoring of upwelled water motions using optical flow method in the Eastern Coasts of Caspian Sea. Journal of Applied Remote Sensing. Jul–Sep 2017, 036016-1, Vol. 11(3)

19. Shebalov A.A., Bazhenov A.N.. Research of performance of optical flow calculation methods. Scientific and technical Bulletin of spbpu Informatika. Telecommunications. Management, 6(2012), 152-158.

20. Gunduz M., Özsoy E.. Modelling seasonal circulation and thermohaline structure of the Caspian Sea. Ocean Sci., 10 (2014) 459–471.

21. Soomere T., Männikus R., Pindsoo K., Kudryavtseva N., Eelsalu M.. Modification of closure depths by synchronisation of severe seas and high water levels. // Geo-Marine Letters. February 2017, Volume 37, Issue 1, pp 35–46.

IRSTI 44.31.31 https://doi.org/10.26577/ijmph.2020.v11.i1.07

M. Gorokhovski

Ecole Centrale de Lyon, Lyon, France
e-mail: saulemaussumbekova@gmail.com

APPLICATION OF OVERFIRE AIR TECHNOLOGY FOR REDUCTION OF HARMFUL EMISSIONS

Abstract. When burning any fossil fuels, one of the most harmful combustion products are nitrogen oxides NOx, which damage both the environment and human health in particular. Reduction of NOx emissions from fuel combustion at TPPs plays an important role in reducing the total level of nitrogen oxides NOx emitted into the atmosphere. One way to reduce the concentration of nitrogen oxides NOx is the stepwise combustion of the pulverized coal mixture, in particular the «Over fire Air» technology. The essence of this method is that the main volume of air is fed into the pulverized burners, and the rest of the air is further along the height of the torch through special nozzles. Structurally, the method of stepwise combustion of fuel can be carried out in boilers with a two-tier arrangement of burners along the height of the combustion chamber. In this case, practically no significant reconstruction of the boiler is required, which is associated with additional costs. In the present work, computational experiments on the use of modern overfire air technology (OFA) in the combustion chamber of the PK-39 boiler of the Aksu TPP were carried out and the fields of the main characteristics of heat and mass transfer, as well as the influence of the mass flow of the oxidant through the OFA injectors on the combustion process were obtained.

Key words: overfire air technology, coal combustion, numerical simulation.

Introduction

As of today Kazakhstan is one of the states possessing a huge stock of hydrocarbons which render essential influence on formation and a condition of the world energy market [1-3]. In the Republic of Kazakhstan, about 80% of the country's energy supply comes from the production of electricity by 69 power plants, the main source of which is Kazakh coal [4-6].

The coal mining in Republic is carried out basically by the open way , which makes this type of solid fuel the cheapest, but low-grade (high ash content in its composition) in our country a source of energy [3,7-8]. At the same time, the coal of Kazakhstan possesses a number of advantages – small sulphur content of coals and a high volatiles content on a dry ash-free basis.

For the sustainable development of heat and power industry of the country in the near future, it is necessary to optimize the combustion of traditional energy fuel (Kazakh coal), to develop and implement clean energy technologies; to protect the environment from harmful dust and gas emissions and ensure the efficiency of power plants. One of the methods for reduction of NO_x concentration is the overfire air technology – OFA.

Technological methods for suppressing the formation of nitrogen oxides are based on a reduction in the peak temperature and oxygen content in the active combustion zone, as well as in the formation in the combustion chamber of zones with a reducing medium, where the products of incomplete combustion, reacting with the formed nitric oxide, lead to the reduction of NO_x to molecular nitrogen N_2.

Thus, in the zone of active combustion, an oxygen-depleted and fuel-enriched combustion zone is formed. Due to the lack of air in this area, the average temperature is lower than in traditional combustion, which allows to reduce the amount of fuel and thermal nitrogen oxides. Further, above the level of the main burners, additional air is supplied through the tertiary air nozzles necessary for afterburning the products of incomplete combustion and an oxidizing medium is formed [9-10].

The most difficult step in realization of the OFA technology is to define the optimal location height and diameter of nozzles through which air will be supplied, and to find the best ratio of air supplying through the main burner and OFA-injectors. These characteristics depend on design of the boilers and the method of supplying fuel-air mixture [10-11].

To effectively implement this technology on an industrial boiler, the height of the OFA injectors should be chosen so that in the active combustion zone a complete burn-out of the fuel and its afterburning to the final combustion products are ensured, since incomplete mixing of fuel and oxidant can increase underburning [12].

Mathematical model of heat and mass transfer processes

For three-dimensional motion of a fluid with variable physical properties, the field of velocity, temperature, and concentration is described by a system of differential equations (1-4)

$$\frac{\partial \rho}{\partial t} = -\frac{\partial}{\partial x_i}(\rho u_i), \qquad (1)$$

$$\frac{\partial}{\partial t}(\rho u_i) = -\frac{\partial}{\partial x_j}(\rho u_i u_j) + \frac{\partial}{\partial x_j}(\tau_{i,j}) - \frac{\partial \rho}{\partial x_j} + \rho f_i, \qquad (2)$$

$$\frac{\partial}{\partial t}(\rho h_i) = -\frac{\partial}{\partial x_i}(\rho u_i h) - \frac{\partial q_i}{\partial x_i} + u_i \frac{\partial \rho}{\partial x_i} + \tau_{ij}\frac{\partial u_j}{\partial x_i} + S_q, \qquad (3)$$

$$\frac{\partial}{\partial t}(\rho c_\beta) = -\frac{\partial}{\partial x_i}(\rho c_\beta u_j) + \frac{\partial}{\partial x_i} + R_\beta, \qquad (4)$$

where i = 1,2,3; j = 1,2,3; β = 1,2,3, ... N.

To simulate turbulent viscosity, the well-known k-ε turbulence model was used, consisting of the equation for the conservation of the kinetic energy of turbulence k, its dissipation rate ε, and the model relation for turbulent viscosity. The K-ε turbulence model is the standard model for forced and natural convection flows. The model include equation of transport of turbulent kinetic energy k and equation of dissipation of turbulent kinetic energy ε:

$$\frac{\partial(\rho k)}{\partial t} = -\frac{\partial\left(\rho u_j k\right)}{\partial x_j} + \frac{\partial}{\partial x_j}\left[\frac{\mu_{eff}}{\sigma_k}\frac{\partial k}{\partial x_j}\right] + P - \rho\cdot\varepsilon, \qquad (5)$$

$$\frac{\partial(\rho\varepsilon)}{\partial t} = -\frac{\partial\left(\rho u_j \varepsilon\right)}{\partial x_j} + \frac{\partial}{\partial x_j}\left[\frac{\mu_{eff}}{\sigma_\varepsilon}\frac{\partial \varepsilon}{\partial x_j}\right] + \qquad (6)$$
$$+C_{\varepsilon,1}\cdot\frac{\varepsilon}{k}\cdot P - C_{\varepsilon,2}\cdot\frac{\varepsilon^2}{k}\cdot\rho,$$

where σ_k, σ_ε – the corresponding turbulent Prandtl numbers; P – turbulent kinetic energy production:

$$P = \left[\mu_{turb}\left(\frac{\partial u_j}{\partial x_j} + \frac{\partial u_j}{\partial x_i}\right) - \frac{2}{3}\rho k \delta_{ij}\right]\frac{\partial u_j}{\partial x_j}.$$

Considering the processes of heat exchange in technical reacting flows in combustion chambers, heat exchange by means of radiation makes the greatest contribution to total heat transfer. In the flame zone, the contribution of radiant heat exchange is up to 90% of the total heat transfer and even more [13]. In this regard, the simulation of heat transfer through radiation in reacting flows in combustion chambers is one of the most important stages in the calculation of heat transfer processes in real combustion chambers.

Physical model of the combustion chamber

To solve the systems of differential equations describing the processes of heat and mass transfer in the combustion chamber of the boiler PK-39 of Aksu TPP, the control volume method [6, 14-16] was used.

The essence of the method is that the space of the combustion chamber is divided into control volumes and for each point of space surrounded by a certain volume, the equations of conservation of physical quantity (mass, momentum, energy, etc.) are solved.

Before the numerical experiments using the PREPROZ program [17], files and startup programs were created for two investigated cases, including initial and boundary conditions, the characteristics of the fuel (elemental composition, heat of combustion, fractional composition of Ekibastuz coal), the geometry of the boiler and burner devices [6, 18]. The main characteristics of the combustion chamber of the boiler PK-39 of Aksu TPP and burnt Ekibastuz coal are presented in table 1.

Table 1 – Characteristics of the combustion chamber of the boiler PK-39 of Aksu TPP and the pulverized coal burned on it (Ekibastuz coal) [3]

The name of the characteristics, dimensionality	**Designation**	**Value**
Fuel consumption per boiler, kg/h	B	87 500
Fuel consumption per burner, kg/h	B_b=B/Z	7291.1
Fuel – Ekibastuz coal Composition of coal,%	W^p	7.0
	A^p	40.9
	S^p	0.8
	C^p	41.1
	H^p	2.8
	O^p	6.6
	N^p	0.8
Calorific value, MJ/kg	Q_H^p	15.87
Volatile, %	V^F	30.0
Coefficient of excess air at the exit from the furnace	α_T	1.25
Coefficient of excess air in the burners	α_r	1.15
Temperature of the air mixture, °C (K)	T_a	150(423)
Temperature of secondary air, °C (K)	T_2	327(600)
Type of burners	Vortical	
Number of burners, pcs	n_B	12
Height of the furnace, m	z(H)	29.985
Width of the furnace, m	Y	10.76
Depth of the furnace, m	X	7.762

Figure 1 provides a general view and a gridding of the boiler: for traditional pulverized coal combustion (Fig. 1a), at implement of secondary air nozzles – OFA (Fig. 1b). The major structural characteristics are presented in table 2. In the work, cases with a percentage of the supply air through the nozzles OFA equal to 0 (base case), 10 and 20% of the total amount of secondary and tertiary air supplied to the combustion chamber.

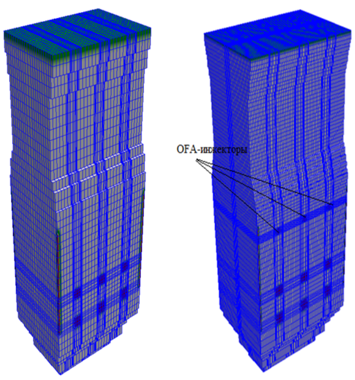

Figure 1 – General view and a gridding of the PK-39boiler

Table 2 – Constructional characteristics of a boiler PK-39 of Aksu TPP at the organization of staged combustion of fuel

The characteristic	**Value**
Number of OFA-nozzles, pcs	6
The height of the tier of the lower burners, m	7,315
The height of the tier of the upper burners, m	10,115
The height of the tier of the OFA-nozzles, m	15,735
Diameter of OFA-nozzles, m	0,7

Results and discussion

Results of researches obtained with the FLOREAN software package [19-22] are presented below in the paper. Figure 2 shows the distribution of the full-velocity vector in different sections of the combustion chamber for the base case (OFA 0%) and with the use of the overfire air technology (OFA 20%). Analysis of the figures shows that with the use of OFA technology, the combustion process in the central part of the combustion chamber is more intense compared to the base case.

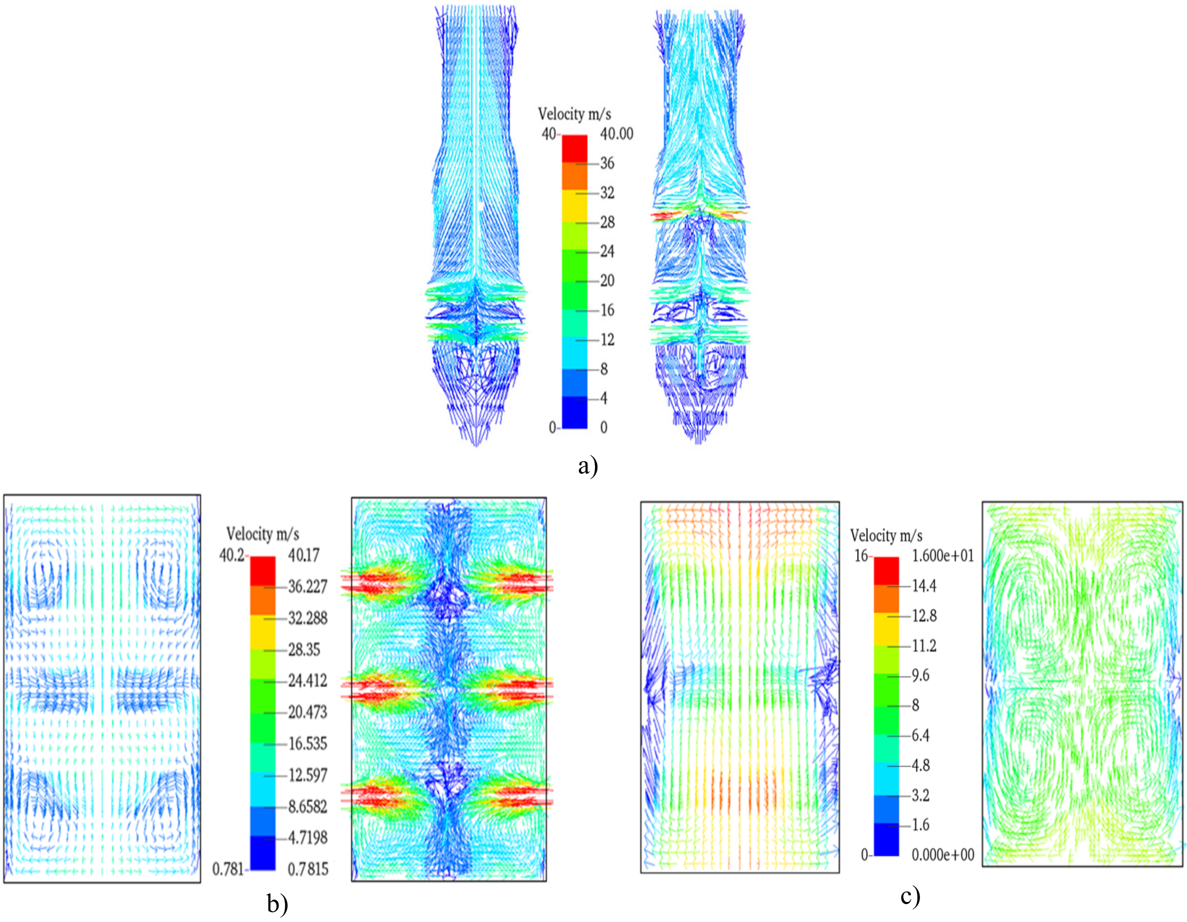

Figure 2 – The distribution of the velocity vector in different sections of the combustion chamber a) Y=5.38 m; b) Z=15.735 m; c) Z=29,595 m

Figure 3 shows the distribution of average temperatures on height of furnace chamber for the investigated cases. The results of full-scale experiment conducted at Aksu TPP [23] are also plotted on the graph. Moving towards the exit of the furnace temperature field is equalized and differences in temperature values for different occasions decrease.

Also, it can be seen that the greatest differences between the results of computational and full-scale experiments are observed in the area of ignition of the pulverized coal mixture. Moving towards the exit from the furnace space, these differences are insignificant, which indicates good consistency and, as a consequence, the adequacy of the used models.

Figures 4-5 show graphs of the distribution of combustion products – carbon CO_2 and nitrogen NO oxides along the height of furnace chamber of PK-39 boiler of Aksu TPP. Analyzing the distribution of carbon monoxide (Figure 4), it can be seen that the greatest differences in the values are noticeable in the area of the burner belt and OFA-injectors. To the exit from the combustion chamber with increasing mass flow of air through the OFA-nozzles, the concentration of carbon dioxide CO_2 is reduced.

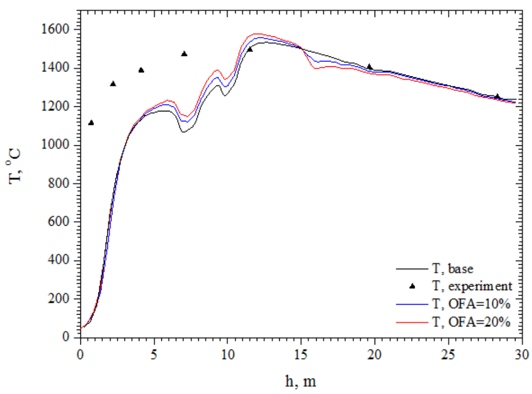

Figure 3 – Temperature distribution over the height of the combustion chamber of the boiler PK-39 for different values of air supplied through the nozzles OFA and comparison with experiment [23]

Figure 5 represents the distribution of the concentration of nitrogen oxide NO along the height of furnace chamber of PK-39 boiler of Aksu TPP.

Analysis of Figure 5 allows us to conclude that an increase in the mass flow of air supplied through OFA injectors leads to a decrease in NO concentration at the outlet from the furnace chamber of PK-39 boiler of Aksu TPP. This is confirmed by the known dependence of NO oxides formed on temperature [24] and analysis of the temperature distribution in the combustion chamber of the boiler PK-39, presented in Figure 3.

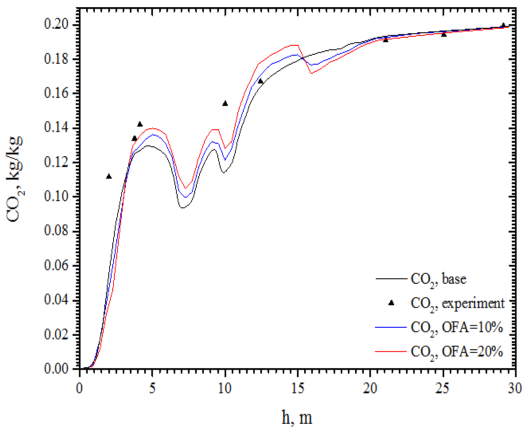

Figure 4 – Distribution of CO_2 concentration along the furnace chamber height for different values of air supplied through the nozzles OFA and comparison with experiment [23]

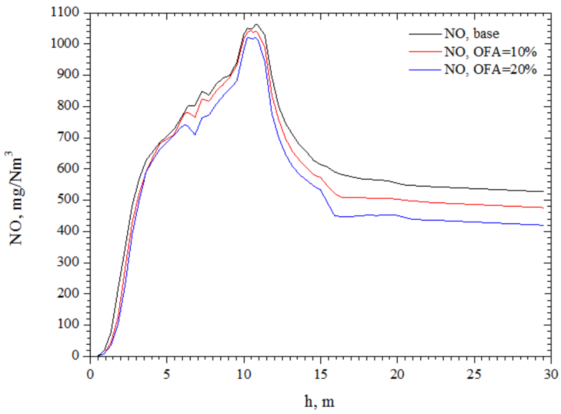

Figure 5 – Distribution of NOx concentration along the furnace chamber height for different values of air supplied through the nozzles OFA

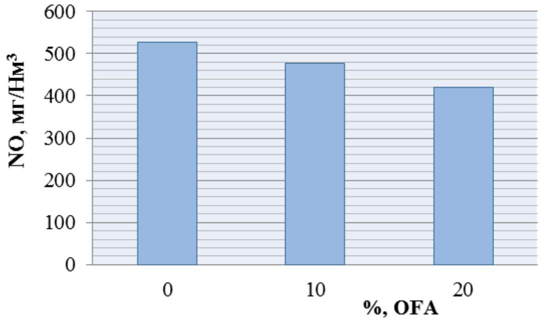

Figure 6 – The effect of the percentage of mass air flow through the OFA injectors on the NO concentration at the outlet from the combustion chamber of the PK-39 boiler of the Aksu TPP

The increase in air supplied through the OFA injectors allows to reduce the concentration of nitric oxide at the outlet from the combustion chamber from for about 20 %. The results of the studies are presented in the form of a diagram in Figure 6.

Conclusion

This paper presents the experiments on the implementation of the overfire air technology on the combustion chamber of PK-39 boiler of Aksu TPP. This technology is based on the separation of the oxidant supplied to the combustion chamber in such a way as to reduce the amount of fuel NO_x in the burner location by reducing excess air, and reduce the amount of thermal NO_x by reducing the temperature of the flame in the region of the location of the OFA-injectors.

Studies show that the implementation of OFA technology on the boiler PK-39 Aksu TPP leads to a change in the distribution of temperature T, the concentrations of carbon CO_2 and nitrogen NO oxides in the combustion chamber.

Thus, the studies in this paper demonstrate that overfire air technology is one of the most promising ways to reduce emissions of harmful substances (nitrogen oxide NO_x and carbon dioxide CO_2) in the atmosphere and can be used in the combustion of high-ash fuels in combustion chambers of coal-fired TPPs.

Nomenclature

τ_{ij} – tensor of viscous tension;

f_i – volume forces, N;

h – enthalpy;

q^{res} – energy flux density due to molecular heat transfer;

S_h – a source of energy;

c_n – mass concentration of the components of the substance;

D_{c_n} – the diffusion coefficient of a component;

S_{c_n} – the source term taking into account the contribution of the chemical reactions in the change in the concentration of components;

k – turbulent kinetic energy per unit mass;

μ_{eff} – effective viscosity;

σ_k, σ_ε – turbulent Prandtl numbers – empirical constants in turbulence model;

P – the production of turbulent kinetic energy, which is determined by the following equation;

ε – dissipation rate of turbulent kinetic energy per unit mass;

δ_{ij} – Kronecker delta;

μ_{turb}– turbulent viscosity;

$c_{\varepsilon 1}$, $c_{\varepsilon 2}$, c_μ – empirical constants;

References

1. Askarova A., Bolegenova S., Bekmukhamet A., Maximov Yu.V., Beketayeva M., Ospanova Sh. Gabitova Z.K. Investigation of turbulence characteristics of burning process of the solid fuel in BKZ 420 combustion chamber. *WSEAS Transactions on Heat and Mass Transfer 9*, (2014): 39-50.
2. Askarova A.S., Bekmukhamet A., Bolegenova S.A., Beketayeva M.T., Maximov Yu.V., Ospanova Sh.S., Gabitova Z.K. Numerical modeling of turbulence characteristics of burning process of the solid fuel in BKZ-420-140-7c combustion chamber. *International Journal of Mechanics* 8 (2014): 112-122.
3. Askarova A.S., Bolegenova S.A., Maximov V.Y., Bekmukhamet A, Beketayeva M.T., Gabitova Z.K. etc. Computational method for investigation of solid fuel combustion in combustion chambers of a heat power plant. *High temperature* 53, Issue 5 (2015): 751-757.
4. Askarova A., Bolegenova S., Bekmukhamet A., Ospanova Sh., Gabitova Z. Using 3D modeling technology for investigation of conventional combustion mode of BKZ-420-140-7c combustion chamber. *Journal of Engineering and Applied Sciences* 9, Issue 1 (2014): 24-28.
5. Askarova A.S., Bolegenova S.A., Bekmuhamet A., Maximov V.Yu. Mathematical simulation of pulverized coal in combustion chamber. *Procedia Engineering* 42, (2012): 1259-1265.
6. Askarova A., Bekmukhamet A., Bolegenova S., Ospanova Sh., Bolegenova Symbat, Maximov V. Beketayeva M., Gabitova Z., Ergalieva A. 3D modeling of heat and mass transfer during combustion of solid fuel in BKZ-420-140-7c combustion chamber of Kazakhstan. *Journal of Applied Fluid Mechanics* 9, Issue 2, (2016): 699-709.
7. Askarova, A.S., Lavrichsheva, Ye.I., Leithner, R., Müller, H., Magda, A. Combustion of low-rank coals in furnaces of Kazakhstan coal-firing power plants. *VDI Berichte* 1988, (2007): 497-502.
8. Askarova, A. S., Vockrodt S., Leithner. et al. Firing technique measures for increased efficiency and minimization of toxic emissions in Kasakh coal firing. *VDI*, *19th German Conference on Flames, Germany, VDI Gesell Energietechn; Verein Deutsch Ingn., Combustion And Incineration, VDI Berichte*, v.1492, (1999): 93.
9. Kuang M., Li Z., Liu C., Zhu Q., Zhang Y., Wang Y. Evaluation of overfire air behavior for a down-fired 350 MWe utility boiler with multiple injection and multiple staging. *Applied Thermal Engineering* 48, (2012): 164-175.
10. Askarova A.S., Messerle V.E., Ustimenko A.B., Bolegenova S.A., Bolegenova S.A., Maximov V.Y., Ergalieva A. Reduction of noxious substance emissions at the pulverized fuel combustion in the combustor of the BKZ-160 boiler of the Almaty heat electropower station using the “Overfire Air” technology. *Thermophysics and aeromechanics* 23, Issue 1, (2016): 125-134.
11. Askarova A.S., Heierle E.I., Bolegenova S.A., Maximov V.Ju., Bolegenova S.A., Manatbayev R., Beketaeva M.T., Ergalieva A.B. CFD study of harmful substances production in coal-fired power plant of Kazakhstan. *Bulgarian Chemical Communications* Special Issue E, (2016): 260-265.
12. Li M., Wang X., Sun S., Zhen X., Li Q., Zhang T. Influence of Overfire air jet form on low NOx retrofit effect of an opposed firing boiler. *Journal of Chinese society of power engineering* 4, (2015): 263-269.
13. Weber K. Dreidimensionale Simulation der Gas–Festoff–Strömung in kohlegefeuerten Dampferzeugern. *Fortschritt–Berichte VDI–Verlag* 6, Issue 415, (1999): 198.
14. Askarova A., Bolegenova S. et al. Influence of boundary conditions to heat and mass transfer

processes. *International Journal of Mechanics* 10 (2016): 320-325.

15. Askarova A., Bolegenova S., Maximov V. et al. On the effect of the temperature boundary conditions on the walls for the processes of heat and mass transfer. *International Journal of Mechanics* 10, (2016): 349-355.

16. Askarova, A. S., Bolegenova, S.A., Maximov, V.Y., Bekmukhamet, A, Ospanova, S.S. Numerical research of aerodynamic characteristics of combustion chamber BKZ-75 mining thermal power station. *Procedia Engineering* 42, (2012): 1250-1259.

17. Askarova A.S., Bolegenova S.A., Bolegenova S., Bekmukhamet A., Maximov V.Yu., Beketayeva M.T. Numerical experimenting of combustion in the real boiler of CHP. *International Journal of Mechanics* 3, Issue 7, (2013): 343-352.

18. Askarova, A.S., Messerle, V.E., Ustimenko, A.B., Bolegenova, S.A., Maksimov, V.Yu. Numerical simulation of the coal combustion process initiated by a plasma source. *Thermophysics and aeromechanics* 21, Issue 6, (2014): 747-754.

19. Leithner R., Müller H. CFD studies for boilers. *Second M.I.T. Conference on Computational Fluid and Solid Mechanics*. Cambridge, (2003): 172.

20. Leithner R., Müller H., Heitmüller R. *Dreidimensionale Simulation von Dampferzeuger-Brennkammern einschließlich der NOx-Schadstoffkinetik.* Essen, 1993.

21. Müller H. Numerische Berechnung dreidimensionaler turbulenter Strömungen in Dampferzeugern mit Wärmeübergang und chemischen Reactionen am Beispiel des SNCR–Verfahrens und der Kohleverbrennung // Fortschritt–Berichte VDI-Verlag, 268 (1992): 158.

22. Gabitova Z.Kh., Gorokhovski M., Septemirova A., Kalybekov A., Bulysheva G. Numerical simulation of heat and mass transfer processes in combustion chamber of pk-39 boiler. *International Journal of Mathematics and Physics* 10, Issue 1, (2019): 99-106.

23. Aliyarov B.K., Aliyarova M.B. Szhiganie kazahstanskih ugley na TES i na krupnyih kotelnyih: opyit i problemyi, Almatyi, 2012.

24. Zeldovich J. The oxidation of Nitrogen in combustions and explosions. *Acta Physicochemica* 21, (1946): 557-628.

IRSTI 27.35.17 https://doi.org/10.26577/ijmph.2020.v11.i1.08

L.A. Nesterenkova, P.A. Nesterenkov, Z.H. Spabekova

Al-Farabi Kazakh National University, Almaty, Kazakhstan,
e-mail: stolkner@gmail.com

ON TWO WAYS TO IMPROVE THE RHEOLOGY OF HIGH VISCOUS OIL IN AN OIL PIPELINE

Abstract. Transportation of highly viscous and high-curing oils through main pipelines requires significant energy costs. Thus, the task of choosing the cheapest pumping modes is very relevant. The article describes and proposes a solution to the oil flow problem in a pipeline using two methods: with preheating and using a Laval nozzle at the inlet of the pipeline. Mathematical models of the flow of high-viscosity oil in the main oil pipeline for the two named pumping methods have been compiled. An algorithm has been developed for calculating temperature, viscosity and pressure along the length of the Uzen-Atyrau pipeline at various oil flow rates. The results of temperature and pressure distribution are analyzed and compared at different oil flow rates along the length of the pipeline for two pumping methods. It is shown that the use of cavitation improves the rheological properties of oil and can significantly reduce the cost of pumping. The research results can be used to predict the operation of main oil pipelines pumping oil both in a heated state and in isothermal mode with a Laval nozzle.
Key words: high viscosity oil, pressure and temperature along the pipeline, cavitation, oil pipelines operation costs.

Introduction

Kazakhstan has the largest deposits of liquid hydrocarbons. In terms of oil reserves, our country is one of the 15 leading countries in the world, and has 3.3% of the world's carbon reserves [1].

The bulk of the oil produced in our country is highly viscous, because it contains a large number of paraffin fractions, resins, asphaltenes and other components. Pipeline transport of such oils require significant energy costs [2].To reduce them, special methods are used to improve the rheological properties of the transported product [2,3]. For example, in the practice of transporting highly viscous high-hardening oils and petroleum products, methods such as pumping in a carrier stream have found application (in this method, oil is cooled to a level where it will be a solid granular body and transferred in a stream of liquefied gas); pipeline transport with continuous heating (using various coolants or electric heating of the pipeline); pumping with diluents (with dilution of oil with external low-viscosity oils, liquefied gas, etc.); hydro-transport (pumping oil with a near-wall water layer); pumping heat-treated oils with improving their rheological properties; preheating pumping and so on [3].

Material and methods

Among the existing methods, the pre-heated pumping method has gained the greatest popularity, which can significantly reduce the viscosity of the transported product [3,4]. In this method of transportation, oil (usually 45 – 65 °C) heated to the optimum temperature is pumped into the main line by pumps. Through certain distances, intermediate heat and pumping stations are established along the pipeline route, where the oil that cools down along the way is heated and pumped to the next station. The distance between pumping stations and thermal stations is determined by the rate of temperature decrease and pressure depression.

The operation of underground heated oil pipelines has a number of related features. first of all, with the influence of the conditions of their heat exchange with the environment. In many cases, there are reasons that adversely affect the temperature regime of the pipeline (annual changes in soil temperature; shutdowns and shutdowns of pumping and heating units, both planned and due to equipment failures, triggering of the automatic protection system; change in the thermal conductivity of the soil due to strong rains, intense melting of snow, floods, etc.). This creates a danger of emergency situations and requires additional capital investments.

Due to the fact that pipelines are being built in regions with different climatic and environmental conditions, problems arise in the selection and justification of laying methods and operation modes of pipelines. When designing them, the selection of the main technological and structural parameters and construction solutions is carried out mainly on the basis of the conditions of stationary operation of the pipeline. This necessitates further improvement of the methods for studying the transport of oil and oil products. In this regard, the issue of using non-standard methods for changing the rheological properties of oils and petroleum products becomes relevant.

One of promising methods for changing the viscosity of oil is cavitation [5,6]. For cavitation to occur, a hollow cylindrical pipe of variable section (tapering, and then expanding part in a certain way) is placed in the pipeline. The fact is that when oil passes through this pipe, called the Laval nozzle, due to cavitation, as a result of a decrease in pressure in the expanding part of the nozzle, a sharp change in its rheological properties occurs. At the outlet of the Laval nozzle, oil has a lower viscosity, higher fluidity, and lower tensile stress [7].

This paper explores the possibility of using a Laval nozzle at the inlet of the pipeline to create cavitation effects of the transported liquid, which can reduce the viscosity of oil by comparing the calculations of the flow of oil through a pre-heated oil pipeline and through a pipeline with a Laval nozzle.

Results and discussion

In a preheated oil pipeline, a steady non-isothermal oil flow in linear sections between intermediate stations is described by a system of differential equations of motion, continuity and energy [3,4].

When constructing a mathematical model of the steady non-isothermal flow of highly viscous fluid in an underground pipeline laid over rough terrain, the following assumptions were made:

- due to the large length of the main pipelines, we use a one-dimensional mathematical model of the flow, the X axis is compatible with the axis of the pipe, and all process parameters are averaged over the pipe section;
- thermal and pumping stations located along the route are considered point-like because of their small size compared to the length of the pipeline;
- the pipeline is divided into sections between thermal and pumping stations (so called "linear sections" in this work);
- along the length of the pipeline there are no intermediate sources of mass;
- oil is considered as a single-phase viscoplastic incompressible fluid;
- heat transfer between the pipeline and the surrounding soil obeys the Newton-Richmann law;
- the coefficients of density ρ, specific heat of oil c and soil thermal conductivity λ are independent of temperature.

Under the assumptions made, the steady non-isothermal flow of oil in the linear sections between intermediate stations will have [3,4]:

$$\left.\begin{array}{c} \frac{dp}{dx} = -\rho \cdot g \cdot \left(\frac{dz}{dx} + \frac{dh_{\text{тр}}}{dx}\right) \\ \frac{dw}{dx} = 0; \end{array}\right\} \tag{1}$$

$$\frac{dT}{dx} = \frac{4 \cdot k}{\rho \cdot c \cdot D \cdot w} \cdot \left(T_{\text{окр}} - T\right) \tag{2}$$

with boundary conditions

$$p(0) = p_n;\ T(0) = T_n;\ w(0) = w_n \tag{3}$$

and interfacing conditions at intermediate stations:

$$p_j^+ = p_j^- + \Delta p_j;\ T_j^+ = T_j^- + \Delta T_j \quad j = \overline{1, N}. \tag{4}$$

where p – pressure in the pipeline, w; T – respectively, the flow velocity and oil temperature; D – internal diameter of the pipeline, z – geodetic height of the pipeline; $T_{\text{окр}}$ – temperature of the soil surrounding the pipeline; $k = 2\lambda / (D \cdot \ln(4h / D))$ – heat transfer coefficient from the oil pipeline to the surrounding soil; h – laying depth to the pipe axles, ΔT_j, Δp_j; – changes in temperature and pressure at the j^{th} station, the j index indicates the station number; the indices "+" and "-"indicate the values of the values on the right and left border of the section; N – number of stations and linear sections between stations.

To determine the frictional pressure loss of viscoplastic oil $h_{\text{тр}}$, will use the Darcy – Leibenzon expression [3,8]:

$$\frac{dh_{\text{тр}}}{dx} = \rho \cdot g \cdot \beta \cdot \left(\frac{\pi \cdot w}{4}\right)^{2-m} \cdot$$
$$\cdot \frac{\nu^m}{D^{m+1}} + \frac{16}{3} \cdot \frac{\tau_0}{\rho \cdot g \cdot D} \quad (5)$$

where m and β are coefficients depending on the flow regime [3].

The kinematic viscosity coefficient ν and the ultimate shear stress τ_0 are largely dependent on temperature. For an analytical description of these dependencies, we use the expressions [3]:

$$\nu = \nu(T_1) \cdot \exp[-a_1 \cdot (T - T_1)];$$
$$\tau_0 = \tau_0(T_1) \cdot \exp[-a_2 \cdot (T - T_1)] \quad (6)$$

where α_1, α_2 are empirical constants, T_1 is a fixed temperature.

The cost of operating the pipeline is mainly determined by fuel consumption level at thermal stations and electricity consumption at pumping stations. For a stationary flow regime, these costs are determined by the expression [4]:

$$S = S_n + S_T =$$
$$= w \cdot t \cdot \left(\sum_{j=0}^{N} \varphi_j \cdot \Delta p_j + \sum_{j=0}^{N} \xi_j \cdot \Delta T_j\right) \quad (7)$$

where t – operating time of the pipeline; φ_j, ξ_j are, respectively, values proportional to the cost of a unit of fuel and electricity of the j[th] station. If the price of fuel and electricity at all stations is the same, the cost functional (7) taking into account (4) will be minimal under the following conditions [4]:

$$T_j^- = T_{min};\ p_j^- = p_{min};\ j = \overline{1, N+1} \quad (8)$$

where T_{min}, p_{min} – the minimum allowable temperature and pressure in the pipe.

From the continuity equation from system (1) we have: $w(x) = const = w_n$.

The energy equation (2) on the linear sections of the pipeline has an analytical solution:

$$T(x) = T_{\text{окр}} + \left(T_j^+ - T_{\text{окр}}\right) \cdot \exp\left(-\frac{4 \cdot k \cdot x}{\rho \cdot c \cdot D \cdot w}\right) \quad (9)$$

The equation of motion from system (1), taking into account (5), (6), contains large nonlinearities, therefore, the pressure distribution along the pipeline route will be calculated numerically using finite-difference schemes. Having divided each linear section j into segments of length Δx_j, and taking into account the boundary conditions, we find the temperature from (9) at each node and then the pressure from (1), (3), (4):

$$T_j^I = T_{\text{окр}} + \left(T_j^{I-1} - T_{\text{окр}}\right) \cdot \exp\left(-\frac{4 \cdot k \cdot \Delta x_j}{\rho \cdot c \cdot D \cdot w}\right)$$

$$p_j^I = p_j^{I-1} - \rho \cdot g \cdot (z_j^I - z_j^{I-1}) + \{\rho \cdot g \cdot \beta \cdot \left(\frac{\pi \cdot w}{4}\right)^{2-m} \cdot$$

$$\cdot \left[\frac{\left[\nu(T_1) \cdot \exp\left[-a_1 \cdot \left(T_{\text{окр}} + \left(\frac{T_j^{I-1} + T_j^I}{2} - T_{\text{окр}}\right) \cdot \exp\left(-\frac{4 \cdot k \cdot \Delta x_j}{\rho \cdot c \cdot D \cdot w}\right) - T_1\right)\right]\right]^m}{D^{m+1}}\right] + \quad (10)$$

$$+\frac{16}{3 \cdot D} \cdot \tau_0(T_1) \cdot \exp\left[-a_2\left(T_{\text{окр}} + \left(\frac{T_j^{I-1} + T_j^I}{2} - T_{\text{окр}}\right) \cdot \exp\left(-\frac{4k\Delta x_j}{\rho c D w}\right) - T_1\right)\right] \quad \} \cdot \Delta x_j;$$

$$p_1^0 = p_n;\ T_1^0 = T_n;\ w_1^0 = w_n = const;$$

$$p_j^0 = p_{j-1}^{M_{j-1}} + \Delta p_j;\ T_j^0 = T_{j-1}^{M_{j-1}} + \Delta T_j;$$

$$i = \overline{0, M_j},\ j = \overline{0, N+1},$$

where M_j is the number of partitions on the j^{th} segment.

The algorithm for solving the thermo hydraulic fuel and energy problem (10) taking into account the cost of costs (7) is implemented as aapplication software. The calculation results for the Uzen-Atyrau trunk pipeline are shown in Figures 1,2.

In an oil pipeline with a Laval nozzle at the inlet, the mathematical model will be slightly different from model (1) – (10).

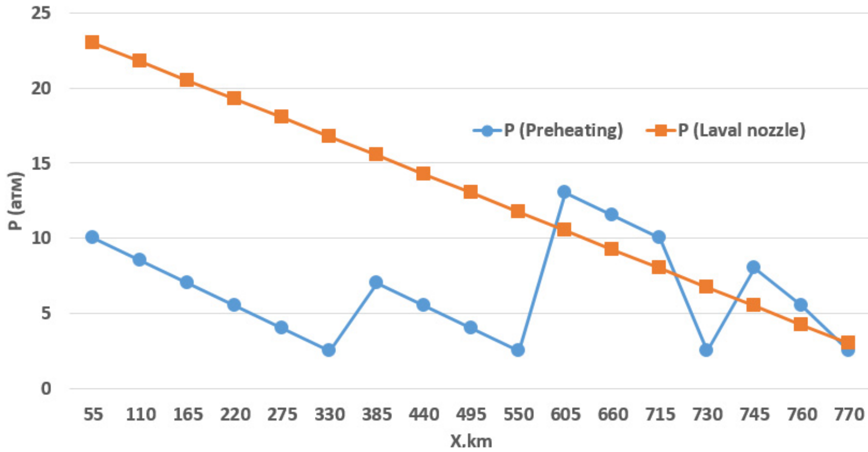

Figure 1 –Pressure distribution along the Uzen-Atyrau oil pipeline

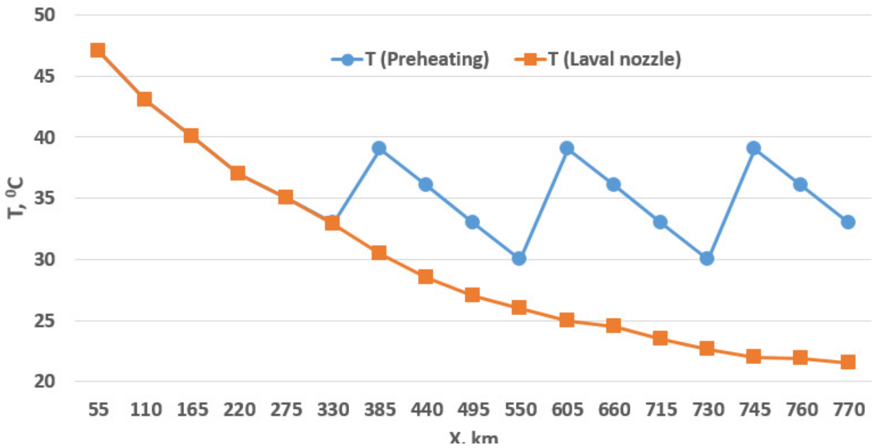

Figure 2 – Temperature distribution along the Uzen-Atyrau oil pipeline

Firstly, oil heating at intermediate stations is not required, because its viscosity decreases as it passes through the Laval nozzle. The decrease in viscosity depends on the nozzle entry angle α and the initial temperature T_n. The empirical formula has the form:

$$\nu=(f\cdot a^2+y\cdot \alpha + n)\cdot exp(u\cdot T_n)$$

where f, y, n, u – are empirical constants.

Note that the viscosity in this case is constant, and oil is a viscoplasticfluid for which dh_{Tp}/dx are described by expression (5).

Secondly, the effect of cavitation and a change in the cross section of the pipe leads to:

$$\tau_0 = 0, \nu = const \tag{11}$$

and pressure losses, which can be calculated by the formulas [6, 9,10]:

$$\left.\begin{aligned} dp_1 &= \gamma_1 \cdot \frac{D}{D_{min}} \cdot \rho \cdot \left(\frac{w_{кр}-w}{2}\right)^2; \\ dp_2 &= dp_{кав} = \gamma_2 \cdot \frac{p-p_{кав}}{\frac{\rho \cdot w_{кр}^2}{2}}; \end{aligned}\right\} \tag{12}$$

where γ_1, γ_2 are empirical constants; $w_{кр}$, $p_{кав}$ are the critical values of pressure and velocity at which cavitation occurs; D_{min} is the minimum diameter in the Laval nozzle.

Thirdly, as the experiment [7] showed, the decrease in viscosity is so significant, that for sufficiently long pipelines intermediate pumping stations can be abandoned using only the head one.

Thus, the stationary process of oil transportation in this case will be described by the system of equations (1), (2), (5), (11), (12), and the linear section is the entire pipeline and N = 1. The boundary conditions taking into account (12) are given in the form:

$$\left.\begin{aligned} p_{1+}(0)&=\Delta p_0-dp_1-dp_2; \\ T_1^+(0)&=T_n;\ w(0)=w_n. \end{aligned}\right\} \quad (13)$$

Since in this case there are no nonlinearities in the model, problem (1), (2), (5), (11) – (13) is solved analytically:

$$\left.\begin{aligned} p(x)&=p_0^+-\frac{\rho\cdot g\cdot\beta}{D^{m+1}}\left(\frac{\pi\cdot w}{4}\right)^{2-m}\cdot v^m\cdot x-\rho\cdot g\cdot(z(x)-z_0); \\ w&=const; \\ T(x)&=T+\left(T_0^+-T\right)\cdot\exp\left(-\frac{4\cdot k\cdot x}{\rho\cdot c\cdot D\cdot w}\right). \end{aligned}\right\} \quad (14)$$

The cost of the pipeline operation (7) in this case will be:

$$S = S_n = w\cdot t\cdot(\emptyset_0\cdot\Delta p_0)$$

and the minimum cost will be achieved with p_1 = p_{min}.

The results of calculations of the oil flow in the pipeline using a Laval nozzle are shown in figures 1,2.

Comparison of the results of calculations of the oil pipeline with preheating and using cavitation at the inlet of the pipeline showed (see Figures 1-3) that its application allows to operate without intermediate heating stations and with much lower energy costs, which is economically very profitable. So, in the case shown in the graphs, the use of a nozzle allows reducing the cost of transporting high-viscosity oil by 3 times.

However, it should be noted that when using a Laval nozzle, high-viscosity oil recovers its original structure over time [5], which can somewhat reduce the positive effect of cavitation.

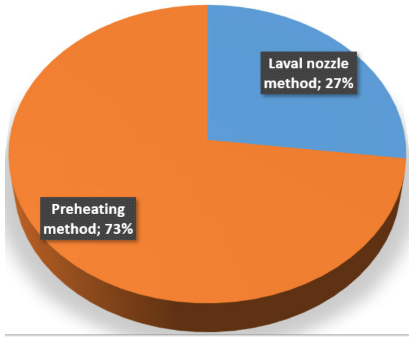

Figure 3 –Comparison of operationcost of the Uzen-Atyrau oil pipeline

Conclusions

Mathematical models of the flow of high-viscosity oil in the main oil pipeline for two pumping methods have been compiled: with preheating and using a Laval nozzle at the pipeline inlet.

An algorithm has been compiled to calculate the temperature, viscosity and pressure along the length of the Uzen-Atyrau pipeline at different oil flow rates.

The paper analyzes and compares the results of the distribution of temperature and pressure at different speeds of oil flow along the length of the pipeline for two pumping methods.

It was found that the viscosity of cavitation-treated oil is four times less than the initial value, which can significantly reduce the cost of pumping.

References

1. Cherdabaev R. *Oil of Kazakhstan*, Astana: "Aldongar", 2012.

2. Abalkin, "Status of pipeline projects in Kazakhstan for December 2015". polismi.org, published 12/31/2015, http://forum.polismi.org/index.php?/topic/13288(accessed 10/17/2019).

3. Agapkin V.M., Krivoshein B.L., Yufin V.A. *Thermal and hydraulic calculations of pipelines for oil and oil products*, Moscow: Nedra, 1981.

4. Nesterenkova L.A., Nesterenkov P.A. Minimization of the cost of a non-isothermal oil pipeline. *VestnikKazNITU*, 2 (2019): 528 – 535.

5. Smorodov E.A., Galiakhmetov R.N., Ilgamov M.A. *Physics and Chemistry of Cavitation*. Moscow: Science, 2008.

6. “Cavitation drip fluid flow”, firing-hydra.ru, https://firing-hydra.ru/index.php?request=full&id=406,(accessed 10/17/2019).

7. Nadirov N.K., Kovachuk T.N., Dukhovny T.S., et al. Patent 788 Republic of Kazakhstan MKI E!17O 1/16 “Method for the preparation of high-viscosity oils for pipeline transportation” (№ 231939/1, published 04.15.1994).

8. Nesterenkova L. A. Mathematical modeling of non-isothermal flow of high-paraffin oil in the pipeline.*Higher School of Kazakhstan, Information Technologies* 2 (2013): 156-159.

9. KamenevaT.Yu., Nesterenkova L.A. A numerical study of the reduction of oil viscosity under the influence of cavitation, *Abstracts of the Kazakhstan-Russian scientific-practical conference "Mathematical modeling – scientific, technological and environmental problems in the oil and gas industry*", Almaty, 1997, p. 96.

10. Hafizov I.F., Aleksandrov A.A., Suschev S.P., et al. Modeling and calculation method of cavitation-vortex apparatus, *Vestnik MGTU named after N.E. Bauman (Natural Sciences)* 1 (2017): 78-91.

CONTENTS

International Journal of Mathematics and Physics, #1 , 2020